A STUDY OF POLAR AURORAL ARCS

AT EUREKA, NWT (89°CGM)

A THESIS

SUBMITTED TO THE COLLEGE OF GRADUATE STUDIES AND RESEARCH

IN PARTIAL FULFILLMENT OF THE REQUIREMENTS

FOR THE DEGREE OF

DOCTOR OF PHILOSOPHY

IN THE

DEPARTMENT OF PHYSICS AND ENGINEERING PHYSICS

UNIVERSITY OF SASKATCHEWAN

SASKATOON

By

Yongliang Zhang

September 1995

UNIVERSITY OF SASKATCHEWAN

College of Graduate Studies and Research

SUMMARY OF DISSERTATION

Submitted in partial fulfillment

of the requirements for the

DEGREE OF THE DOCTOR OF PHILOSOPHY

by

YONGLIANG ZHANG

Department of Physics and Engineering Physics

University of Saskatchewan

Spring 1996

Examining Committee:

Dr. R. McKercher	~~Dean~~/Associate Dean/~~Dean's Designate, Chair~~ College of Graduate Studies and Research
Dr. K. Paulson	Department of Physics and Engineering Physics
Dr. D.J. McEwen	Supervisor, Department of Physics and Engineering Physics
Dr. G. Sofko	Department of Physics and Engineering Physics
Dr. A. Hirose	Department of Physics and Engineering Physics
Dr. E.J. Llewellyn	Department of Physics and Engineering Physics
Dr. H. Wood	Department of Electrical Engineering

External Examiner:

Dr. S. Murphree
Dept. of Physics and Astronomy
University of Calgary
2500 University Drive NW
Calgary, AB
T2N 1N4

A STUDY OF POLAR AURORAL ARCS AT EUREKA

($89°CGM$)

Sun-aligned arcs threading across the polar cap to link dayside aurora with the nightside auroral oval represent a significant part of the mystery and dynamics of the aurora borealis. Observations of these arcs were carried out at the Canadian Network for Space Research observatory at Eureka. located near the north magnetic pole. to study their characteristics and morphology. A total of 656 arcs were recorded by an all-sky imager during the 4-winter period with arcs being present 8% of total observing time. Most of the auroral forms were sub-visual and with the high sensitivity of meridian scanning photometers operating at the observatory polar auroras were observed (above a 50 Rayleigh threshold) nearly one-half of the time.

A detailed study of polar auroras has revealed much of their occurrence patterns, their relation to solar wind parameters and ionosphere-magnetosphere linkages. For example, an observed diurnal variation in occurrence frequency of polar arcs may be due to differing regions of the magnetotail connecting with the Eureka viewing area as the day progresses.

The lifetimes of polar arcs suggest that the intrinsic time constant of the magnetosphere related to polar arcs is below 20 minutes. A rapid development of special features (bifurcation and wave structure) of polar arcs indicates the time constant is of a few minutes for the related plasma instabilities in the magnetosphere or the ionosphere.

Polar arcs and global magnetic activity as depicted by K_p level were found not correlated. Most polar arcs occurred with the interplanetary magnetic field (IMF) oriented northward. However, there were substantial numbers observed with the IMF stably southward. It was also found that the mean frequencies of polar arcs over the winter periods positively correlated to solar activity (10.7 cm flux or sunspot number).

Solar wind dynamic pressure enhancements played a very important role in inducing polar arcs. Polar arcs were found to be generated following all major solar wind enhancements with long (70 min) time delays when the IMF was northward and short (18 min) time delays with the IMF was southward. Two electron source regions were identified: the deep magnetotail and the solar wind. Mapping of polar arcs by using the Tsyganenko 1989 magnetic field model confirmed that the location of the electron sources of polar arcs is usually in the magnetotail lobe region.

Copyright

Abstract

A ground-based optical study of polar arc characteristics is presented. An All-sky Camera (ASC) and Meridian Scanning Photometer (MSP) were operated at Eureka ($89°N$, Corrected Geomagnetic Latitude), Northwest Territories, over winter periods from 1990 to 1994 with 656 polar arcs detected by the ASC. Polar arcs were observed on average 8% of the time (above 300 R, 557.7 nm) by the ASC, with a diurnal variation peaking around local midnight. The amplitude of the diurnal variation was about 37 % of the mean occurrence rate. This may be due to the fact that the viewing area of the ASC in the ionosphere was magnetically connected to a magnetotail region which was closer to the plasma sheet around the local midnight hours. Polar arcs were detected by the MSP with a threshold of 50 R 30 % of the time from 557.7 nm emissions and 49 % of the time from 630.0 nm emissions. These suggest that the precipitated electrons exciting the polar arcs were often very soft. It was also found that the mean frequencies of polar arcs over the winter periods correlated with solar activity (10.7 cm flux or sunspot number). Most polar arcs (78%) occurred with northward IMF B_z. However, there were significant numbers (16 %) observed with the IMF B_z stably southward. Polar arcs also tended to occur with the IMF B_x near zero and the IMF B_y slightly positive. One half of the polar arcs (above 300 R, 557.7 nmm) had lifetimes less than 20 minutes.

There were 25 solar wind dynamic pressure enhancements detected by the IMP-8 satellite during the 1991-92 and 1992-93 winter periods. All the enhancements were followed by polar arcs. A short time delay (18 min on average) between the enhancements and the polar arcs with southward IMF B_z suggests direct access of solar wind particles into the polar ionosphere and an open magnetospheric configuration in the polar cap region. A positive correlation between the intensity of 630.0 nm emission of the polar arcs and the magnitude of the enhancements supports the direct access of the solar wind particles. The long time delay (70 min on average) for polar arc appearance following the enhancements with northward IMF B_z suggests the particle source for the polar arcs in this case was located in the magnetotail. This finding shows the solar wind dynamic pressure enhancements do generate or induce energetic

electron precipitation in the polar cap with either northward or southward IMF B_z. Mapping of polar arcs by using the Tsyganenko magnetic field model (T89) suggests electron source regions for polar arcs are mostly located in the magnetotail lobe region. The mapping supports a bifurcated magnetotail model or an expanded plasma sheet (plasma sheet boundary) model.

Suggestions for future work include the relation between the energy of precipitated electrons and the polarity of the IMF, generation of field-aligned electric fields, the relation between the lifetimes of polar arcs and stability of the northward IMF B_z or solar wind dynamic pressure, and development of fine structure in polar arcs in relation to plasma instabilities in the magnetosphere or the ionosphere.

Acknowledgments

First I would like to thank my research supervisor, Dr. D.J. McEwen, for his continued guidance, support, and encouragement throughout this thesis project.

It is very important that I thank the operators of the Eureka observatory, A. Maione, D. Harris, G. Hammel and N. Rolheiser. I would like to thank Drs. I. Oznovich and N. Lloyd for their advice and suggestions. I would also like to thank D. Harris for his help in showing me the operation of the instruments. Special thanks should be given to G. Hammel for his computer code necessary for the processing of the photometer data which were utilized in this thesis. I would also like to thank the Department of Physics and the Institute of Space and Atmospheric Studies (ISAS) for the access to their facilities.

Finally, I would like to greatly thank the Canadian Network for Space Research (CNSR) for their funding for this project. Financial assistance was provided by my supervisor, and I thank him for that. I would like to thank Dr. R.P. Lepping and NASA Data Center for the interplanetary magnetic field data and solar wind data. A note of appreciation to Mrs. J.H. Meek and Mrs. B.W. Currie, as I received the John Henry Meek and B.W. Currie Memorial Scholarships which are awarded annually in honor of their late husbands. I thank the University of Saskatchewan for the Graduate Scholarship I received. I would also like to thank my wife, Binbin Yuei, for her full support during the writing of this thesis.

Contents

List of Figures

List of Tables

Chapter 1

INTRODUCTION

1.1 Historical background

The mysterious and beautiful luminosity which we call aurora has excited the curiosity and wonder of the Human since the dawn of history. Unlike other impressive phenomena of nature such as the sunsets, the rainbows or the thunderstorms, it is both physically and conceptually remote since it occurs well above the lower layers of the atmosphere and its explanation involves some of the more recent disciplines of physics.

The name *aurora borealis* (northern dawn) was given by Gassendi in a book describing observations in southern France before 1621. The corresponding *aurora australis* was used by Cook in 1773. Cavendish made a reasonable height measurement in 1784. By 1873 the northern auroral zone had been mapped as a result of the work of Muncke, Loomis and Fritz. The connection between aurora and magnetic storms was recognized by Celsius in 1741. The sunspot cycle was discovered by Schwabe about 1844 and within 10 years the connection between sunspot maxima and magnetic storms was recognized. The auroral spectrum was first observed by Angstrom about 1868.

The discovery of the electron around 1880 paved the way for the proposal of Birkeland in 1896 that aurora was caused by electrons ejected from the Sun and guided to the auroral zones by the Earth's field. Birkeland showed by means of laboratory

experiments that an electron beam would behave qualitatively as proposed. By 1910, Stormer began to calculate mathematically such particle orbits, so that quantitative testing of the theory could begin. Subsequently Stormer [1955] carried out definitive studies of auroral heights and extent by photographic triangulation.

The most prominent feature of the auroral spectrum, the green line at 557.7 nm , had been a mystery but was finally identified as a forbidden transition of atomic oxygen by McLennan and Shrum in 1925. The hydrogen lines and their Doppler shift were identified and measured by 1950 in the work of Vegard, Gartlein and Meinel. In the following decade the exploration of the spectrum was virtually complete as detailed by Chamberlain [1961].

The aurora is the most readily observed consequence of the dynamic magnetosphere and the most obvious characteristic of the high-latitude ionosphere. People must have been looking at the northern and southern lights in the night sky, the aurora borealis and the aurora australis, for thousands of years, which surely puts them among the oldest known geophysical phenomena; though it is only in the last part of the 20th century that any proper explanation has become possible. Early 'theories' range from the fanciful to some that were unwittingly near the truth: sunlight reflected from polar snow and ice (wrong), elastic fluids (vague), electric discharge (plausible). Only in the early 1950s was it proved that the immediate cause of auroral emissions is excitation of atmospheric gas by energetic particles, and it was not until 1958, when rockets were fired into an aurora, that energetic electrons were identified as the primary source. Because of these in-situ measurements, auroral science has developed from a somewhat mysterious and imprecise specialty into a major topic central to the space physics discipline. An understanding of the source of those electrons has had to wait for a fairly detailed knowledge of the structure and physics of the magnetosphere.

Aurora consists of a luminosity, usually distributed in regular or irregular horizontal bands which sometimes have vertically oriented striations or rays. Most commonly seen auroras have their lower limits between 100 and 120 km above the Earth's surface

and have a vertical extent of a few atmospheric scale heights. Most auroras are too low in intensity to reach the color threshold of the eye so that they are seen by scotopic vision and hence appear without definite color. More intense auroras appear green or more rarely red, purple, violet and blue are seen.

The overall probability of seeing aurora reaches a maximum in an approximately circular zone of radius $\sim 22°$ centered on the geomagnetic poles. This is called the auroral zone. However, if local time is taken into consideration the locus of maximum occurrence is an oval aligned along the sun-earth direction with radii from the geomagnetic pole of about 12° and 22°, respectively, in the solar and anti-solar directions. This is the auroral oval. The most intense aurora is seen in the midnight region of the oval. The area in the vicinity of the magnetic pole and surrounded by the auroral oval is called the polar cap. Auroras observed in the polar cap are called polar cap auroras or polar arcs. They are quite different from those in the auroral oval.

The intensity of auroras in the auroral oval is variable from a just detectable level comparable to that of the Milky way, to 1000 times brighter. Active displays of aurora tend to follow a pattern called a substorm during which the most spectacular feature is an explosive increase in intensity in the midnight region of the oval followed by a spreading of the brightening poleward, westwards and eastwards. Rapid motions of the auroral forms take place at the height of each substorm and strong local magnetic perturbations are observed below on the ground due presumably to large electric currents at auroral heights.

The study of the spectra of aurora in the auroral oval and direct measurements by rockets and satellites have shown that most bright auroras are excited by energetic electrons guided downwards along the lines of the Earth's magnetic field. The average energy of the electrons is of the order of 2 to 10 keV. In addition to exciting the atoms and molecules of the atmosphere to emit optically, the bombarding electrons produce ionizations which gives rise to various radio wave absorption and reflection effects. Radio aurora is a reflection of VHF and UHF waves from ionization more or less closely

associated with visual aurora. It appears however that plasma instabilities associated with the presence of electric fields are necessary to generate the structure from which the radio waves are reflected. Electric fields also give rise to electric currents in the ionized regions and these currents generate strong magnetic field disturbances on the ground beneath many auroral forms.

Higher energy components of auroral electrons fluxes can generate X-ray emission detectable at balloon altitudes below aurora as well as VLF radio emission. Such higher energy electrons also cause radio wave absorption due largely to the ionization they produce below 100 km. Both X-ray and particularly absorption observations have been widely used in synoptic studies since they give a measure of the entry of the higher energy component of auroral electrons independent of atmosphere conditions or time of day.

In addition to electrons, there are fluxes of energetic protons capable of producing a low level of luminosity in the same height range as electron aurora. This is called proton aurora. Sometimes it is spatially separated from electron aurora and sometimes intermingled with it. Because of charge exchange processes, incoming protons spend part of the trajectories as hydrogen atoms, thus escaping from the control of the Earth's magnetic field. This permits the proton beam to spread laterally and consequently a proton aurora never shows the detailed structure of electron aurora but rather takes the form of a broad diffuse emitting surface. Viewed in the magnetic zenith (i.e. parallel to the Earth's magnetic field lines), the hydrogen Balmer lines of proton aurora show a Doppler shift which historically provided the first evidence that auroral phenomena are caused by particle bombardment.

Auroras observed in the polar cap are usually caused by precipitated electrons with energy lower than that in the auroral oval. Their characteristics are quite different from those of auroras in the auroral oval. A full understanding of all these auroras requires knowledge of coupling between the magnetosphere and ionosphere, and the interaction between the solar wind and the magnetosphere.

1.2 Solar Terrestrial Environment

1.2.1 The solar wind

The story of the solar wind begins with the work of S. Chapman and V.C.A. Ferraro on magnetic storms. Some storms commence with a sharp increase in the geomagnetic field as recorded with ground-based magnetometers. By way of explanation, Chapman and Ferraro [1931] suggested that during a solar flare a cloud of plasma is ejected from the sun, reaching the Earth about a day later. Theoretical studies by Chapman and E.N. Parker subsequently proved that, unlike the Earth's atmosphere, the solar corona is not in hydrostatic equilibrium but expands continuously, with matter leaving the Sun and streaming out into space. Parker called this flow the *solar wind.* The existence of the solar wind was verified by space probes in the early 1960s.

Our planet is embedded in the solar wind. Fig. 1.1 is a sketch of the solar-terrestrial environment (after J.K. Hargreaves, 1992). It shows the solar wind emitted from the Sun and interacting with the Earth's magnetosphere. The solar wind is basically a proton-electron plasma that streams past the Earth with a mean velocity of 400-500 km/sec and a typical proton and electron density of about 5 cm^{-3}. The temperature of the solar wind is about 10^5 K [Axford, 1968]. Therefore, the solar wind carries energy and momentum to the vicinity of the Earth. The variability in the density and speed of the solar wind is shown over one solar rotation in Fig. 1.2. There is a degree of anti-correlation between density and speed. The solar wind is the principal medium by which the activity of the Sun is communicated to the vicinity of the Earth, and it is extremely important in solar-terrestrial relations.

The solar wind plasma interactions with the Earth's intrinsic magnetic field and the resulting interaction has important repercussions on space systems operating in the near Earth environment. The only visible manifestation of this interaction is the aurora, which frequently lights up the sky at polar latitudes (both north and south). Intermixed with the streaming solar wind plasma is a weak magnetic field, called the

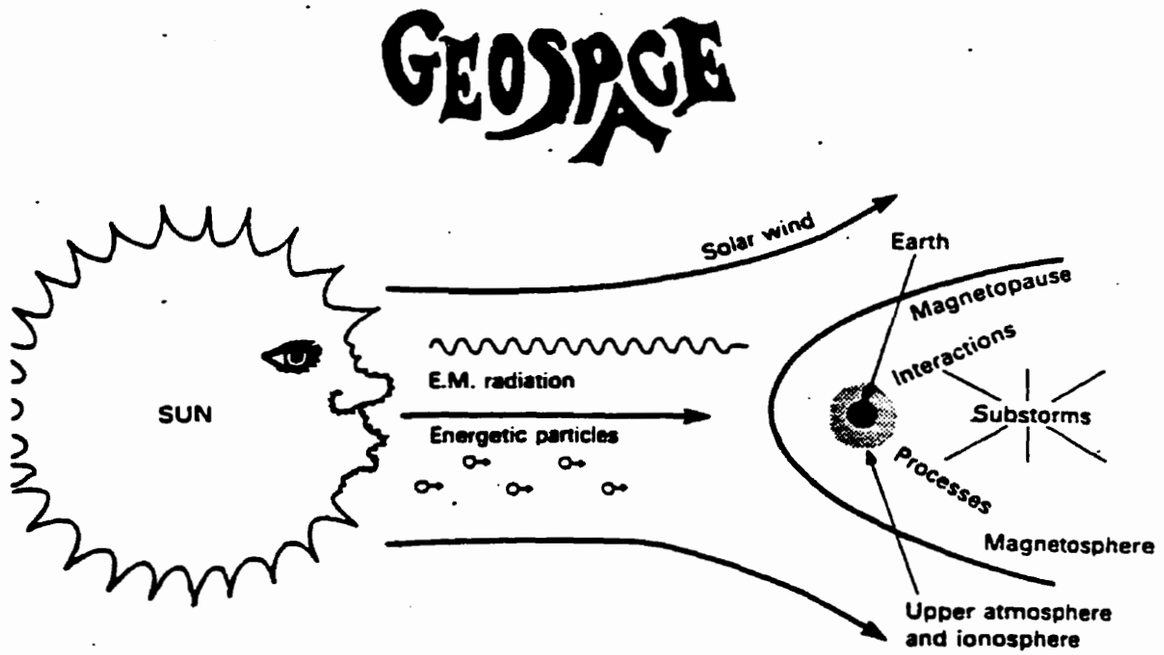

Figure 1.1: Summary of solar-terrestrial environment. (after a sketch by J.K. Hargreaves, 1992).

interplanetary magnetic field (IMF). The IMF is about 1/10000 the strength of the Earth's surface magnetic field. However, it plays a very important role in the interaction between the solar wind and the Earth's magnetosphere. The orientation of the IMF determines whether the IMF will couple with the Earth's magnetic field which, in turn, allows solar wind particles easy access to the magnetosphere.

1.2.2 The magnetosphere

In the absence of an interplanetary plasma, the Earth's dipole magnetic field would extend indefinitely in all directions. However, the geomagnetic field produces a semi-permeable obstacle to the solar wind and the resulting interaction produces a cavity around which most of the plasma flows. The extent of this obstacle called the magnetosphere where the movement of plasma is controlled by the geomagnetic field. It

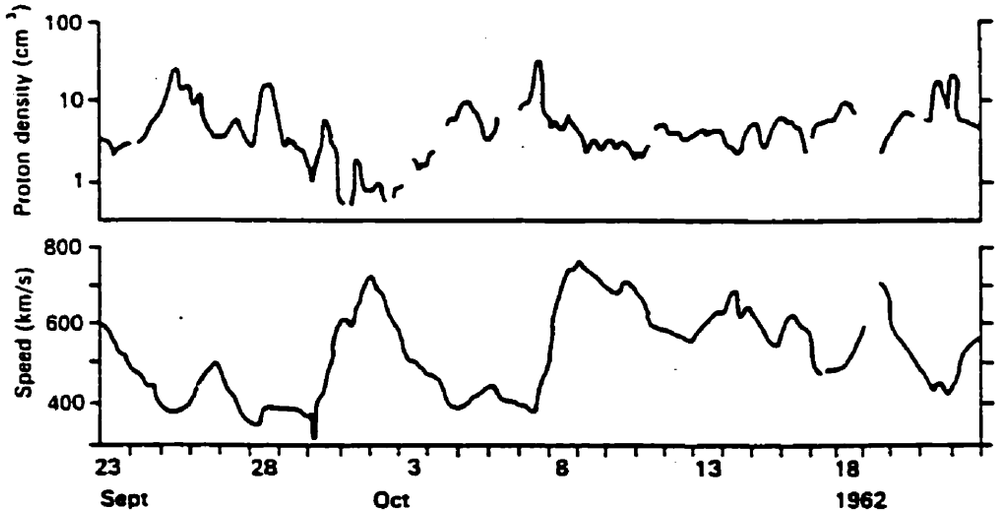

Figure 1.2: Density and speed of the solar wind over one solar rotation in 1962, measured by Mariner-2. (after H. Rosenbauer, 1982).

is modified by changes in the solar wind density and velocity, and to variations in the strength and orientation of the interplanetary magnetic field (IMF). The magnetosphere consists of several regions which play distinctly different roles in formation of auroras (both auroral oval and polar cap). Fig. 1.3 shows the cross section of the magnetosphere. The magnetosphere includes the plasmasphere, radiation belt region, the plasma sheet, magnetotail lobes, plasma mantle region, magnetopause, magnetosheath, dayside boundary layer, magnetotail boundary layer and cusp region. The auroral oval also can be seen in the Fig. 1.3.

1.2.3 Bow shock

The solar wind plasma can behave like a fluid because of the existence of propagating wave modes, the Alfven and magneto-acoustic waves. The solar wind plasma flow speed (Mach 8+) exceeds the speed of these waves. Upon encountering the magnetosphere, a shock wave (called the bow shock) forms in the solar wind 2 or 3 Earth radii (R_E) upstream of the magnetopause. Fig. 1.4 shows that the measured and calculated

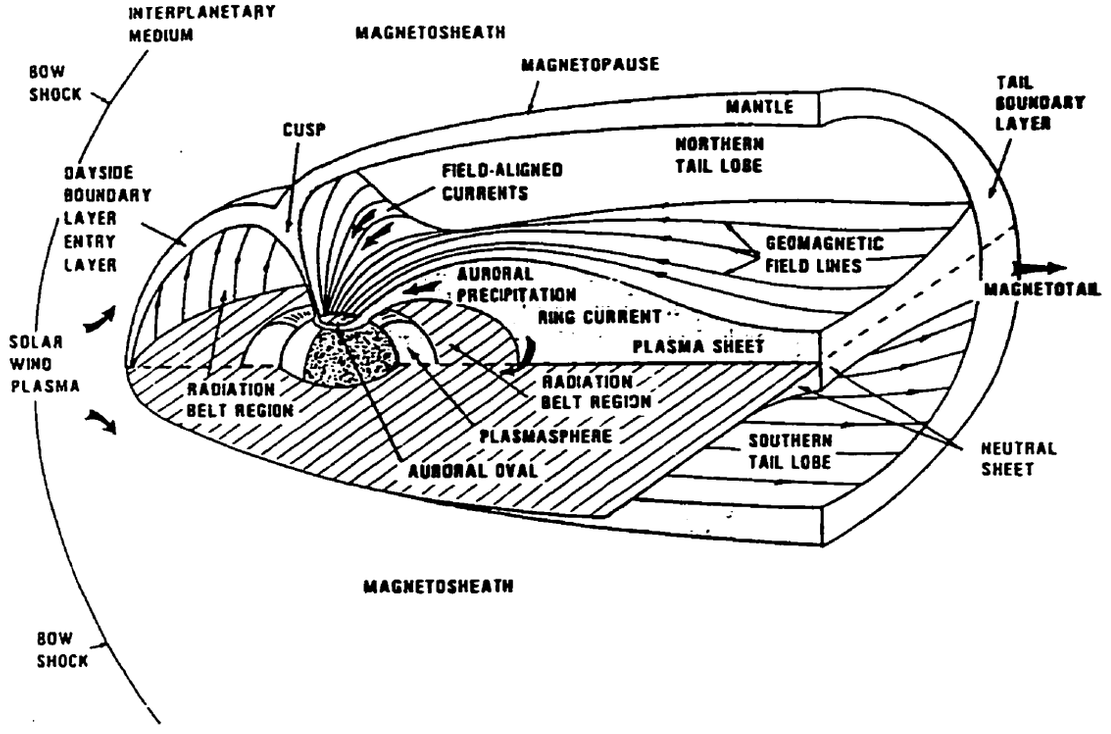

Figure 1.3: A sketch of the magnetospheric structure (Cross section of the magnetosphere).

position of the bow shock is around 13 - 14 R_E from the Earth.

1.2.4 Magnetosheath

Between the bow shock and the magnetopause lies a region of compressed and heated solar wind plasma called the magnetosheath. Crossing the bow shock, solar wind plasma is slowed down to about 250 km/s and the corresponding loss of directed kinetic energy is dissipated as thermal energy, increasing the temperature of the solar wind plasma to 5×10^6 K. Therefore magnetosheath plasma is more turbulent and irregular than the solar wind plasma before it travels across the bow shock. The location of the magnetosheath, as shown in Fig. 1.3., is between the bow shock and the magnetopause.

1.2.5 Magnetopause

The magnetopause is a surface or thin layer where the outward force of the compressed geomagnetic field along with the gas pressure of the magnetospheric plasma is balanced by the force of the magnetosheath plasma . The normal position of the magnetopause is about 9 to 12 R_E (see Fig. 1.4). The position is mainly controlled by solar wind dynamic pressure; the higher the solar wind dynamic pressure, the closer the magnetopause is to the Earth. The magnetopause is recognized by a strong change in direction of $\vec{B}$ during negative B_z. Otherwise, it is recognized mostly by a change in particle energy from one side to the other.

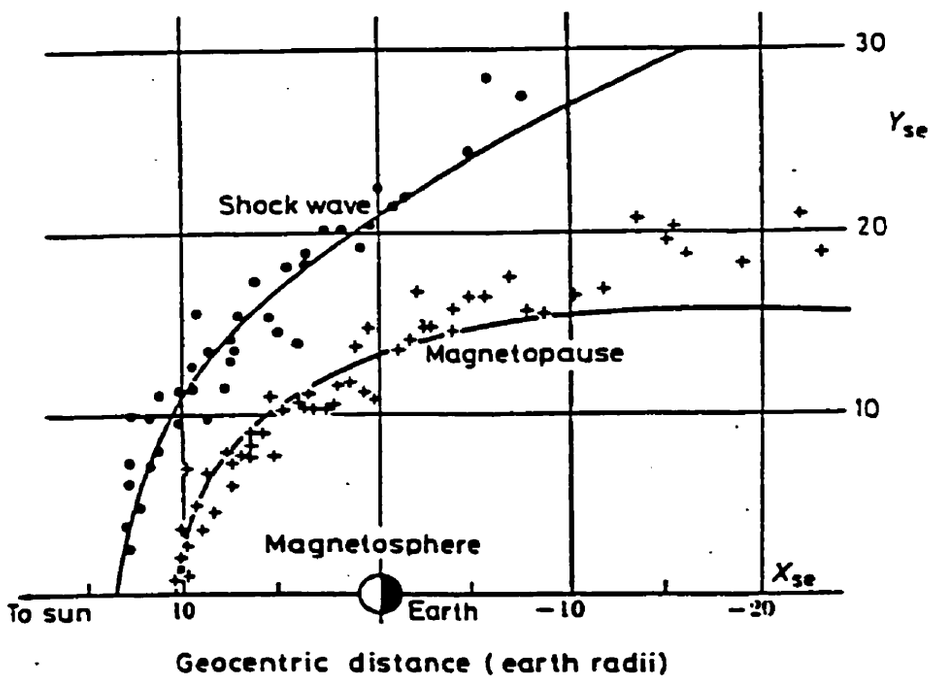

Figure 1.4: Observed and calculated positions of the magnetopause and the shock in the solar-equatorial plane. (after N.F. Ness et al., 1964).

1.2.6 Cusp

Simple magnetosphere models predict two neutral points on the magnetopause where the total field is zero. These points connect along field lines to places on the Earth's surface near $\pm 78°$ magnetic latitude. These are the only points that connect the Earth's surface to the magnetopause and all the field from the magnetopause converges to those two points. They are, therefore, regions of great interest where solar wind particles (from the magnetosheath) can enter the magnetosphere without having to cross field-lines. There is good direct evidence that this happens. Particles with energy typical of the magnetosheath are observed over some 5° of latitude around 77°, and over 8 hours of local time around noon. Being more extended than points, these regions are now called the *polar cusp or clefts.* The significance of the cusps is that they serve as the main particle entry regions from the solar wind.

1.2.7 Plasmasphere

The plasmasphere represents the relatively cold ionospheric plasma which is co-rotating with the Earth due to frictional coupling. The co-rotation extends out to several Earth Radii (4-5 R_E at the equator) with particle densities ranging from about 10^4 cm^{-3} at low altitudes (1000 km) to 10 - 100 cm^{-3} near its outer edge. The plasmasphere nevertheless persists as a permanent feature of the inner magnetosphere. The boundary between plasmasphere and inner magnetosphere is called the plasmapause. Plasma densities drop at least a factor of 10 across this boundary. The plasmapause was discovered by D.L. Carpenter in 1963 in observing VLF propagation of 'whistlers' generated by lightning [Carpenter, 1988].

1.2.8 Magnetotail

In the antisunward direction the magnetosphere is extended into a long tail, usually known as the *magnetotail,* which is perhaps the most remarkable feature of the magnetosphere. Spacecraft magnetometers found that on the nightside of the Earth the geomagnetic field beyond 10 R_E tends to run in the sun-earth direction, and there is a

central plane where the field reverses direction. This is called *neutral sheet.* The field points toward the Earth in the northern lobe, and away from the Earth in the southern lobe. The tail is roughly cylindrical, some 30 R_E (2×10^5 km) across, and of uncertain length thought it has been detected downward beyond 10^7km ($1500R_E$). Therefore, the magnetotail extends well beyond the orbit of the Moon (60 R_E). Other satellites have made measurements in the tail which showed that the tail is very dynamic, and it is the source region for magnetic storms, substorms and auroral activities.

1.2.9 Currents in the magnetosphere

There are five major current systems in the magnetosphere. They are the ring current, magnetopause current, plasma sheet current (neutral sheet current), tail current, and Birkeland (field-aligned) currents. The location of these currents are shown by a sketch in Fig. 1.5. All these currents are related to the convection pattern of the magnetosphere. The changing of these currents causes magnetic disturbances, such as magnetic storms and substorms.

1.2.10 Magnetic substorm

At times, the geomagnetic field is disturbed by magnetic storms or substorms. The substorm has been identified with large-scale changes in the magnetotail in which the total flux is suddenly reduced, thus producing large induced electric fields which drive the tail plasma toward or away from the Earth. The circulation of the magnetosphere is driven (mainly) by magnetic merging on the sunward side of the magnetopause, but its continuity depends on reconnection in the tail plasma sheet. When the IMF turns southward, the connection rate increases and more open field is then being produced than removed. The coupling between the solar wind and the magnetosphere becomes very strong and this induces large currents in the magnetotail. These may cause a *substorm.* The substorm was originally identified from ground-based studies of the aurora, and three phases have been identified: the growth phase, the expansion phase, and the recovery phase. The most visible products of substorms are bright, active and extensive auroras. It is fair to say that the basic elements of magnetic substorms or

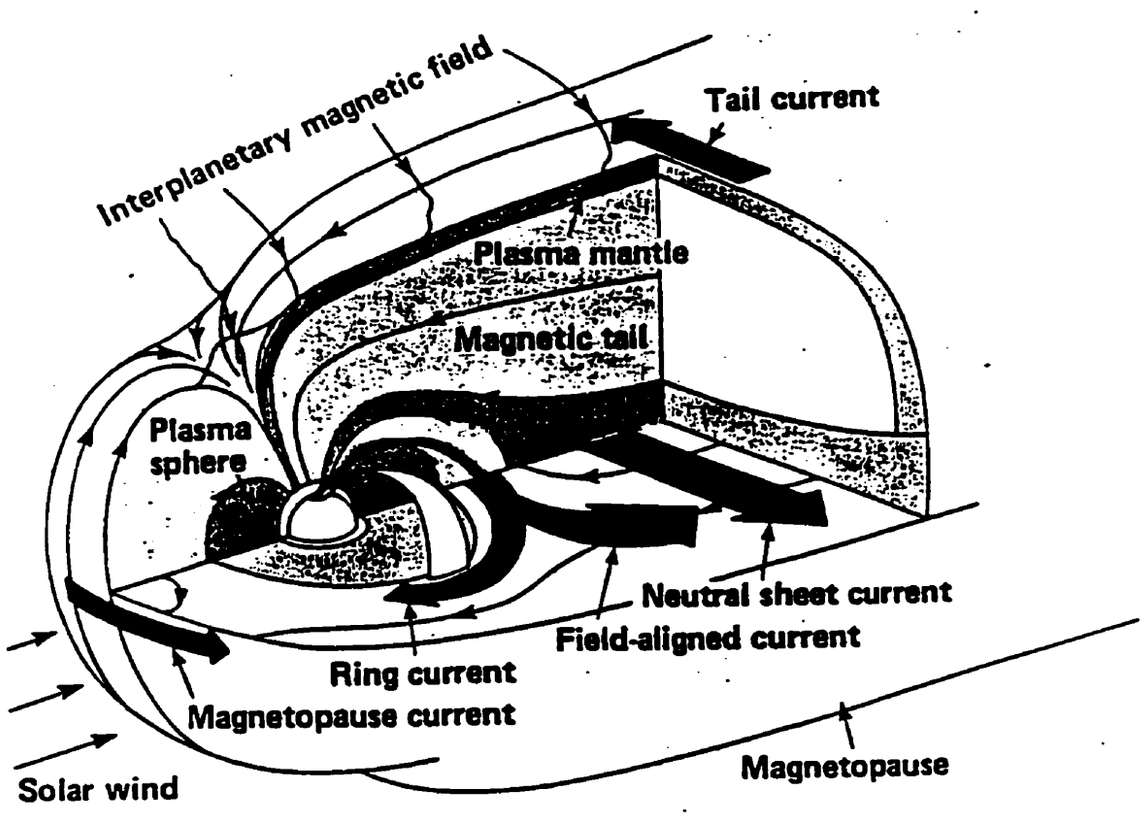

Figure 1.5: Currents in the magnetosphere. (after T.A. Potemra, 1983)

storms are moderately well understood. But our theoretical understanding of how the solar wind triggers a magnetic substorm is still far from complete [Tascione *et al.*, 1988].

1.3 Modern view of auroral oval and polar cap auroras

The auroral oval is one of important boundaries of geospace. The auroral intensity has a maximum near 67° (magnetic latitude) at midnight. It is around 77° at noon. The polar cap is then defined as the area surrounded by poleward edge of the oval. Both discrete and diffuse auroras can be observed in the oval. But generally only discrete auroras, also call polar arcs, are observed in the polar cap.

Auroras on the Earth have been observed for many centuries. However, the scientific study of polar cap auroras just started at the beginning of this century with the pioneering work of D. Mawson. *Mawson* [1916, 1925] was the first scientist to report the occurrence of aurora at very high latitudes based on visual observations during the Australian Antarctic expedition of 1907-09. Those auroras were found to be nearly aligned with the sun-earth direction with velocities of motion of the order of 100 ms^{-1}. During the international Geophysical Year (IGY), it was realized that this type of aurora only developed at latitudes poleward of the auroral oval [Weill, 1958; Denholm and Bond, 1961; Davis 1960]. A few years later it was discovered that the sun-aligned arcs preferentially developed when the interplanetary magnetic field pointed northward [Berkey et al., 1976], and during periods of quiet magnetic conditions [Davis, 1963; Lassen, 1972; Ismail et al., 1977]. More precise measurements of the morphology of the polar cap aurora indicated these arcs were sun-aligned only in a first approximation. These observations suggested that the the appearance of polar arcs was associated with a special magnetospheric topology.

A new era of polar auroral research was initiated by satellite measurements of electron precipitation. The particle sensors on-board satellites in the Defense Meteorogical Satellite Program (DMSP) revealed that the polar cap aurora was co-located with low-energy (< 500 eV) electron precipitation. The spectrum of this soft precipitation was found to contain characteristics similar to the electrons injected at the poleward boundary of the auroral oval [Meng, 1981a, b]. Three kinds of polar cap auroral arcs were classified according to the study of global auroral imagery obtained by DMSP [Ismail and Meng, 1982]: Type 1, the distinctly sun-aligned polar arcs; Type 2, the morning/evening polar arcs expanded from the auroral oval and Type 3, the hook shaped arcs connecting the polar cap arc with the oval arcs. Over both hemispheres, the polar arcs were observed mostly during northward IMF. Type 1 arcs were observed mostly during low geomagnetic activity conditions, bright Type 2 arcs during the recovery phase of the substorms and Type 3 did not occur during the recovery phase of the substorms. The later observations suggest that arcs of Type 1 may be non-conjugate.

Based on a theoretical model, two types of polar arcs were predicted according to their plasma sources: the magnetosheath arc and the plasma sheet arc [Chiu et al., 1985]. It was pointed out that during extended periods of B_z northward conditions, the polar cap was observed to be contracted into a teardrop shape [Murphree et al., 1982] and that the poleward flanks of the oval expand and occupy much of the otherwise polar cap region [Meng, 1981a]. The expanded auroral oval model implicitly suggests that the polar arcs are located in the region of closed field lines mapping to the boundary layers of the magnetosphere. Satellite excursions in the magnetosphere (for example bt the ISEE 1 satellite) have determined that the low-latitude boundary layer (LLBL) widens during positive B_z values [Mitchell et al., 1987]. This gives further credit to the oval expansion model.

A different view in the study of polar cap auroras arose from the analysis of data obtained by the DE 1 satellite. The imager on-board the high-altitude DE 1 provided a global view of the auroral oval and revealed the existence of the transpolar auroras extending between the midnight oval and the midday auroral zone. This auroral configuration is called the theta aurora [Frank et al., 1982, 1986]. The precipitating particles in the center of the theta aurora were observed to clearly resemble a population of plasma sheet particles in density, temperature and differential fluxes. Conjugate measurements on both hemispheres have indicated that the theta aurora in fact occurs simultaneously at both poles [Mizera et al., 1987; Obara et al. 1988, Craven et al., 1991]. ISEE2 excursions downtail discovered the presence of filaments of plasma sheet plasma intruding into the tail lobes [Huang et al., 1987, 1989]. This suggests a bifurcated magnetotail [Frank et al., 1986].

In addition to the model of a bifurcated tail, other models such as the expanded plasma sheet, expanded LLBL, rotated x-line and open magnetotail model were suggested based on different observations [Weiss et al., 1994].

Ground based high-sensitivity photometers have observed a type of subvisual, sun-aligned arcs which are present in the polar cap more often than is implied by satellite

imager data [Weber and Buchau, 1981]. These weak polar arcs are associated with gradients in velocity pattern and with low-energy ($< 500eV$) precipitating electrons. These arcs have been named F region arcs, because most of the electron energy is deposited at altitudes above 240 km. An instrumented rocket launched into a polar cap F region arc [Weber et al., 1989] measured sunward flow within the polar arc and a particle spectral shape with characteristics of boundary plasma sheet and magnetosheath populations. This fact suggested that some of the polar arcs could map to regions of open field lines [Kan and Burke, 1985]. Another rocket measurement of polar arcs [Weiss et al., 1994] was consistent with a model in which the arc is formed on open field lines on the duskside of a bifurcated polar cap or alternatively on closed field lines threading an expanded low-latitude boundary layer. Hardy [1984] observed intense fluxes above polar rain levels which were embedded in the polar rain suggesting that the polar cap arcs were not attached to the auroral oval and consequently were on a region of open field lines. More recently, Gussenhoven and Mullen [1989] have reported observations of relativistic electrons concurrent with precipitating electrons and ions associated with a polar cap aurora. Their measurement argues in favor of the formation of polar arcs on open field lines. It is also shown that polar arcs of typical electron energy ($\leq$ 1 keV) can be produced by downward acceleration of polar rain electrons by parallel potential drops on open field lines [Chiu, 1989]. Whether polar cap arcs are on open or closed field lines has important implications not only for topological considerations but also for energy implications and the determination of whether particle energy can be stored or directly precipitated into polar arcs [Hardy et al., 1982].

The strong observational evidence in favor of both closed field line models and open field line models of polar cap arcs can be understood if each model corresponds to a specific class of polar arcs [Meng and Mauk, 1991]. It is also possible that the development of several models was stimulated by the large number of different sensors all with distinct sensitivity thresholds which have been used to measure characteristics of polar arcs [Valladares et al., 1994].

1.4 Thesis objective

The thesis project is to study the statistical characteristics of polar arcs based on a large data set recorded at Eureka near the north magnetic pole over the four winter periods (1990-94) and to determine how polar arcs are related to the IMF vector and the solar wind activity via coupling between the solar wind and the magnetosphere. Polar auroras are also related to auroras in the auroral oval, but their characteristics are significantly different. They respond to activities in the interplanetary medium in different ways. Compared to the auroral oval auroras, polar auroras and their relation to the solar wind and magnetospheric conditions are less well understood. Much attention has been paid to polar auroral studies in recent years. Chapter 2 is a short description of instruments and data used in the study. Chapter 3 is a detailed study of polar arc occurrence patterns, and the relationship between polar arcs, solar wind parameters and global magnetic activity. Solar wind dynamic pressure enhancements play a very important role in inducing polar arcs. The relationship between the enhancements and polar arcs is shown in Chapter 4. Mapping of polar arcs using a magnetic field model is presented in Chapter 5. Discussion and conclusions are found in Chapter 6 and Chapter 7 respectively.

Chapter 2

Eureka site, instruments and data

2.1 Site of observations

An observatory very close to the north magnetic pole has been in operation at Eureka (80.0°N, 274.1°E) by the University of Saskatchewan since the winter of 1990-91 [Zhang *et al.*, 1993] and continuous winter observations have been made there with an all-sky camera (ASC) and a meridian scanning photometer (MSP). Fig. 2.1 shows that Eureka is located in the central polar cap very near the north magnetic pole (in Corrected Geomagnetic Coordinates [CGM], 1990 epoch). Because of this, the ASC at Eureka can view all 24-hour local magnetic sectors at any time. The shaded area is the mean position of the auroral oval for a K_p level of 3. The magnetic latitude of Eureka is 88.9° N. The instruments were operated through the whole dark winter period at Eureka (November through February in general). At 80°N, full 24-hour operation was possible for most of this period. Some other instruments were operated in the polar cap at Resolute Bay, Cambridge Bay by the Universities of Nagoya and Tokyo, Japan, and at Thule by the US Phillips Laboratory. Eureka (88.9°N, 318.0°E CGM), Resolute Bay (84.5°N, 316°E CGM) and Cambridge Bay (77.6°N, 306°E CGM) form a chain in the polar cap (see Fig. 2.1). This chain provided opportunity to observe transpolar arcs and motion of polar arcs from the midnight sector to the central polar cap.

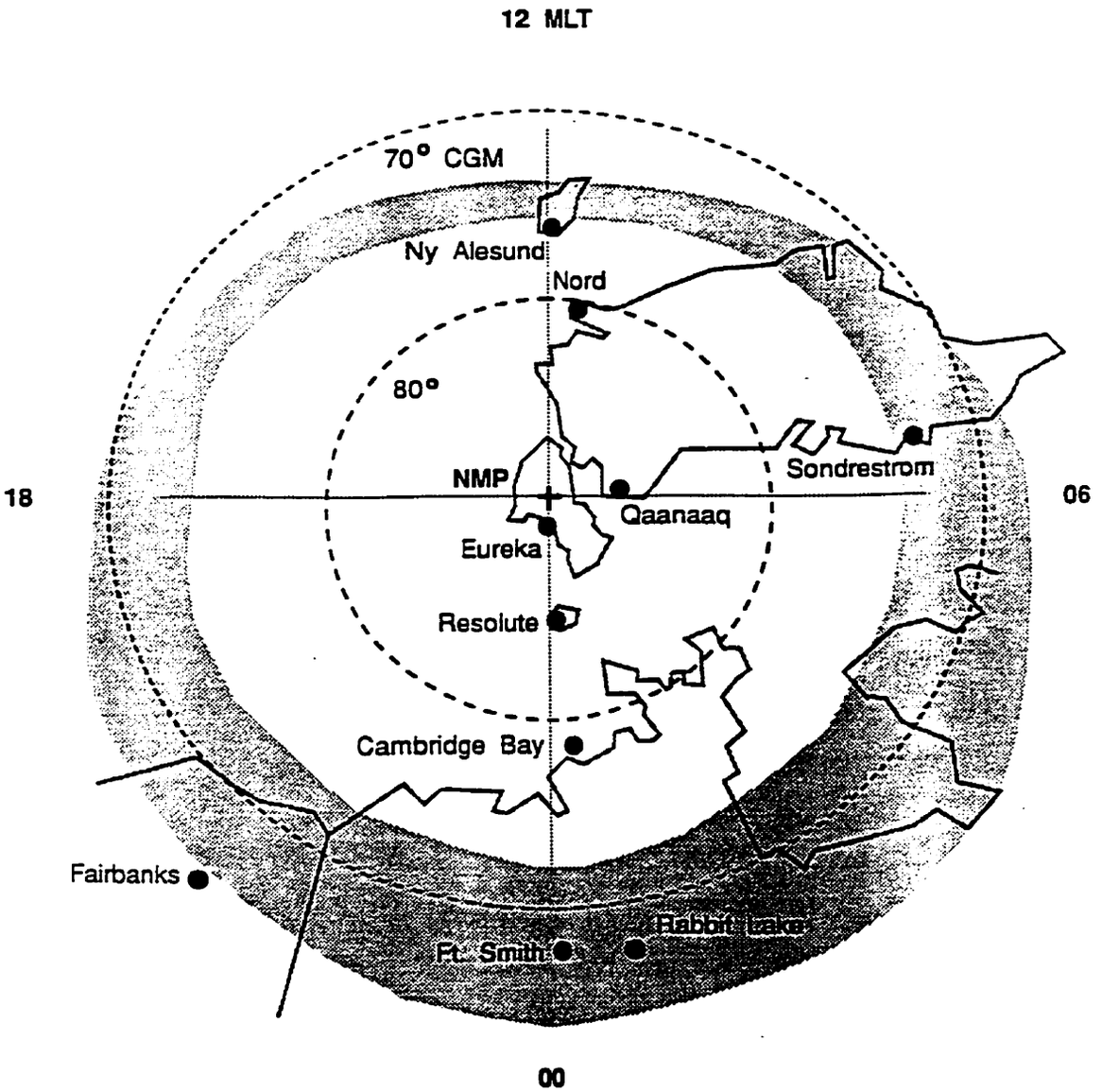

Figure 2.1: Locations of Eureka, Resolute Bay and Cambridge Bay *etc.* under CGM coordinate at Eureka local magnetic midnight. (after D.J. McEwen, 1994).

2.2 Instruments

Fig. 2.2 (left) shows a picture of the ASC. The mirror at the bottom enables the intensified TV camera on the top to view the whole sky. The ASC was operated with 557.7 nm, 630.0 nm filters and open frame alternately under the control of an IBM personal computer. Fig. 2.2 (right) also shows details of the shutter - filter assembly. The ASC was operated to take images of the sky every 4 seconds with a sensitivity threshold of about 300 rayleigh (557.7 nm) [Oznovich and McEwen, 1994]. ASC images were first digitized by a frame grabber and then stored in the computer memory. Those digitized images were then integrated and finally written on VHS magnetic tapes by a time lapse video recorder.

The MSP was run with 6 channels including the 557.7 nm and 630.0 nm channels with a threshold of detection of about 5 rayleigh (R) at 557.7nm. Fig. 2.3 shows a picture of the MSP. The MSP scanned the sky from 0 to 180 degrees of elevation angle in 40 seconds (5 Hz mode) or 20 seconds (10 Hz mode) with spatial resolution of 1 degree/step under the control of an IBM personal computer [Steele and McEwen, 1990; McEwen and Huang, 1993]. The MSP could be operated either at a fixed orientation or in a rotating dawn-dusk direction.

The flux gate magnetometer was operated by the University of Tokyo, Japan. The magnetometer collected 3 components of the geomagnetic field each second.

2.3 Data

Observations of polar arcs by the ASC and the MSP at Eureka were continued for five winters from 1990-91 to 1994-95 winter. Detailed periods of operation are listed in table 2.1. The instruments were operated manually during the first winter period (1990-91 winter). The instruments had been run automatically since the second winter period. There were about 21 thousand images and 10 MB data collected by the

All-Sky Camera - Eureka

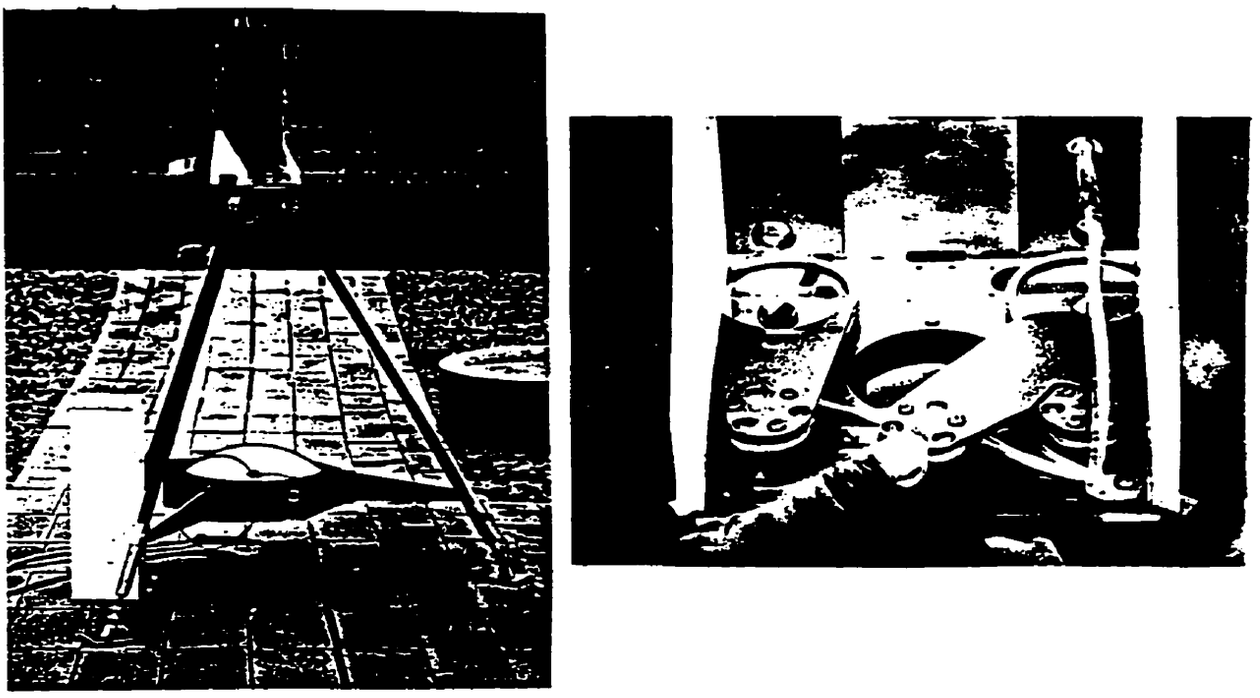

- **RCA Intensified Silicon-Intensifier Target (ISIT) all-sky TV camera.**
- **Frame rate options: - free running, 32 frames/second**
- **- programmable with PC controller and frame-grabber**
- **- time lapse with 0 - 32 frames/second**
- **Operational control: - ephemeris control for on-off times (>8° solar depression)**
- **- photocell protection**
- **Recording: Panasonic Time Lapse VCR on VHS tape**
- **shutter modes: - open**
- **- 558 nm filter**
- **- 630 nm filter**

Figure 2.2: A picture of the All-Sky Camera (left image) and a picture of shutter-filter assembly in the camera (right image). Technical parameters are shown at the bottom.

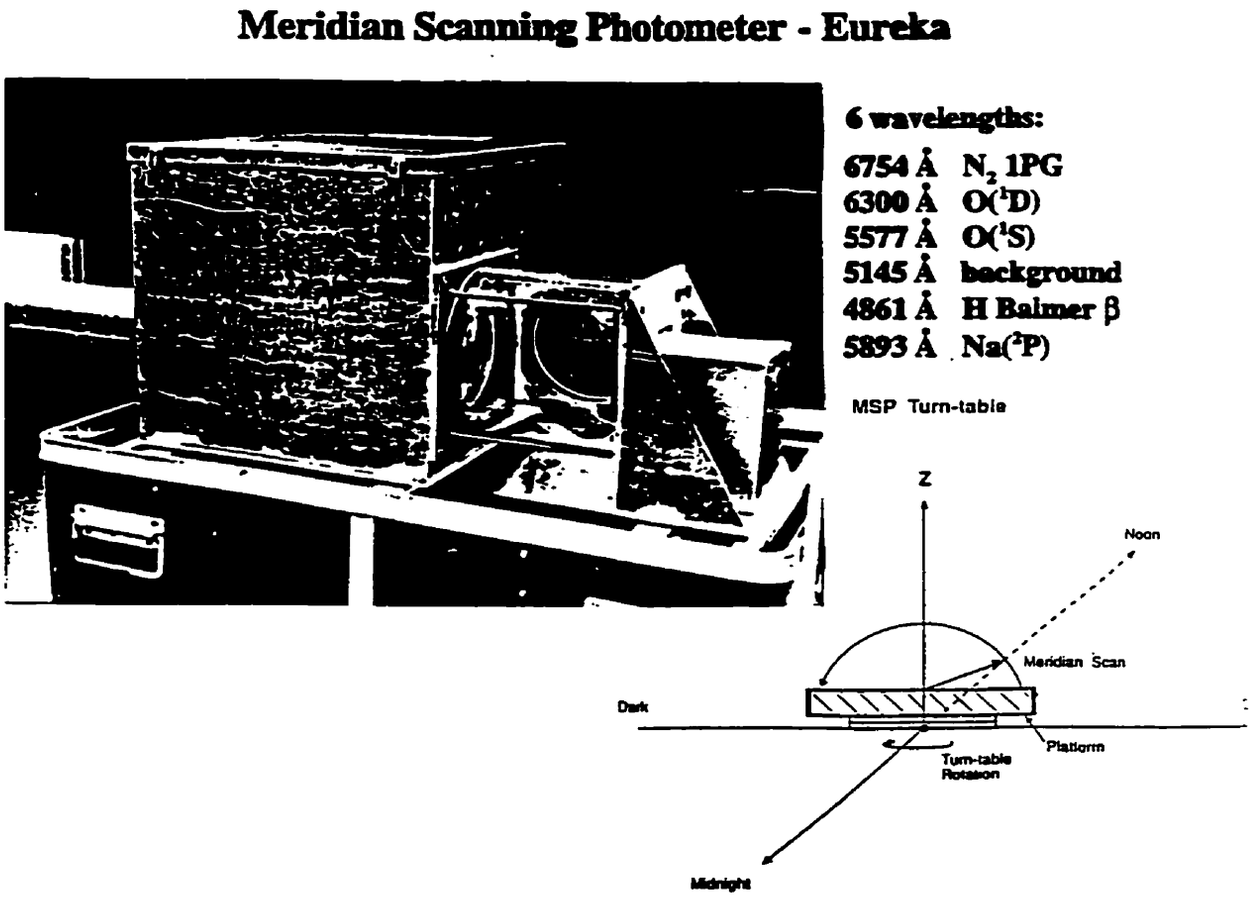

Figure 2.3: A picture of Meridian Scanning Photometer. Technical parameters are shown at the bottom.

ASC and the MSP respectively each full 24-hour day of operation. The instruments at Eureka were operated by participants of Project 3 of the Canadian Network for Space Research. The author went to Eureka to operate the instruments for two 1-month intervals during the 1993-94 and 1994-95 winter periods.

The ASC operating at Eureka recorded, on rare occasions, auroras at the poleward edges of the dayside or the nightside auroral oval. These observed auroras at the poleward edge of the dayside auroral oval were due to contraction of the auroral oval with a strong northward IMF. Those auroras at the poleward edge of the nightside auroral oval were due to poleward expansion during southward IMF and usually with a magnetic storm or substorm. These few auroras at the poleward edge of the auroral oval were excluded from the statistical study.

The MSP raw data (count rate) were processed to convert to intensities of emissions. All the MSP raw and processed data were stored in 8 mm tapes. IMP-8 solar wind speed, density and IMF data were provided by the National Aeronautical and Space Administration (NASA) National Space Science Data Center (NSSDC) at Greenbelt, Maryland. Ground magnetic field data from Eureka were provided by the University of Tokyo. K_p data were provided by the World Data Center at Boulder, Colorado. All the software for the ASC image and satellite data processing were written by the author.

Table 2.1: Periods of observation at Eureka

Winter	Start - end date	Numbers of days
1990 - 91	Dec. 11 - 19, 1990	9
	Jan. 6 - 25, 1991	20
1991 - 92	Oct. 15/91 - Mar. 9/92	146
1992 - 93	Oct. 30/92 - Feb. 23/93	117
1993 - 94	Oct. 18/93 - Mar. 27/94	161
1994 - 95	Oct. 17/94 - Mar. 14/95	149

Chapter 3

Statistical characteristics of polar arcs

3.1 Introduction

Ground-based observations at Eureka (89° N magnetic latitude), a location very close to the north magnetic pole, provide an unique opportunity for study of polar arcs. The entire field of view (174°) of the ASC is inside the polar cap at all local times under normal circumstances. The most recent statistical study of the polar arcs [Valladares *et al.*, 1994] is based on ASC (155° field of view) observations of the 630.0 nm emission from Qaanaaq during the local night time for one winter (1986-87). The statistical study of polar arcs here is based on ASC and MSP observations for 4 winters at Eureka. The location of Eureka allows the ASC to view all 24 hr local magnetic time sectors in the central polar cap. There were 656 polar arcs observed during the 4 winters from 1990 to 1994 and these polar arcs form the largest data set used for statistical studies of polar arcs so far. The data set provide a significant opportunity to examine the characteristics of the polar arcs. The physical characteristics of the polar arcs (occurrence, lifetimes, motions, etc) were studied. Their relations to IMF, solar wind and geomagnetic K_p index were also investigated. As the data set covered a period of 4 winters, from the 22nd solar cycle maximum (1990) to near minimum (1994), it was possible to study the effect of solar cycle on the occurrence of polar arcs.

3.1.1 Examples of observed polar arcs

One good example of a polar arc is shown here to illustrate the appearance of polar arcs. This is a polar arc (probably a transpolar arc [Zhang, *et al.*, 1994]) observed on November 15, 1993. Fig. 3.1 shows the images of the polar arc recorded by the ASC. The sunward direction is indicated by a small arrow at the edge of the images. The dawn sector is clockwise from the sunward direction. The geographic north is at the top of the images. The polar arc was detected from 0740 UT to 1257 UT by the ASC. The polar arc first appeared in the morning sector with a relatively low intensity at the lower-right corner near the horizon. It was sun-aligned as indicated in Fig. 3.1. The polar arc brightened around 0921 UT and began to move duskward. The polar arc expanded and moved dawnward after 0947 UT. A structure developed at one end of the arc (see images at 1026 UT and 1052 UT). A new polar arc appeared around 1117 UT near the zenith. Both the new arc and the polar arc (original) moved duskward after 1117 UT. Then the new arc faded and disappeared by 1148 UT. The polar arc moved to the zenith of the ASC and reached its maximum intensity around 1148 UT and continued its duskward motion thereafter. The polar arc finally disappeared in the dusk sector. The polar arc remained in a sun-aligned direction during its lifetime.

The MSP was mounted on a rotating table and arranged to scan in the dawn-dusk direction during the 1993-94 winter [McEwen, 1994]. Therefore, it scanned perpendicular to the polar arc observed on November 15, 1993 all the time. This provided a good opportunity to study the motion of the polar arc in the dawn-dusk direction with detail. Fig. 3.2 is a plot of the 4-minute averaged intensity (557.7 nm and 630.0 nm channels) of the polar arc along the dawn-dusk scans of the MSP from 0730 UT to 1400 UT. The plot shows the polar arc first appeared in the dawn sector with low intensity from 200 R to 500 R (557.7 nm). The polar arc moved duskward and then dawnward between 0730 and 0830 UT. This pattern of motion was repeated between 0830 UT and 1000 UT. The intensity of the polar arc increased gradually and reached 4 kR (557.7 nm) around 0950 UT. The intensity decreased after 1000 UT and and a new arc

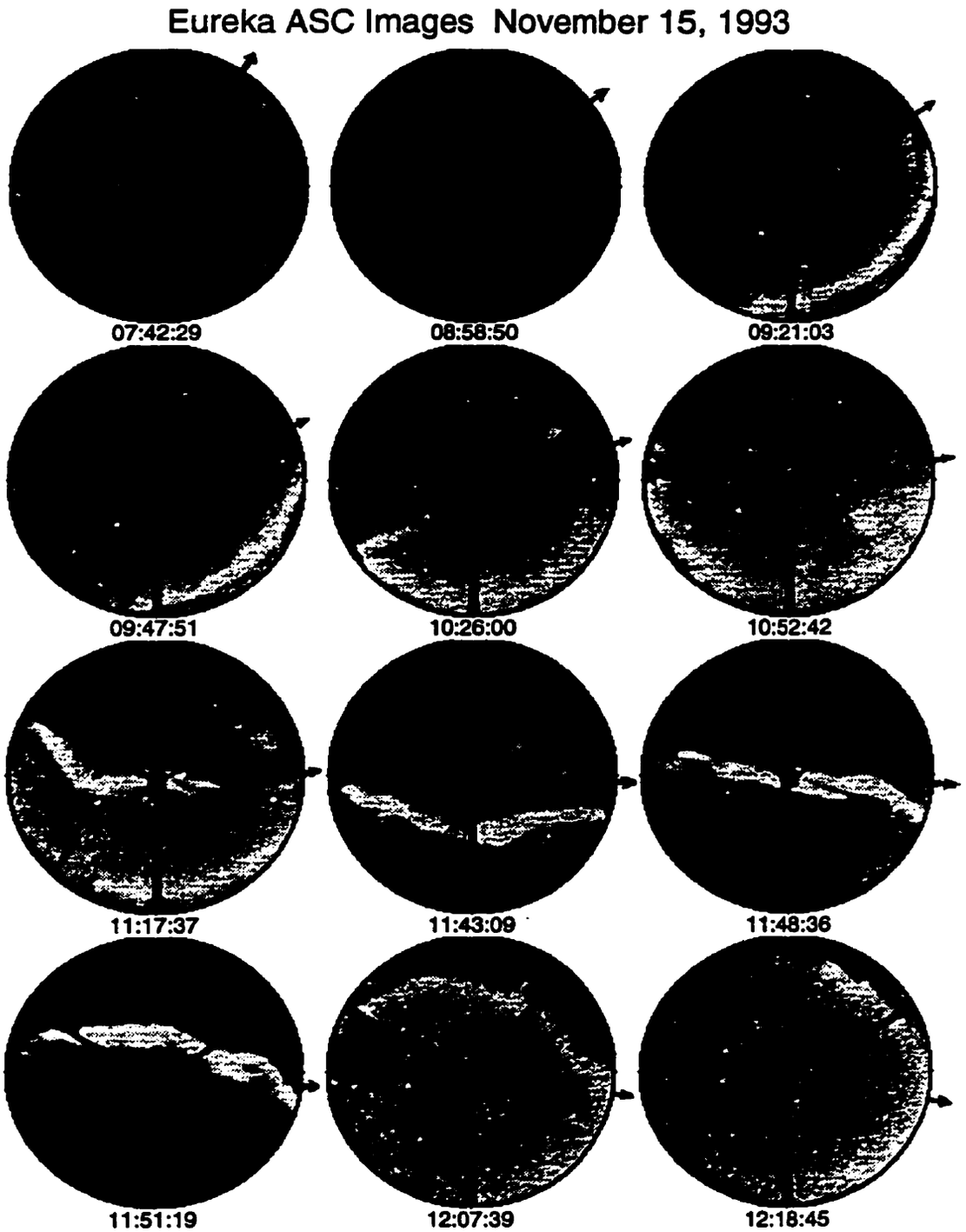

Figure 3.1: A selected sequence of ASC images of a transpolar arc from 0742 UT to 1218 UT on November 15, 1993. The geographic north direction is at the top of these images. The sunward direction is indicated by a small arrow at the edge of the images. The dawn sector is clockwise from the sunward direction.

appeared around 1100 UT. Both the polar arc and the new arc moved duskward after 1100 UT and their intensity increased quickly. The new arc disappeared or merged with the polar arc around 1150 UT. The polar arc continued its duskward motion after it reached its maximum intensity around 1200 UT. The intensity of the polar arc decreased quickly to about 1 kR (557.7 nm). Overall, the intensity of the polar arc changed each 4-minute averaged scan. The polar arc finally disappeared in the dusk sector.

Both the ASC images and the MSP scans show some characteristics of polar arcs, such as motion in dawn-dusk direction, changing of intensity and multiple arcs.

3.1.2 Observability of polar arcs

Observability of polar arcs depends on the sensitivity of the instrument used. Polar arcs with intensity below about 300 R of 557.7 nm can not be detected by the ASC. The MSP operated at a higher sensitivity threshold (50 R at 557.7 nm) [McEwen, 1994]. Due to the dawn-dusk MSP scans, the MSP was able to detect sun-aligned arcs at any local time, just as the ASC. Fig. 3.2 (plot at 557.7 nm) shows that in addition to the transpolar arc described in the last subsection, there are many short lived polar arcs which have lifetimes around or less than 4 minutes and low intensity down to 100 R. The plot at 630.0 nm of Fig. 3.2 shows more weak polar auroras with intensity down to 50 R. Such weak polar auroras could not be detected by the ASC (see Fig. 3.1). Intensities of polar arcs cover a wide range from R to kR (557.7 nm). Therefore, the MSP detects more polar arcs and for longer periods than the ASC due to their difference of sensitivity threshold.

3.2 Occurrence of polar arcs - ASC observations

Observations of polar arcs at Eureka by the ASC and the MSP were continued for five winters (see table 2.1 for detailed periods of operation for each of the winters). There were 656 polar arcs recorded by the ASC during the first four winter periods and these were the bases for the statistical study. There was only a preliminary analysis of the

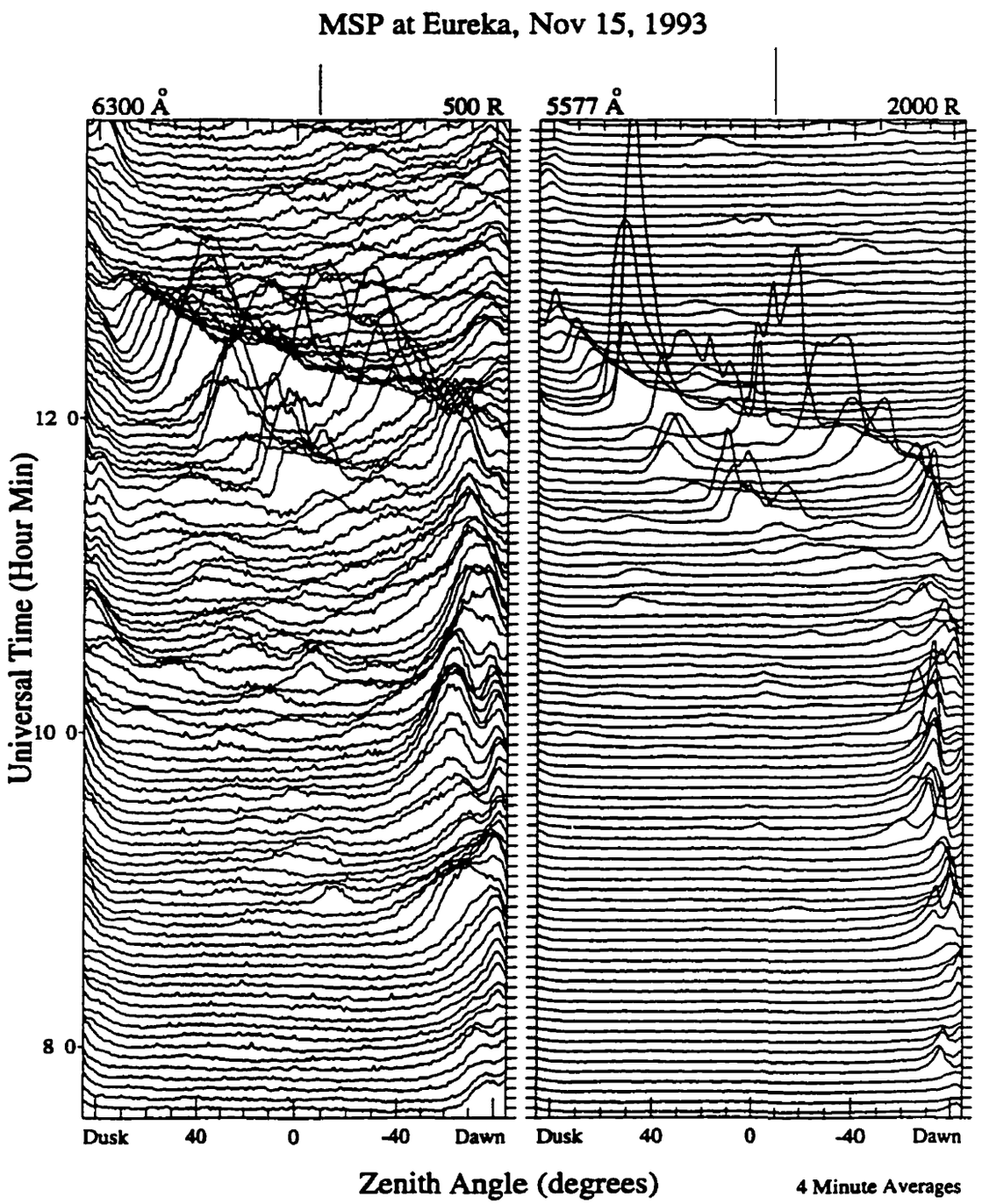

Figure 3.2: Intensity of 557.7 nm and 630.0 nm emissions along the dawn-dusk scans of the MSP on November 15, 1993 with a 4 min average. The lowest intensity of the detected auroral emissions at 557.7 nm is about 50 R. The highest intensity is 20 kR (557.7 nm). The vertical lines at the top of the diagrams indicate the intensity scales: 500 R for 630.0 nm and 2000 R for 557.7 nm.

data for the 5th winter.

Occurrence of polar arcs was first studied based on investigation of images of these polar arcs. In order to determine occurrence patterns of polar arcs, all observed ASC image data were binned into 15 minute time intervals each day (24 hours). Occurrence of polar arcs during each 15-min time bin (interval) was obtained by taking the total auroral events in each 15-min time bin divided by total operation time with clear sky in that 15-min time bin. As the ASC has a threshold of sensitivity of 300 R (557.7nm), the occurrence based on the ASC images applies to only those polar arcs with intensity above 300 R (557.7nm). The following subsections show the polar arc occurrence patterns for each of the winters.

3.2.1 1990-91 winter

The first winter of polar arc observation at Eureka was 1990-91. A campaign covering two dark-moon periods was conducted with operators in attendance. The field site was operated from Dec. 11, 1990 to Dec. 19, 1990 and from Jan. 06, 1991 to Jan. 25, 1991. It covered a period of 29 days. During that period, 72 polar arcs were recorded by the ASC. The occurrence of polar arcs (the percentage of time with recorded polar arcs) was calculated based on investigation of the 72 polar arcs. Fig. 3.3a shows a distribution of the occurrence of polar arcs by universal time (UT) for that winter period. The occurrence between 0500 UT and 1300 UT appears higher than that of other UT regions. Polar arcs were observed 8.6 % of time by the ASC during the 1990-91 winter. That is, auroral arcs were detectable in the ASC tapes 8.6 % of the dark hours when skies were clear. The field of view of the ASC covered most of the region above 80° of magnetic latitude. This included all of the central polar cap. Therefore, auroral arcs with intensity larger than 300 R (557.7 nm) were detected about 8.6 % of the time on average in the central polar cap for the first winter period.

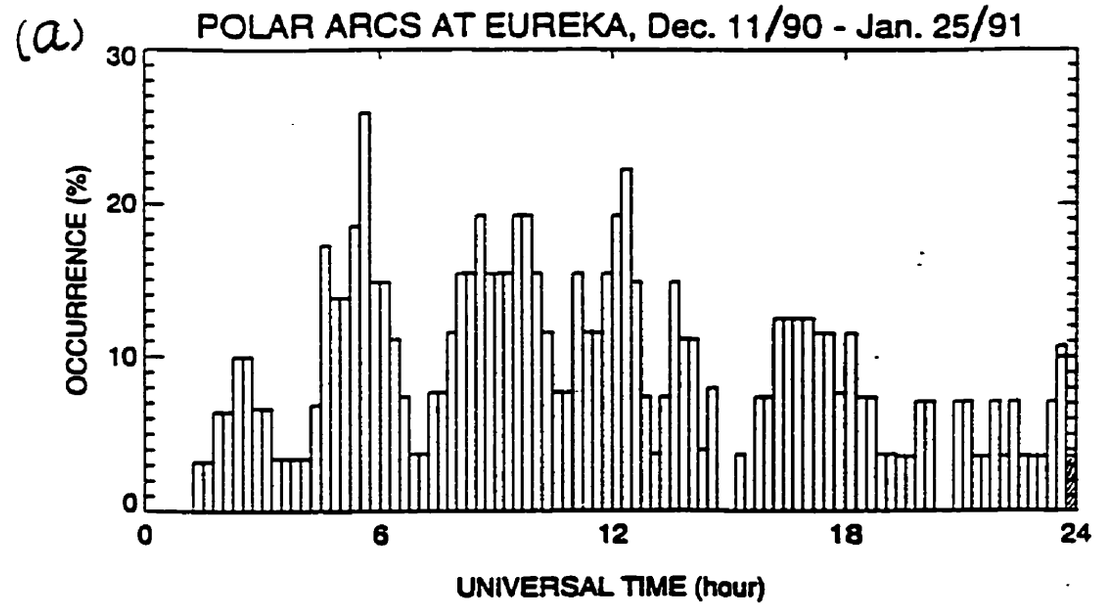

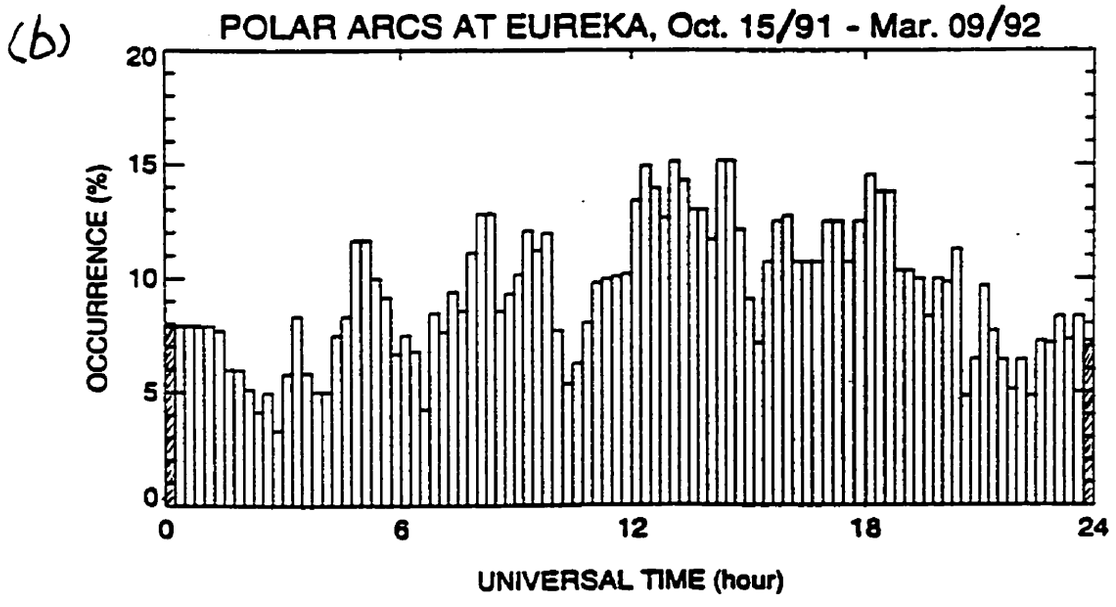

Figure 3.3: Occurrence of polar arcs observed during (a) 1990-91 winter period, (b) 1991-92 winter period.

3.2.2 1991-92 winter

Observations of polar arcs at Eureka were continued during the 1991-92 winter (the second winter). The instruments were operated automatically during this winter and the following winters . The observations covered 5 months (146 days) from October 15, 1991 to March 9, 1992. The ASC detected 218 polar arcs during this winter. Fig. 3.3b is a plot of the occurrence distribution of polar arcs for the 1991-92 winter. It indicates that the occurrence distribution is relatively uniform over 24 hour UT, except the slightly higher level of the occurrence between 1200 UT and 1800 UT. As the duration of observations in this winter was five times that of the 1990-91 winter, more polar arcs were observed and there is a smoother distribution. Polar arcs were observed on average 9.3 % of the time during the 1991-92 winter.

3.2.3 1992-93 winter

Observations of polar arcs in the third winter (1992-93 winter) started on October 30, 1992 and ended on February 23, 1993. The observations were continued for 117 days. The ASC detected 143 polar arcs. Fig. 3.4a shows a plot of polar arc occurrence distribution by Universal Time for this winter. The occurrence distribution appears to have a strong UT dependence. The occurrence between 0200 UT and 1200 UT is much higher than that between 1600 UT and 2000 UT. The average occurrence of polar arcs for the 1992-93 winter was 7.6 % of the time. This is somewhat lower than that of previous winter.

3.2.4 1993-94 winter

Observations of polar arcs in the fourth winter started on October 18, 1993 and ended on March 27, 1994. They covered a period of 161 days, which was the longest period among the first 4 winters, and 223 polar arcs were observed. Fig. 3.4b shows the occurrence distribution of polar arcs for the 1993-94 winter. The occurrence distribution appears to have a UT variation. The maximum of the occurrence distribution locates around 1000 UT. Polar arcs in the 1993-94 winter occurred, on average, 6.5 % of the time, which is significantly less than the first 3 winters.

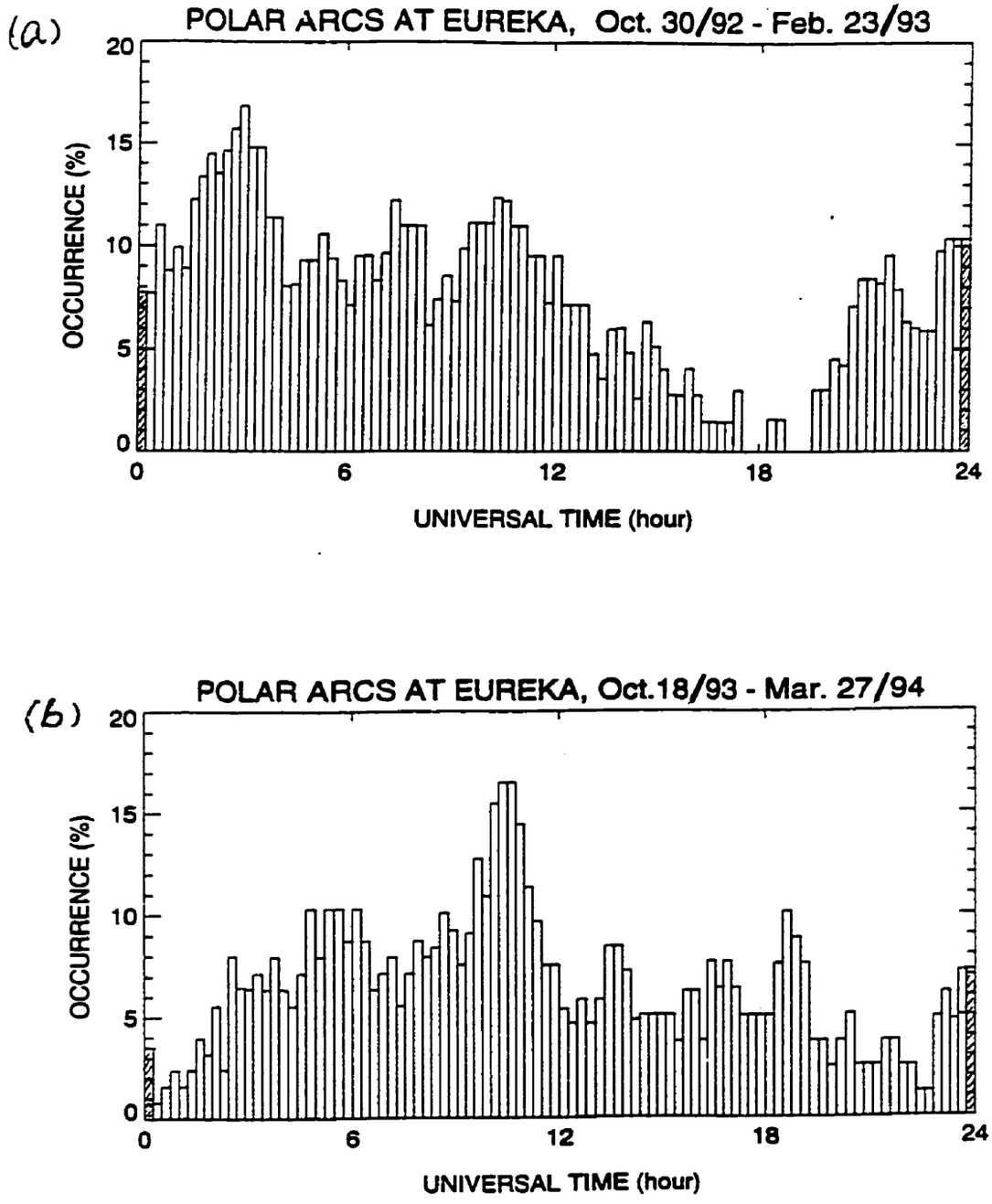

Figure 3.4: Occurrence of polar arcs observed during (a) 1992-93 winter period, (b) 1993-94 winter period.

Polar arcs observation at Eureka was continued in the 1994-95 winter, from October 17, 1994 to March 14, 1995. A preliminary review of polar arcs observed in this winter indicates the average occurrence of polar arcs was around 6 % of the time. This is the lowest occurrence among that of the five winters.

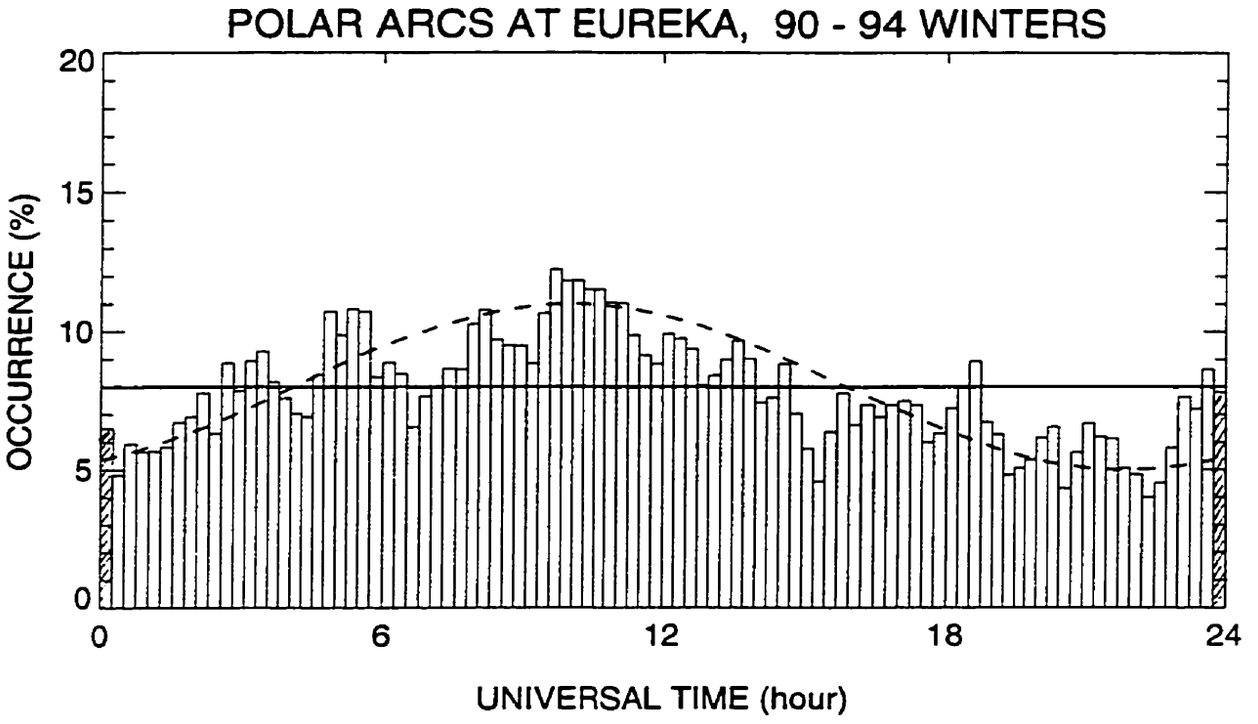

Figure 3.5: Occurrence of polar arcs observed over 4 winters from 1990 to 1994.

3.2.5 Average over 1990 - 1994 winters

All 4 winters of observations were combined to show the average occurrence pattern of polar arcs. Fig. 3.5 shows this distribution for the four winters from 1990 to 1994. Polar arcs were present, on average, 8 % of the time over the four winter period. Fig. 3.5 also indicates that the occurrence of polar arcs was higher between 0300UT and 1400UT than between 1400UT and 0300 UT. The maximum and minimum occurrences

were observed around 1000 UT and 2200 UT respectively. This occurrence distribution is best seen from the fitted dashed line curve in Fig. 3.5. This diurnal variation of the occurrence has an amplitude of 37 % of the mean occurrence rate. Over all, the occurrence is fairly evenly distributed during the 24 hour period. Because Eureka is very close to the the north magnetic pole and the ASC can view all 24 hours of local (or magnetic) time, then it is natural that the polar arc occurrence distribution is continuous. Note that the occurrence pattern shown here is based on the ASC images and is valid only for polar arcs with intensity over 300 R (557.7 nm).

3.3 Comparision between the ASC and the MSP observations

The sensitivity of the MSP for detection of aurora (threshold of 50 R at 557.7 nm) is higher than that of the ASC (threshold of 300 R at 557.7 nm). In order to find the difference between the ASC and the MSP observations of polar arcs, 38 days with clear skies (no clouds, no ice crystals, no moon, and no twilights) were selected for investigation from the 1993-94 winter period. Because the MSP scanning was arranged from the dawn to the dusk during the 1993-94 winter period, then the MSP was able to detect all sun-aligned arcs in the central polar cap region with intensity above the MSP threshold. The percentage of the time with polar arcs were observed for each of the 38 days was obtained from the analysis of the data from the ASC and the MSP 557.7 nm and 630.0 nm channels. Only discrete emission structures on the MSP scans were identified as polar arcs. Fig. 3.6 is a plot of the percentages of the time arcs were observed through two channels (green and red) of the MSP and and one channel (green) of the ASC for each of the 38 days. The diagram shows all three plots (solid line: MSP 630.0 nm channel, dotted line: MSP 557.7 nm channel and dashed line: the ASC). They followed a similar pattern of variation during the selected 38 days. The similarity among them suggests that they are proportional to each other generally. There were some cases of arcs detected in the MSP green channel which were below the level of detection on the MSP red channel. More frequently, arcs were detected in the MSP red channel and they lasted longer than those detected in the green channel.

The average percentages of the time (or occurrences of polar arcs on average) with observed polar arcs for the 38 days by the ASC, the MSP scans at channels of 557.7 nm and 630.0 nm are 8 %, 30 % and 49 % respectively. This indicates that there are about 4 times as many polar arcs with intensity above 50 R (557.7 nm) than there are polar arcs with intensity over 300 R (557.7 nm). This implies that more polar arcs or polar arcs with longer lifetimes will be observed by instruments with higher sensitivities. Therefore, polar arcs occur at least 30 % (557.7 nm) of the time or 49 % of the time (630.0 nm) above threshold of 50 R. A significant point here is that many polar arcs are seen better from the red line emission than from green line emission. This will be discussed in relation to the energy of precipitated electrons in Chapter 6.

3.4 Lifetimes and development of polar arcs

The distribution of lifetimes of the 656 polar arcs from the ASC was determined. The lifetimes are defined as the time interval between appearance and disappearance of the polar arcs as seen within the field of view of the ASC. The vast majority of the arcs observed in the ASC images did originate and disappear well within the field of view. This field, for an assumed auroral emission height of 150 km, extended 9° of latitude from Eureka. Fig. 3.7a is a distribution of the observed polar arcs according to their lifetimes. Lifetimes of the polar arcs are usually from a few minutes to a few hours. The shortest lifetime of the polar arcs observed at Eureka was two minutes. The longest lifetime (observed on November 15, 1993) was about 10 hours, and it is not included in Fig. 3.7a. The distribution quickly decreased for polar arcs with lifetimes longer than 40 minutes. As shown by Fig. 3.7a, over 50 % of the observed polar arcs have lifetimes less than 20 minutes. Due to this fact, a more detailed lifetime distribution between 1 and 30 minutes is shown in Fig. 3.7b. It indicates that the observed polar arcs were distributed mainly between 3 min and 20 min of lifetime.

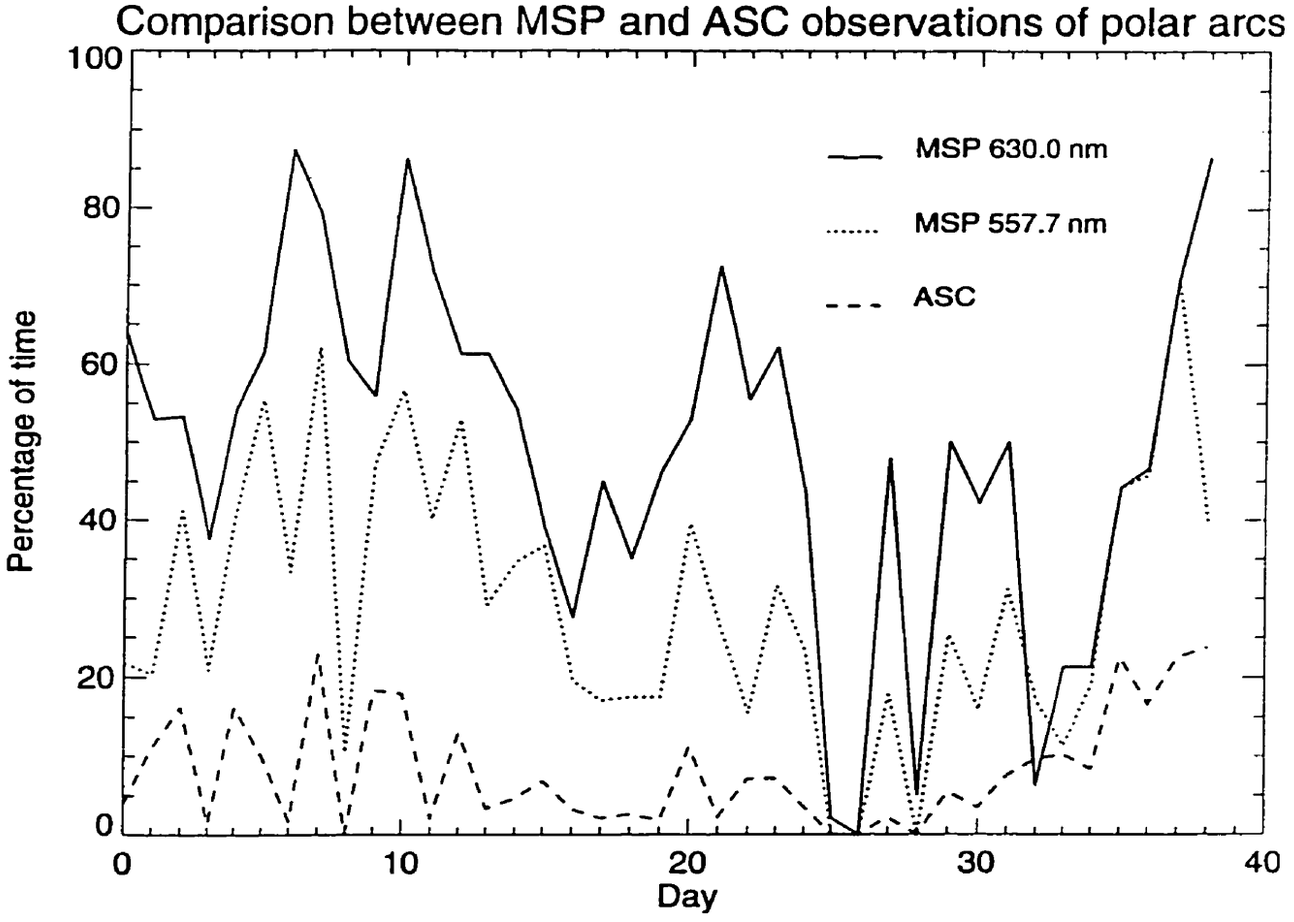

Figure 3.6: Plots of percentage of time with polar arcs observed each day by the ASC (dashed line), the MSP 630.0 nm channel (solid line) and the MSP 557.7 nm channel (dotted line) for the selected 38 days in the 1993-94 winter period.

3.5 Motion, shape and bifurcation of polar arcs

Generally speaking, polar arcs moved mainly either duskward or dawnward. In order to study these differing motions of polar arcs, the polar arcs observed in the 1990-93 winter periods were divided into two groups - dusk sector and dawn sector. Fig. 3.8a shows the direction of motion of polar arcs observed in the dusk sector with respect to the sun-aligned direction. Positive angle implies velocity of the motion has a dawnward component and the negative angle shows the motion has a duskward component. The distribution indicates that most of polar arcs in the dusk sector

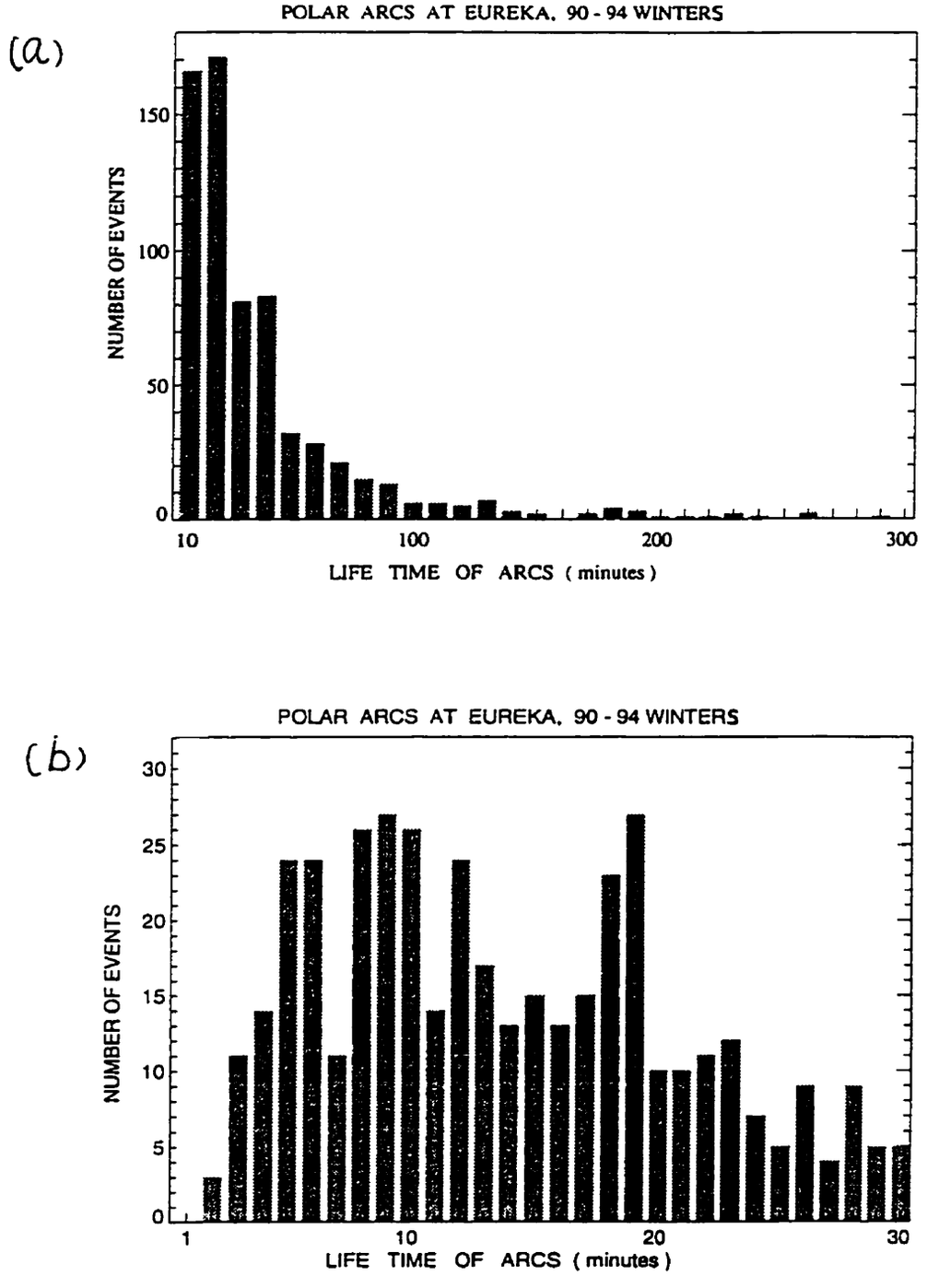

Figure 3.7: (a) The lifetime distribution of polar arcs observed by ASC during the 4 winters (1990-1994). (b) The lifetime distribution detailed between 1 and 30 minutes.

moved either in the duskward direction or dawnward direction. The polar arcs moving duskward (or equatorward direction) are twice as numerous as those moving dawnward. Only a few of the polar arcs moved in other than dawn-dusk directions. Fig. 3.8b shows that the polar arcs observed in the dawn sector also moved mainly in either dawnward or duskward directions. This is the same as that of those polar arcs observed in the dusk sector. However, the polar arcs observed in the dawn sector had almost the same probability of moving either dawnward or duskward. The distribution also indicates that the polar arcs in the dawn sector can move in virtually any direction, though the occurrence rate of polar arcs which moved in directions other than the dawn-dusk direction is not significant. This suggests that the polar arcs are predominantly sun-aligned with a few cases of non sun-aligned polar arcs as only motion perpendicular to the polar arcs could be detected from the ASC images. The motion in the dawn-dusk direction is considered to be controlled by the IMF B_y component [Valladares *et al.*, 1994]. Speed of the motions varied from tens of meters per second to up to 1 km/s.

Polar arcs also changed their shape in addition to their motion in the dawn-dusk direction. While polar arcs are usually in a straight line, they are also often observed with wave structures as illustrated in Fig. 3.9. The diagram shows that a polar arc first appear as a straight and thin arc around 1930 UT. The arc began to take a bow shape (half wave) about 75 minutes later. The arc then developed into a S-shaped (one full wave) arc within 5 minutes. Finally the arc took a shape of wave (multi-S) form around 2103 UT.

Multiple arcs, bifurcation of a single arc, merging of double arcs and other special features, such as approximated the shape of the letters C, E, V, S and H were also observed. Fig. 3.10 and 3.11 show a polar arc appeared as a C and then changed to E and finally took a straight line shape. Those shapes of polar arcs other than a straight line indicate a special configuration structure in the magnetosphere.

An example of bifurcation of a single polar arc is shown in Figure 3.12, which is a selected sequence of the ASC images of a strong polar arc observed on November 1, 1991 from 0439 UT to 0451 UT (just the first 12 minutes of the lifetime of the arc). The polar arc appeared around 0439 UT as a thin sun-aligned arc. Both the width and intensity of the arc increased quickly with time and the single polar arc split into two

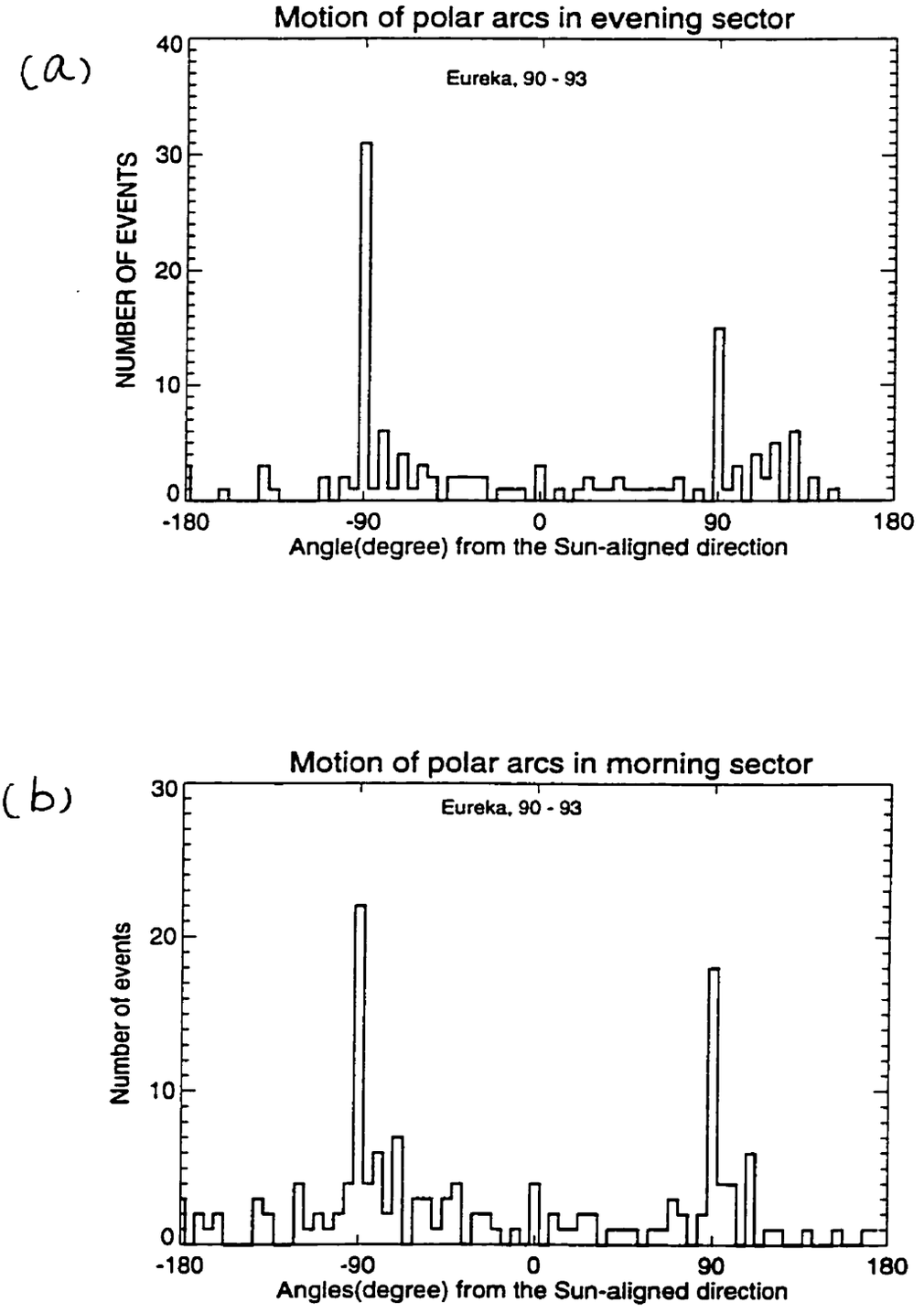

Figure 3.8: The distribution of directions of motion of polar arcs observed in (a) the dusk sector (127 arcs) and (b) the dawn sector (131 arcs) from 1990-93 winter periods.

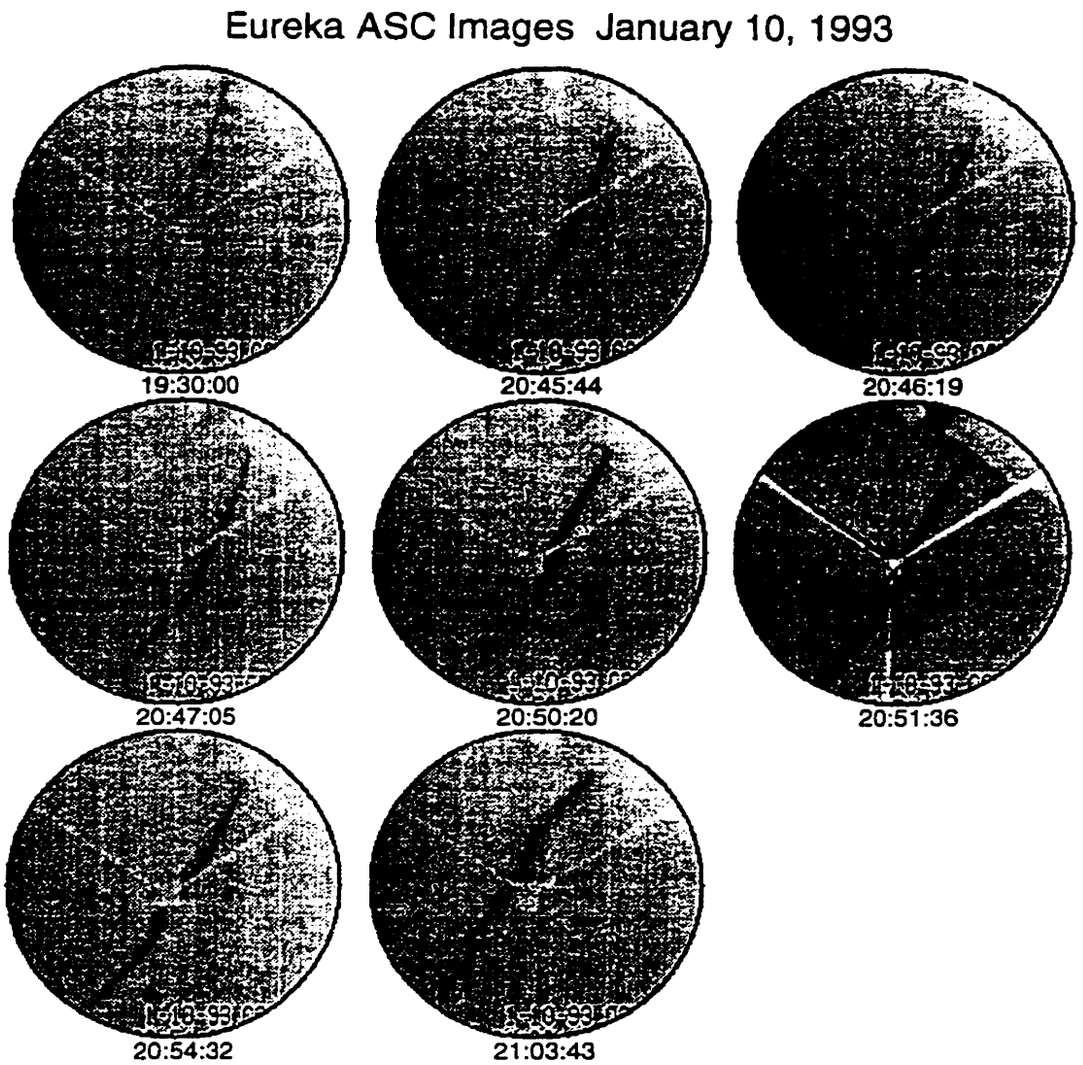

Figure 3.9: A sequence of the ASC images of a polar arc observed on January 10, 1993. The first image was taken at 19:03:00 UT and the last image at 21:03:43 UT. All the images were taken with green (557.7 nm) filter except the image at 20:51:36 UT which was taken without any filter. The sequence of images shows how a thin and straight polar arc developed to take a half wave form, a single wave form (S shape) and wave form (multi-S shape).

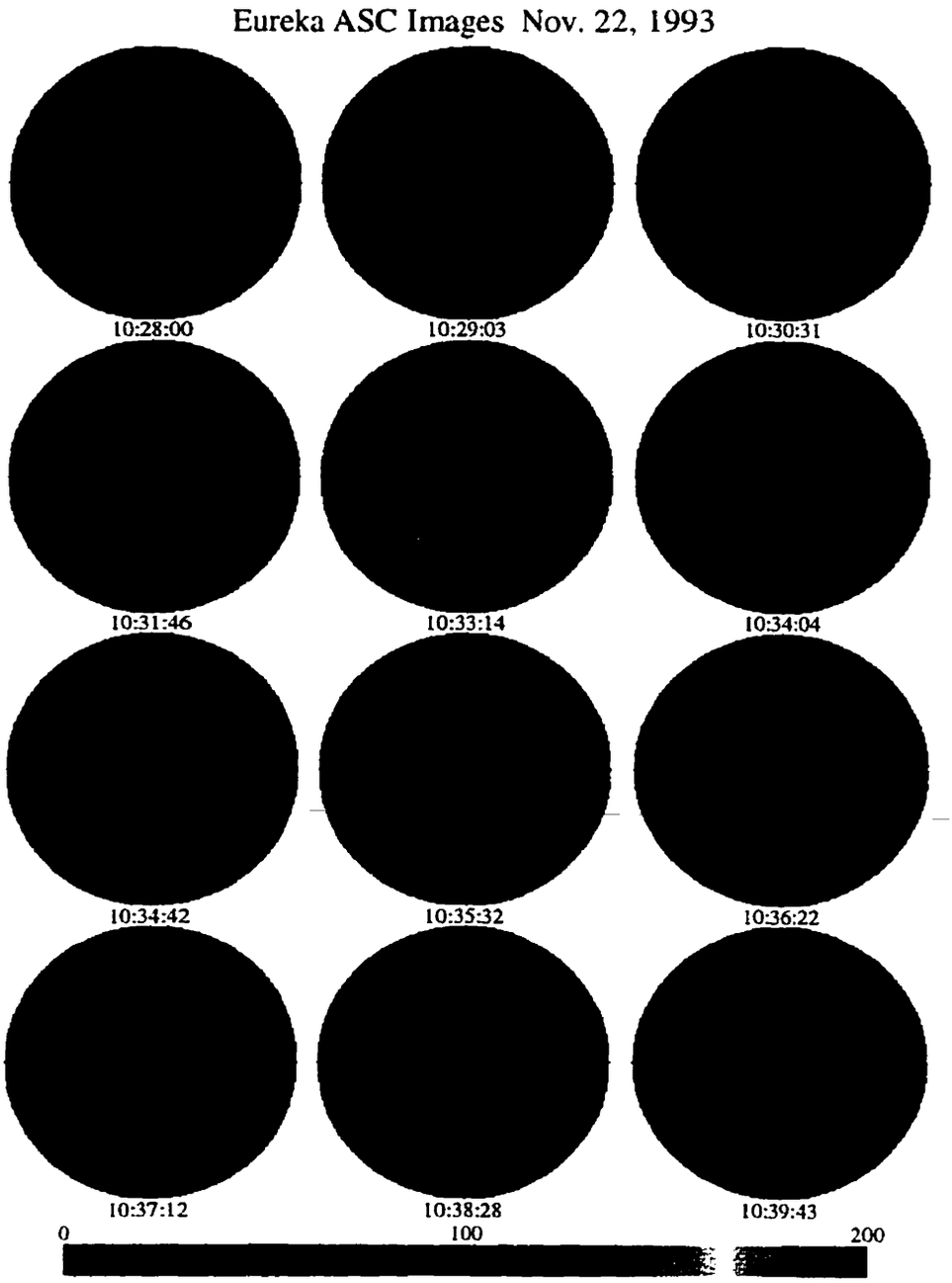

Figure 3.10: A selected sequence of the ASC images observed on Nov. 22, 1993 from 10:28:00 UT to 10:39:43 UT. The first 5 images from 10:28:00 UT to 10:33:14 UT show the formation of a polar arc which approximates the shape of the letter C. The remaining images indicate how the arc changed to E shape.

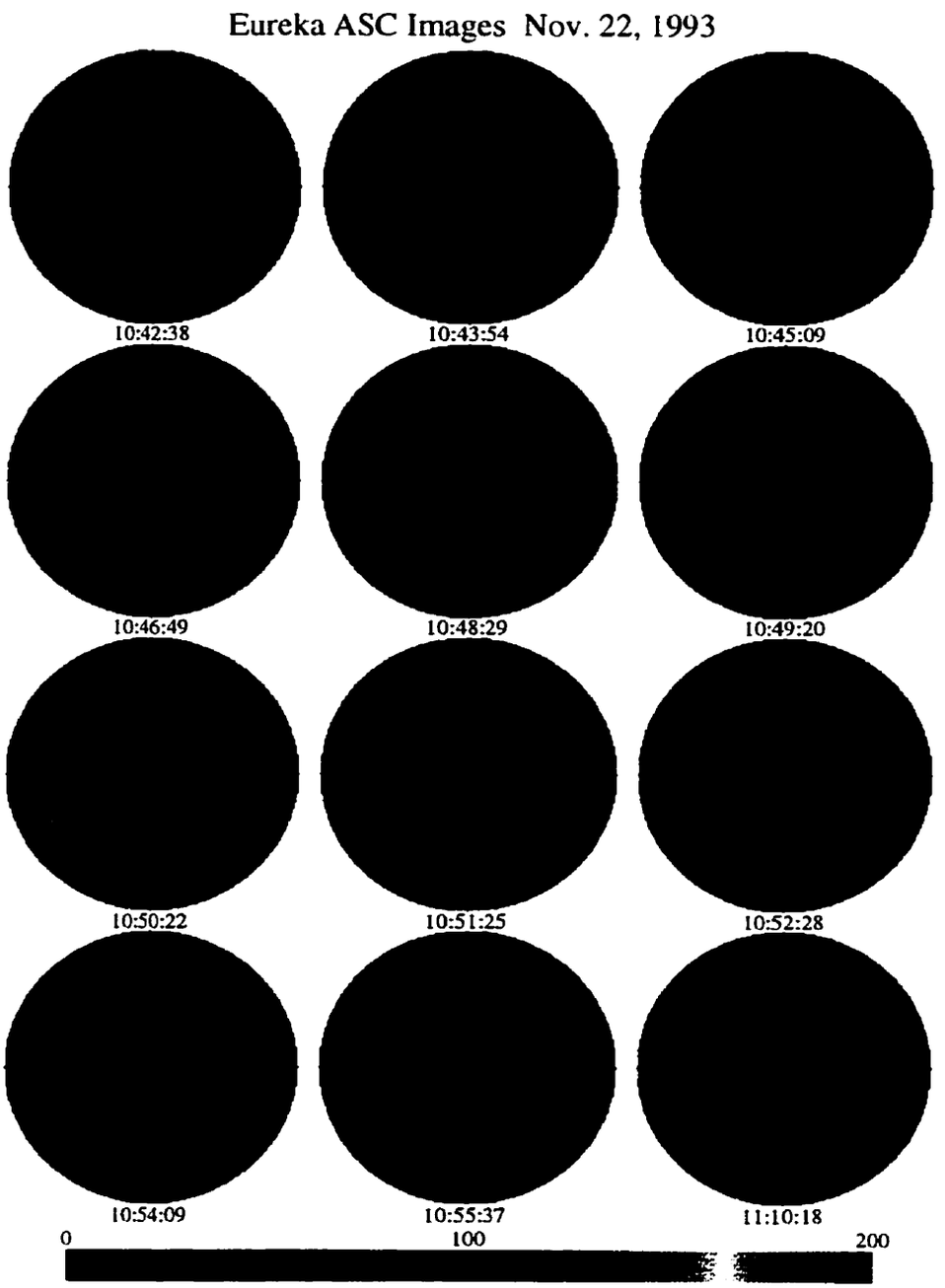

Figure 3.11: A sequence of the images following the images shown in last Figure. The sequence is from 10:42:38 UT to 11:10:18 UT. It shows how the E shaped arc gradually changed to a sun-aligned arc.

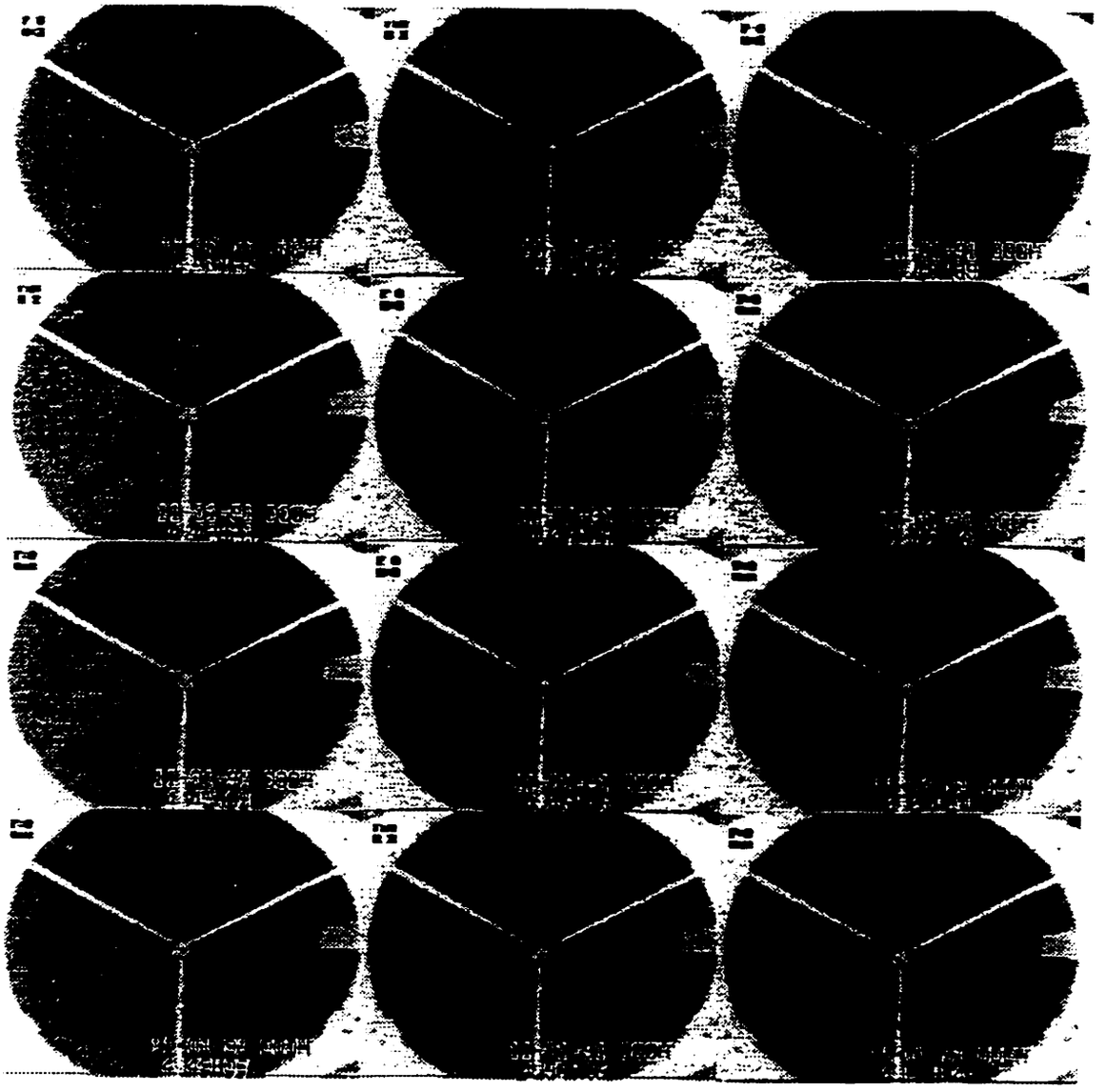

Figure 3.12: A sequence of ASC images of a polar arc observed on November 1, 1991 from 0439 UT to 0451 UT, taken at about one minute intervals. The arc first appeared as a thin weak arc around 0439 UT and then it brightened and bifurcated around 0441 UT.

arcs at 0441 UT just two minutes after its first appearance. One segment of the double arc (the short one) faded within one and half minutes. The intensity of the remaining arc kept increasing and reached 10 kR (557.7 nm) at 0445 UT. This example indicates that bifurcation occurred when the single polar arc brightened and it was a transient phenomenon. During the period of the arc, the IMF B_z quickly dropped from 20 nT at 0400 UT to 0 nT at 0530 UT and the IMF B_y stayed above 20 nT with a quick change between 0400 UT and 0500 UT.

Another example of polar arc bifurcation is shown in Figure 3.13, which is a selected sequence of the ASC images from 2040 UT to 2053 UT on November 9, 1992. The polar arc appeared at 2039 UT and disappeared at 2100 UT. The polar arc began to to brighten around 2042 UT. About 3 minutes later, around 2045 UT, the arc split when it reached maximum intensity. Multiple polar arcs were formed around 2046 UT. These multiple polar arcs decayed into a pair of parallel polar arcs around 2048 UT. This example further suggests that bifurcation occurs only when a single polar arc brightens. The IMF B_z changed quickly from 18 nT at 2040 UT to 0 nT at 2100 UT. IMF B_y changed quickly from 8 nT at 2035 UT to 18 nT at 2045 UT. These abrupt changes in the IMF occurred very shortly before the arc brightening and bifurcation. Whether the two events were related is uncertain.

3.6 Polar arcs and K_p index

The relation between polar arcs and K_p levels was studied based on the 4 winter data sets (656 polar arcs). K_p is a measure of the level of global magnetic activity, and those data are available continuously while solar wind data are intermittent. In order to see possible solar cycle effects, the relation between polar arcs and K_p level was examined for each winter from 1990 to 1994.

Fig. 3.14 shows the number distributions of polar arcs against K_p level for each of the four winters from 1990-91 to 1993-94. These figures show very similar distributions. The peaks of the distributions are at K_p level of 1, 3, 2 and 2 from the winter 90-91 to winter 93-94 respectively. These indicate that polar arcs occurred predominately with middle or middle-low K_p level. Polar arcs were also observed at extremely low

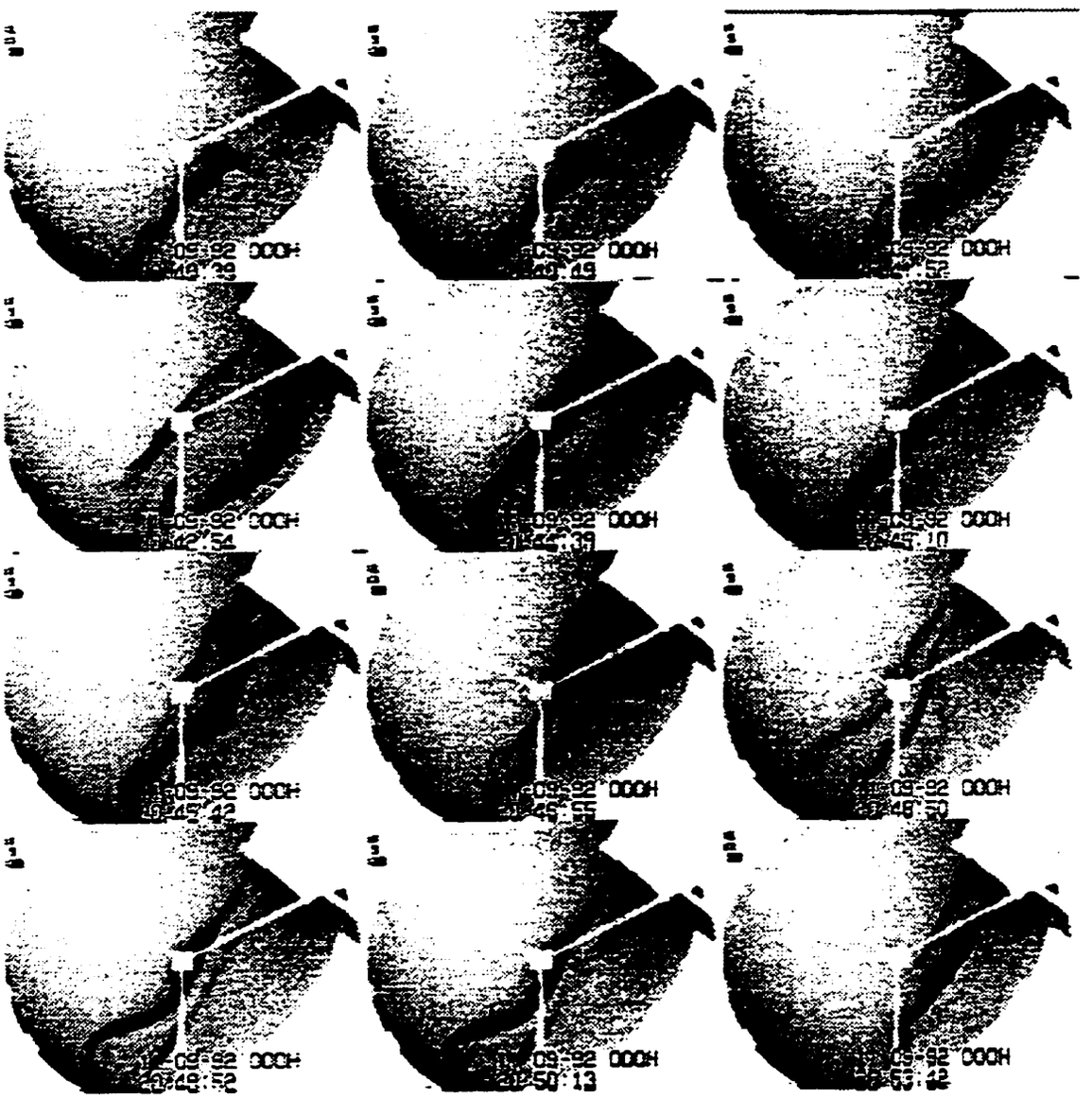

Figure 3.13: A sequence of the ASC images of a polar arc observed on November 9, 1992 from 2040 UT to 2053 UT. The arc extended from dayside to the nightside and moved duskward before 2042 UT. It moved dawnward after 2042 UT and brightened when it reached the zenith of the ASC. Bifurcation began around 2044 UT and multiple polar arcs formed around 2047 UT due to the development of the bifurcation. These multiple polar arcs finally decayed into two arcs with a wave structure.

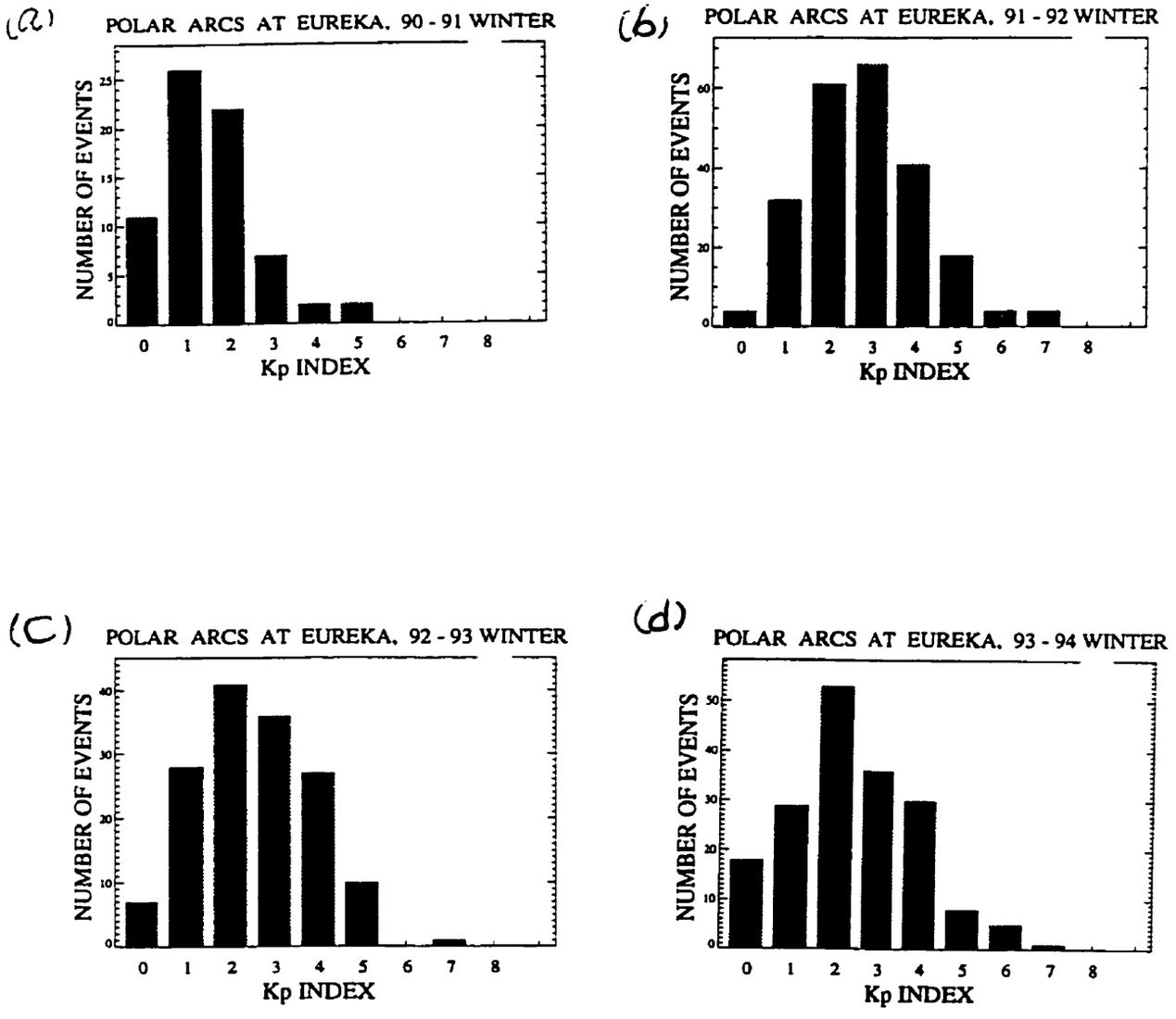

Figure 3.14: Polar arc number distribution by K_p level: (a) 1990-91 winter, (b) 91-92 winter, (c) 92-93 winter and (d) 93-94 winter.

magnetic activity ($K_p = 0$) and very disturbed magnetic conditions ($K_p = 7$). It was not possible to draw a conclusion from these distributions of polar arcs by K_p level because the distribution of K_p level itself is not uniform. Fig. 3.15a shows the distribution of K_p level itself for the 1990 to 1992 winters. The peak of the distribution is at $K_p = 2$. In order to make a comparison between the polar arc distribution and the K_p distribution, the polar arc distributions for the 4 winters shown in Fig. 3.14 were combined and plotted in Fig. 3.15b. It shows the peak of the distribution is at $K_p = 2$, which is the same as that of the K_p distribution. Overall, both distributions are very similar to each other. The normalized polar arc distribution (Fig. 3.15b by Fig. 3.15a) is relatively uniform. This suggests that (a) polar arcs occur independently of the level of K_p, or (b) both polar arcs and K_p levels are similarly influenced by solar activity.

3.7 Polar arcs and IMF orientation

The orientation of the interplanetary magnetic field affects the configuration of the magnetosphere and the coupling between the solar wind and the magnetosphere. Therefore, the orientation of the IMF must influence the occurrence of polar arcs. The following subsections investigate how polar arcs are related to IMF B_x, B_y and B_z. IMF data which were collected by the Interplanetary Magnetic Field Probe (IMP-8) satellite were available during the lifetimes of only 208 of the 656 polar arcs observed. The following analysis is based on those 208 polar arcs.

3.7.1 Effect of IMF B_x

The IMF B_x is the component along the sunward direction. Fig. 3.16a is a plot of polar arc occurrences as a function of IMF B_x from -20 nT to 20 nT. The dashed line is a fitted curve of the distribution by using a least-square polynomial fit although the distribution does have three peaks at $B_x = -5, 0$ and 5 nT. The largest peak is locates at $B_x = 0$. The distribution is symmetric around $B_x = 0$ nT. Forty percent of the polar arcs occurred with negative IMF B_x, 12.5 % with IMF $B_x = 0$ and 47.5 % with positive IMF B_x. In order to find the relation between polar arcs and IMF B_x

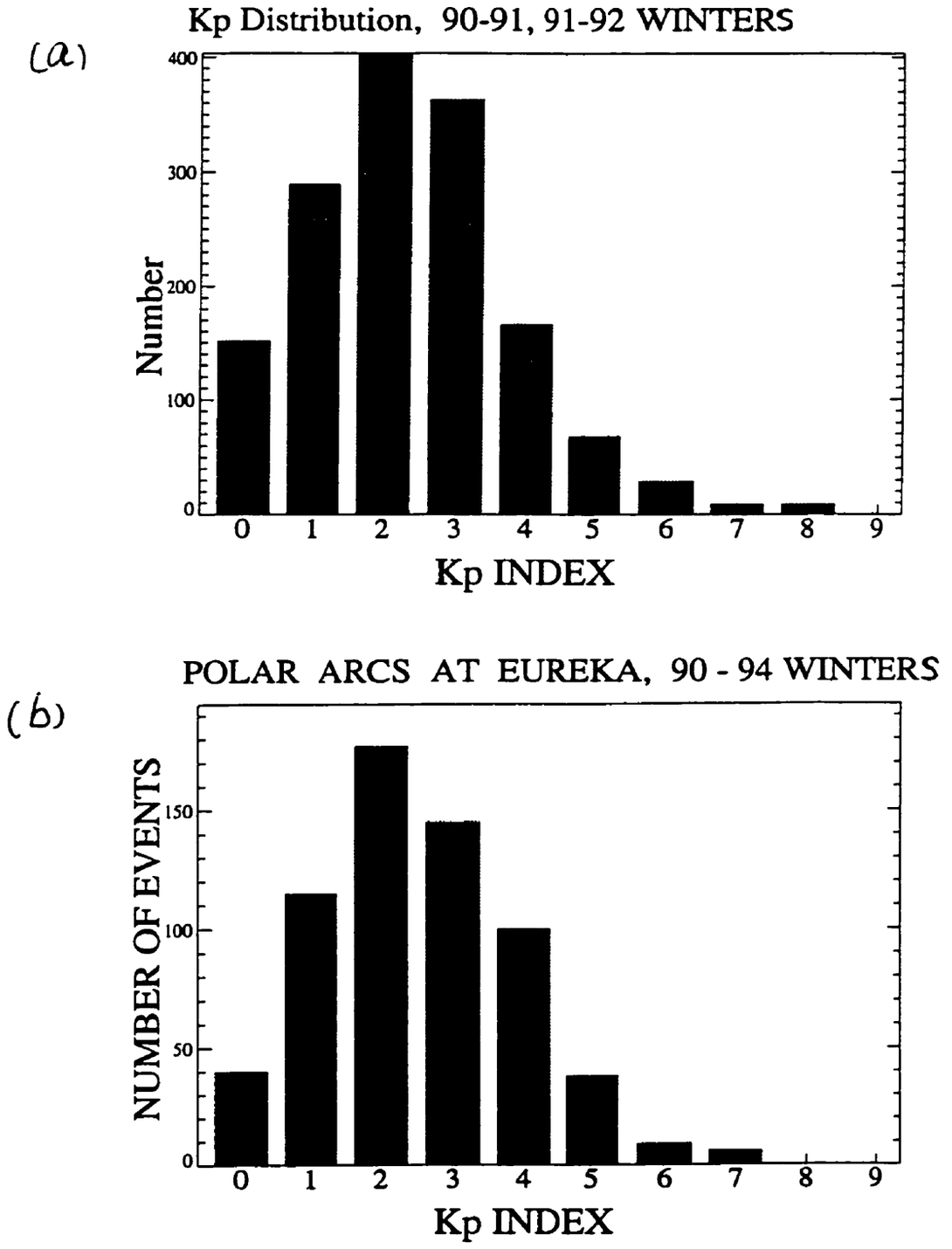

Figure 3.15: (a) The distribution of K_p level itself. (b) The polar arc distribution by K_p level for the 4 winters (1990-94).

component, it is necessary to investigate the distribution of IMF B_x itself. Fig. 3.16b shows a distribution of numbers of minutes when an All-sky Image Photometer (ASIP) was on during a period of 1986-87 winter as a function of B_x (after Valladares et al, 1994). It is assumed here that this distribution does not change with solar cycle. The figure shows a symmetric distribution with two peaks at $B_x = -4$ and +3 nT and a local minimum around B_x=0 nT. Comparing Fig. 3.16a and Fig. 3.16b, it is suggested polar arcs occur preferentially when IMF B_x is near 0 nT.

3.7.2 Effect of IMF B_y

It is believed that the IMF B_y component controls the dawn-dusk position of polar arcs. Fig. 3.17a, similar to Fig. 3.16a, is a plot of polar arc distribution with IMF B_y from -20 nT to 20 nT. The dashed line is again a fitted curve. Those polar arcs which occurred with IMF $B_y > 20$ nT or IMF $B_y <$ -20 nT were counted as cases of IMF $B_y =$ 20 nT or -20 nT. The distribution is not symmetric around B_y=0. It has two peaks at $B_y =$ -1 nT and 4 nT. Some 38 % of the polar arcs occurred with negative IMF B_y, 14 % with B_y =0, and 48 % with positive B_y. Therefore more polar arcs occur with positive or duskward B_y. Fig. 3.17b is similar to Fig. 3.16b, but as a function of IMF B_y. This shows the B_y component has a roughly symmetric distribution and slightly more negative (dawnward) B_y component than positive (duskward) B_y. This shows that more polar arcs occurred with positive B_y component than those with negative IMF B_y.

3.7.3 Effect of IMF B_z

Polar arcs have been considered to be strongly influenced or controlled by the the sign of the IMF B_z. The orientation of the IMF B_z directly affects coupling between the solar wind and the magnetosphere. Fig. 3.18a illustrates the distribution of polar arcs by IMF B_z. All cases with $B_z > 20$ nT were counted B_z=20 nT. The dashed line is a fitting curve. The major part (78 %) of polar arcs occurred with positive (northward) B_z, 6 % with B_z=0, and 16 % of the polar arcs occurred with negative

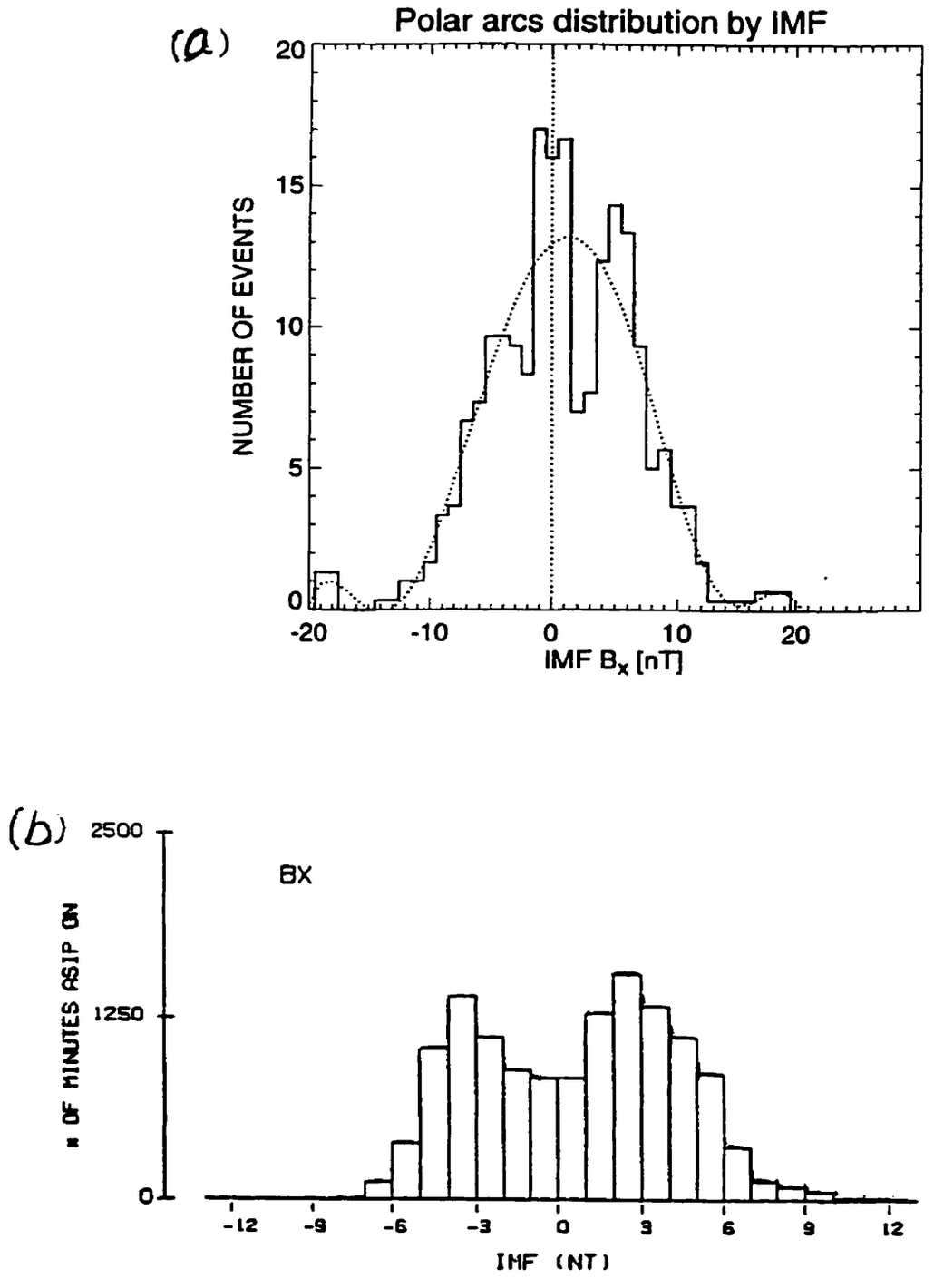

Figure 3.16: The distribution (a) of polar arcs in relation to the IMF B_x component and (b) of the number of minutes when the All-sky Image Photometer (ASIP) was on during a period of 1986-87 winter as a function of the IMF B_x level. (after Valladares et al., 1994).

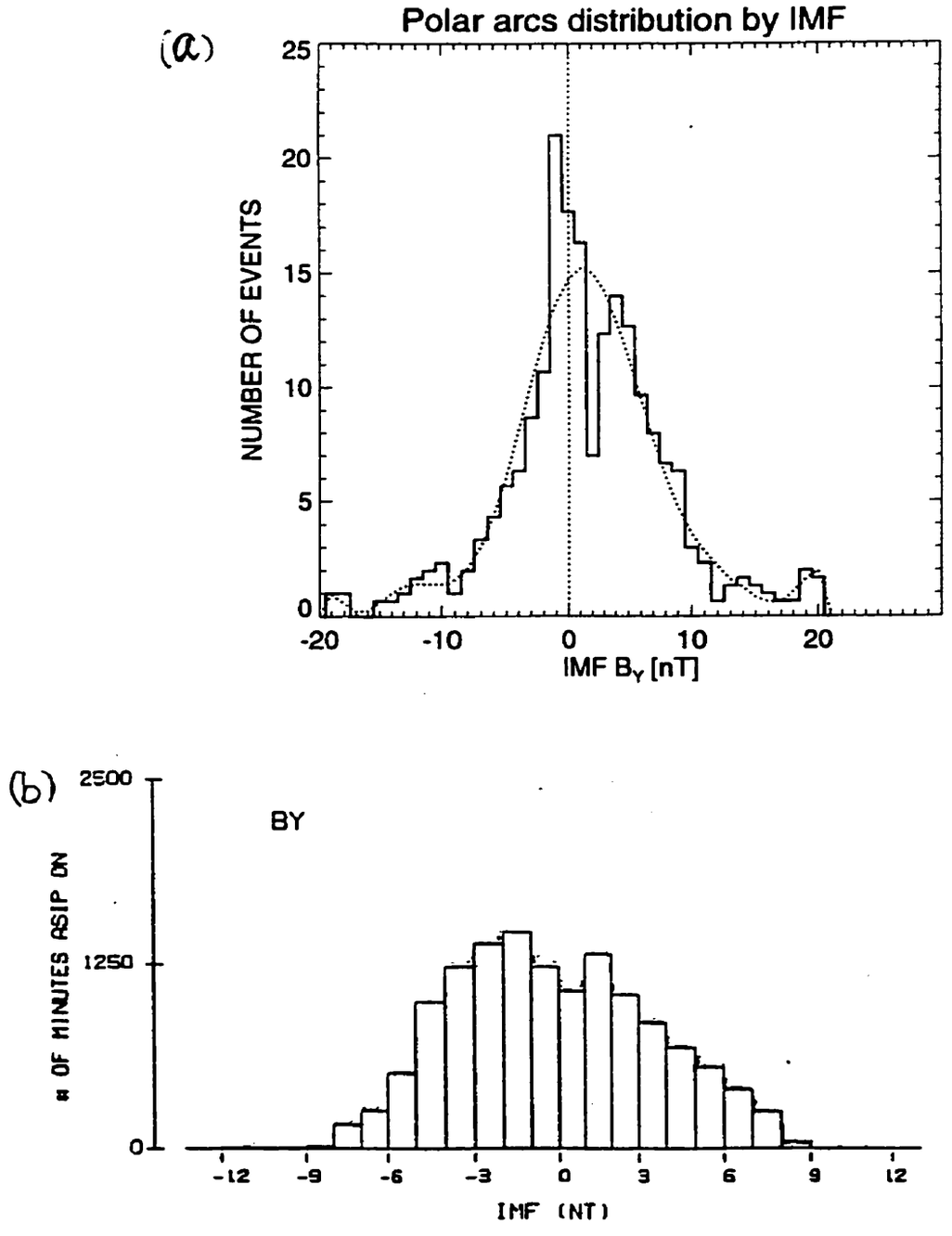

Figure 3.17: The distribution (a) of polar arcs in relation to the IMF B_y component and (b) of number of minutes when the ASIP was on during a period of 1986-87 winter as a function of the IMF B_y. (after Valladares et al., 1994)

IMF The peak of the distribution is located at B_z=3 nT. Fig. 3.18b is a plot of IMF B_z distribution, similar to the plot of IMF B_x in Fig. 3.16 from Valladares et al., [1994]. This distribution shows that the IMF B_z is positive about 60 % of the time. This shows that polar arcs occurred predominantly with positive IMF B_z.

3.8 Polar arcs and the solar wind

Solar wind plasma is generally the energy and particle source for activity in the magnetosphere, including the polar auroral activity. The orientation of the IMF especially the B_z component, affects occurrence of polar arcs. It is worthwhile here to see how solar wind parameters such as solar wind speed, density and dynamic pressure are related to polar arcs by examining the solar wind data in conjunction with the polar arc data. Solar wind data from the IMP-8 satellite were provided by the NSSDC/NASA.

3.8.1 Solar wind speed and polar arcs

Solar wind speed is considered to be one independent parameter relating to polar arcs [Gussenhoven, 1982]. Fig. 3.19a is a polar arc occurrence distribution according to solar wind speed. The peak of the distribution is located at solar wind speed of 350 km/s. There is a sharp drop of the distribution around solar wind speed 360 km/s. The distribution doesn't change very much with solar wind speed larger than 360 km/s. Fig. 3.19b is a histogram of solar wind speed (after Gosling, 1972). It shows that the median solar wind speed was 380 km/s around solar minimum. When this histogram of solar wind speeds is normalized to compare with the polar arc distribution of Fig. 3.19a the two curves are seen to be roughly similar. This suggests that solar wind speed may not have a major effect on occurrence of polar arcs.

3.8.2 Solar wind density and polar arcs

Solar wind density varies from a few to over one hundred particles per cubic centimeter. The large variations in the solar wind density do change momentum flux and dynamic pressure so they may affect the polar auroras. Fig. 3.20a is a plot of the polar arc

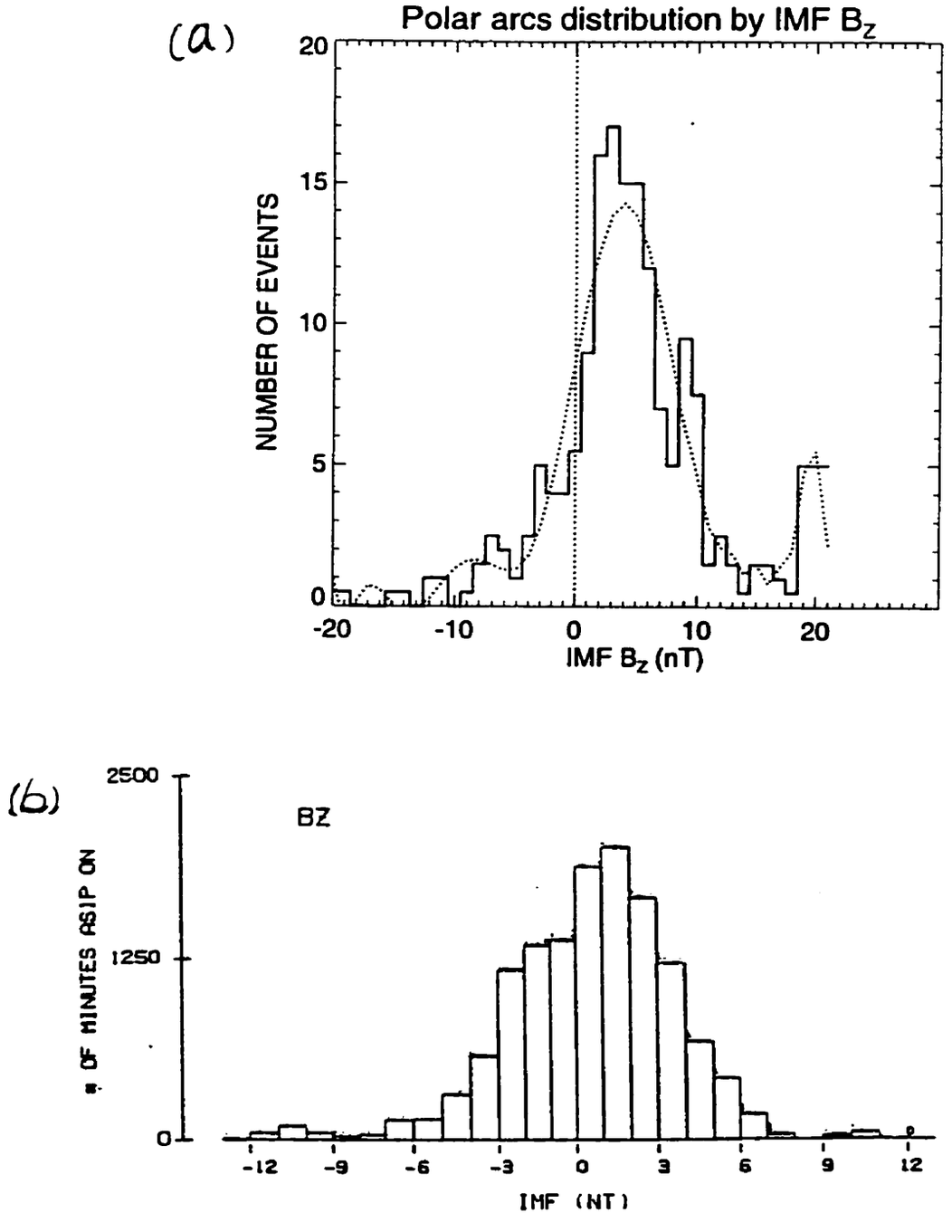

Figure 3.18: The distribtution (a) of polar arcs in relation to the IMF B_z component and (b) of number of minutes when the ASIP was on during a period of 1986-87 winter as a function of IMF B_z. (after Valladares et al., 1994).

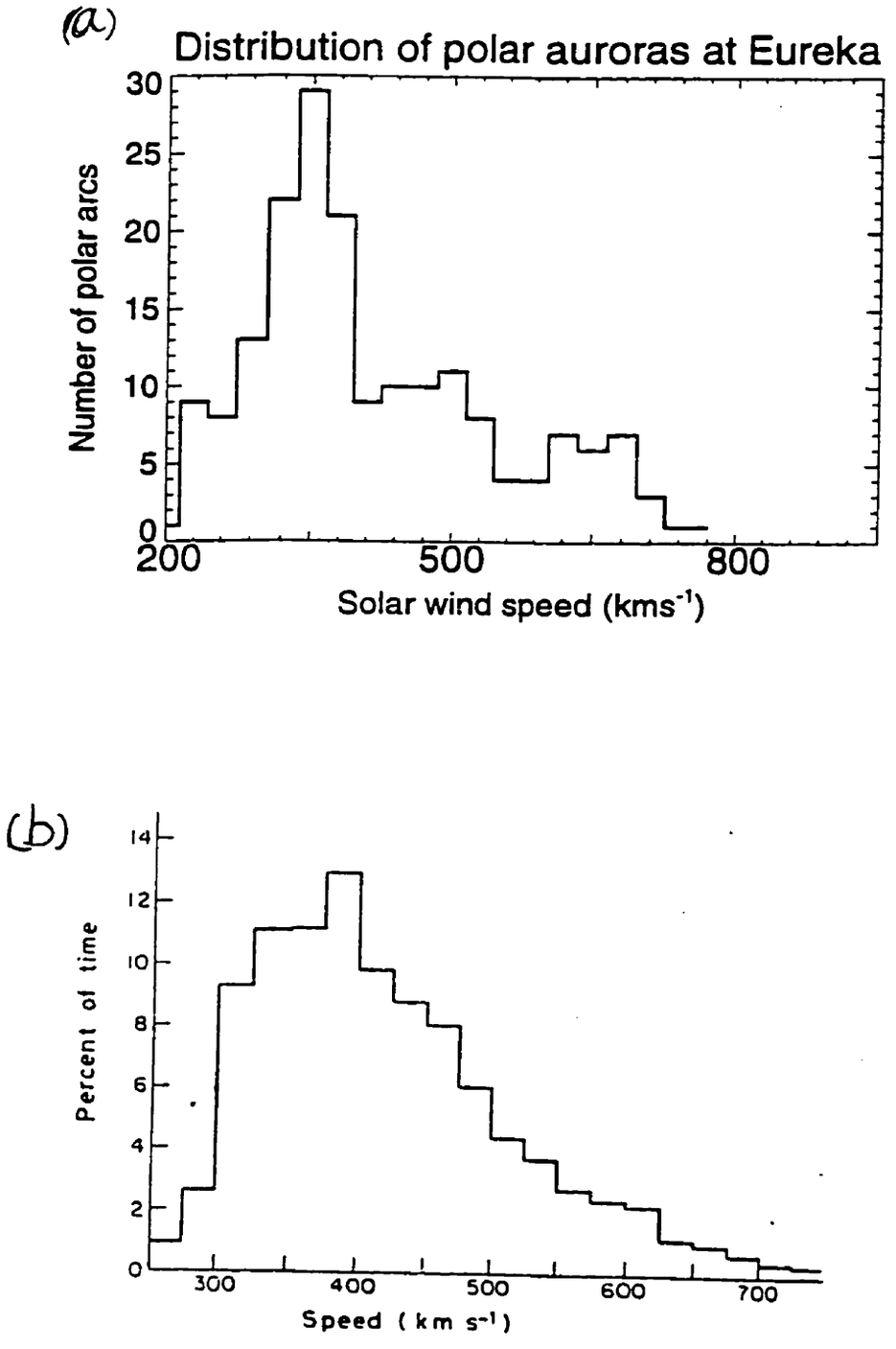

Figure 3.19: (a) The distribution of polar arcs in relation to solar wind speed. (b) The distribution of solar wind speed itself in relation to observing time (after Gosling, 1972).

distribution observed as a function of solar wind density. The distribution appears similar to the solar wind density distribution itself [Rosenbauer, 1982].

3.8.3 Solar wind dynamic pressure and polar arcs

Solar wind dynamic pressure controls the size and shape of the magnetosphere. Fig. 3.20b is a plot of the polar arc occurrence distribution with solar wind dynamic pressure. Because of the linear relationship between the solar wind density and solar wind dynamic pressure, Fig. 3.20b is very similar to Fig. 3.20a. How solar wind dynamic pressure changes induce polar arcs is investigated in the next chapter.

3.9 Energy of precipitated electrons: A preliminary result

3.9.1 Relation between auroral intensity ratio and electron energy

The energy of precipitated electrons determines which auroral emissions will be most efficiently excited. Therefore, the energy of precipitated electrons could be estimated from the intensity ratio of different emissions. Two empirical formulas were obtained between 630.0, 557.7, 427.8 nm emission ratios and precipitated electron energy [Steele and McEwen, 1990], namely

$$\frac{I_{630.0}}{I_{427.8}} \approx 3.3 \times E_o^{-2.1} \tag{3.1}$$

$$\frac{I_{557.7}}{I_{427.8}} \approx 5.6 \times E_o^{-0.3} \tag{3.2}$$

where $I_{630.0}, I_{557.7}$ and $I_{427.8}$ are the intensities (in rayleighs) of auroral emissions at 630.0 nm, 557.7 nm and 427.8 nm respectively and E_o is the characteristic energy of the precipitated electrons in keV. Combining these two equations, we have,

$$E_o \approx [\frac{3.3}{5.6} \times \frac{I_{557.7}}{I_{630.0}}]^{\frac{1}{1.8}} = 0.8 \times [\frac{I_{557.7}}{I_{630.0}}]^{\frac{1}{1.8}} (keV) \tag{3.3}$$

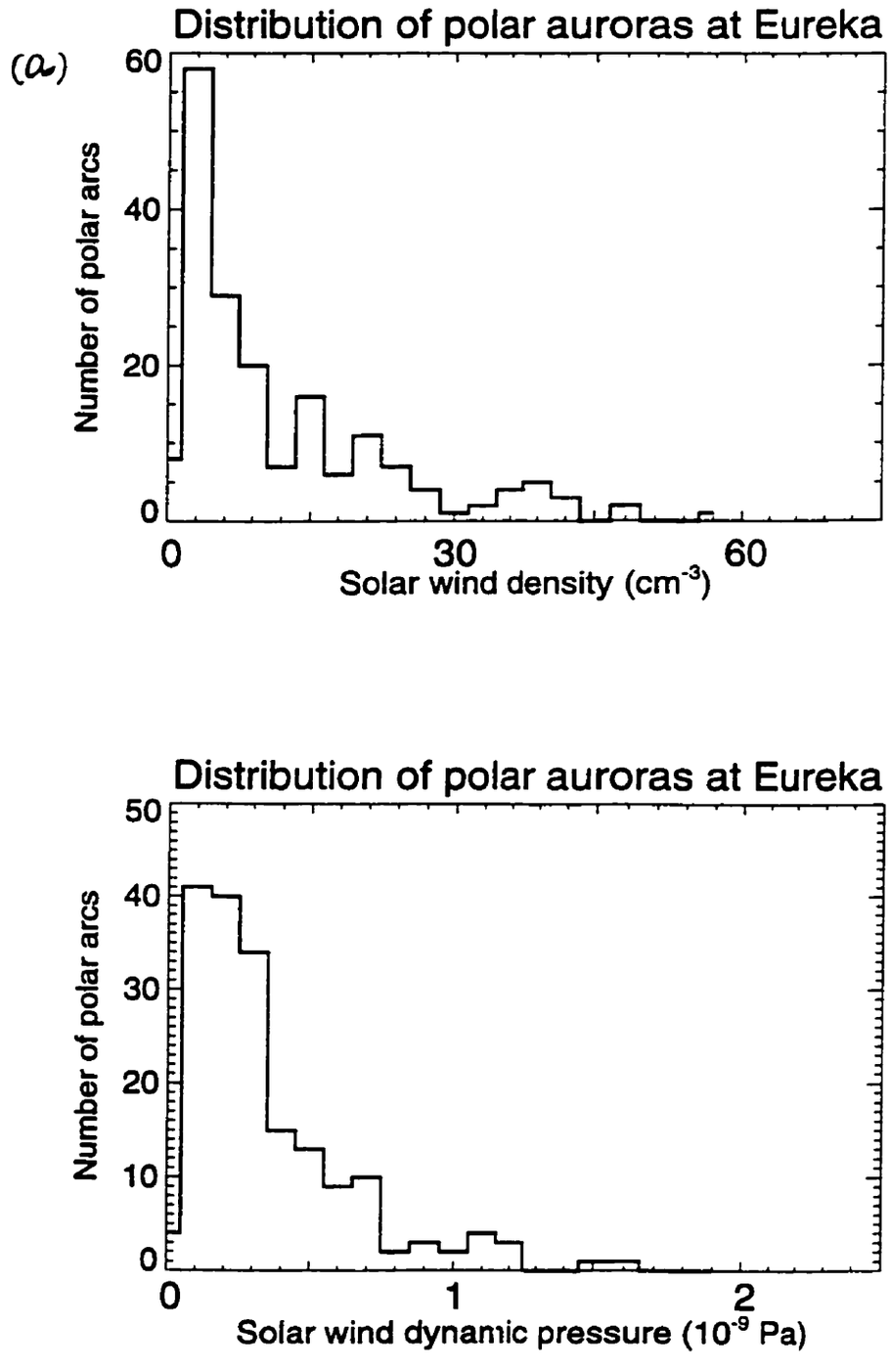

Figure 3.20: The distribution of polar arcs in relation to (a) solar wind density and (b) solar wind dynamic pressure.

This equation can be used to estimate precipitated electron energy based on the intensity ratio of 557.7 nm and 630.0 nm emissions.

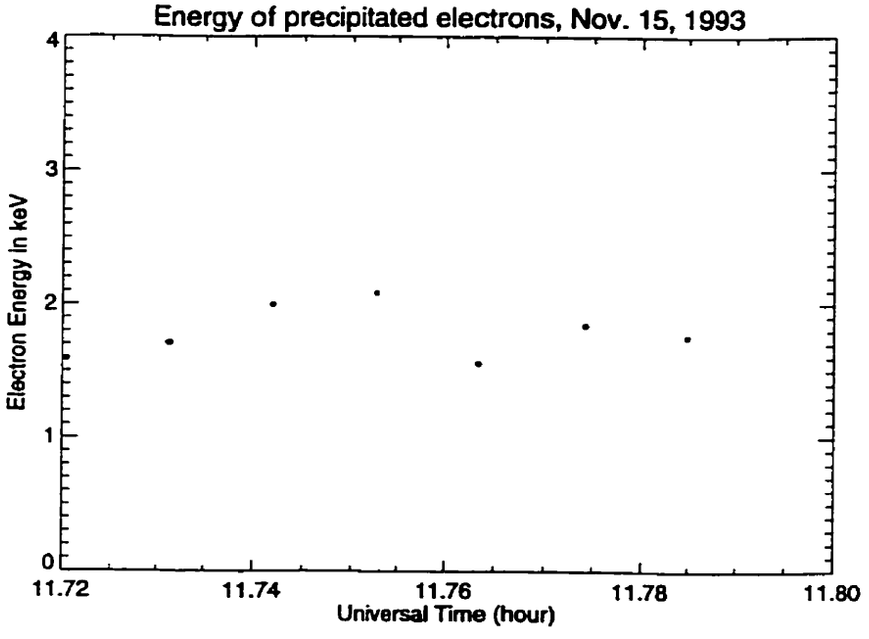

Figure 3.21: The estimated energy of precipitated electrons which caused the transpolar arc on November 15, 1993.

3.9.2 Examples

The formula shown above requires the auroral volume emission intensity ratio in calculating the electron characteristic energy [Steele and McEwen, 1990]. Therefore, the energy of precipitated electrons was estimated when the polar arcs were at or very close to the zenith using intensities measured by the MSP. Fig. 3.21 is a plot of electron energy between 1146 UT and 1148 UT on November 15, 1993 associated with a transpolar arc. It shows the characteristic energy of the precipitated electrons is from 1.5 keV to 2.1 keV. This is well above the typical energy (a few hundred eV, see Fig. 3.22) of precipitated electrons for polar arcs [Meng and Makita, 1986].

Fig. 3.22 shows a second example of electron energy associated with a sun-aligned polar arc observed on December 16, 1993. The electron energy is from 0.5 keV to 0.9 keV in this case.

The third example is an arc expanded poleward from the nightside auroral oval. The arc was observed with a magnetic storm on February 21, 1994. Fig. 3.23 is a plot of electron energy between 0922 UT and 0928 UT. The figure shows the electron energy is from 2.1 keV to 3.3 keV. During the period of the magnetic storm (and polar arc), the Geotail satellite was located on the dayside of the magnetosheath. It recorded the energy of peak electron flux between 2.0 and 3.0 keV, see Fig. 3.24 (from Mukai, Tokyo University), in qualitative agreement with the ground observations.

3.10 Summary

Polar arcs were observed with high resolution and sensitivity with an ASC and MSP through the four winters from 1990 to 1994 in the central polar region. Their main statistical characteristics are:

(a) There were 656 polar arcs observed by the ASC during the four winter periods. The polar arcs occurred 8 % of time on average. There was a diurnal variation on the occurrence pattern of the polar arcs. The amplitude of the diurnal variation was 37 % of the mean occurrence rate.

(b) The lifetimes of the polar arcs varied from 2 minutes up to 10 hours. Their mean lifetime is was minutes. However, half of the polar arcs had lifetimes less than 20 minutes.

(c) Bifurcation of a single arc was likely to happen when the intensity of the arc increased quickly.

(d) Of the polar arcs observed, 78 % were with the IMF B_z northward and 16 % were with the IMF B_z southward. (for the remaining 6 %, B_z was zero.)

(e) Polar arcs above a 50 R threshold were observed 30 % of the time from the 557.7

nm emission and 49 % of the time from the 630.0 nm emission on average.

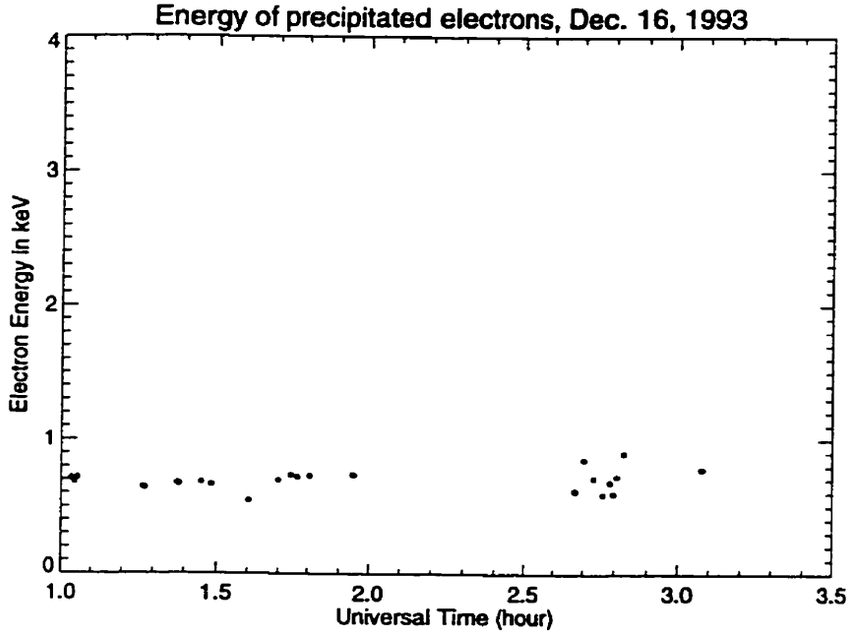

Figure 3.22: The estimated energy of precipitated electrons which caused the polar arcs on December 16, 1993.

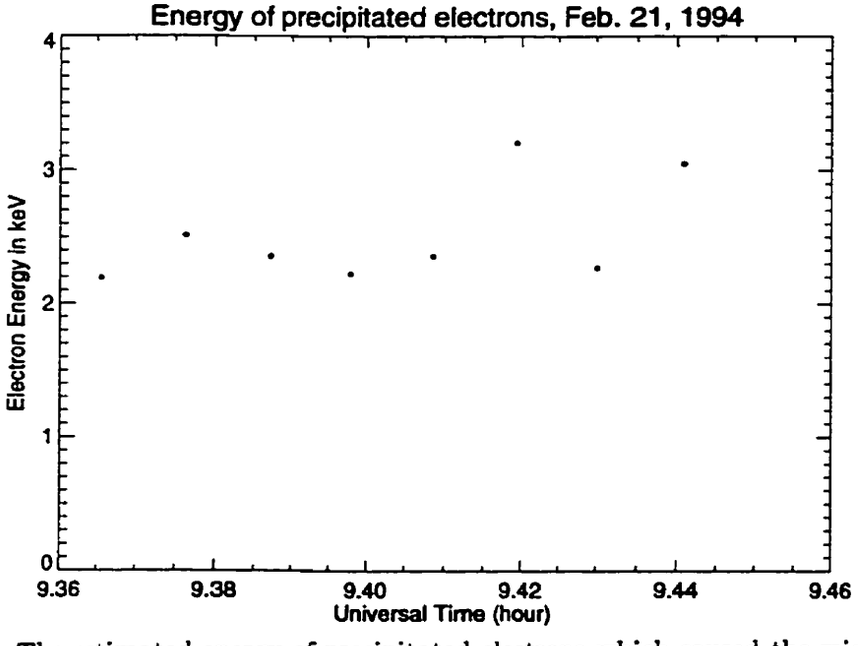

Figure 3.23: The estimated energy of precipitated electrons which caused the mid-night auroral oval expansion arcs on February 21, 1994 (with a magnetic storm).

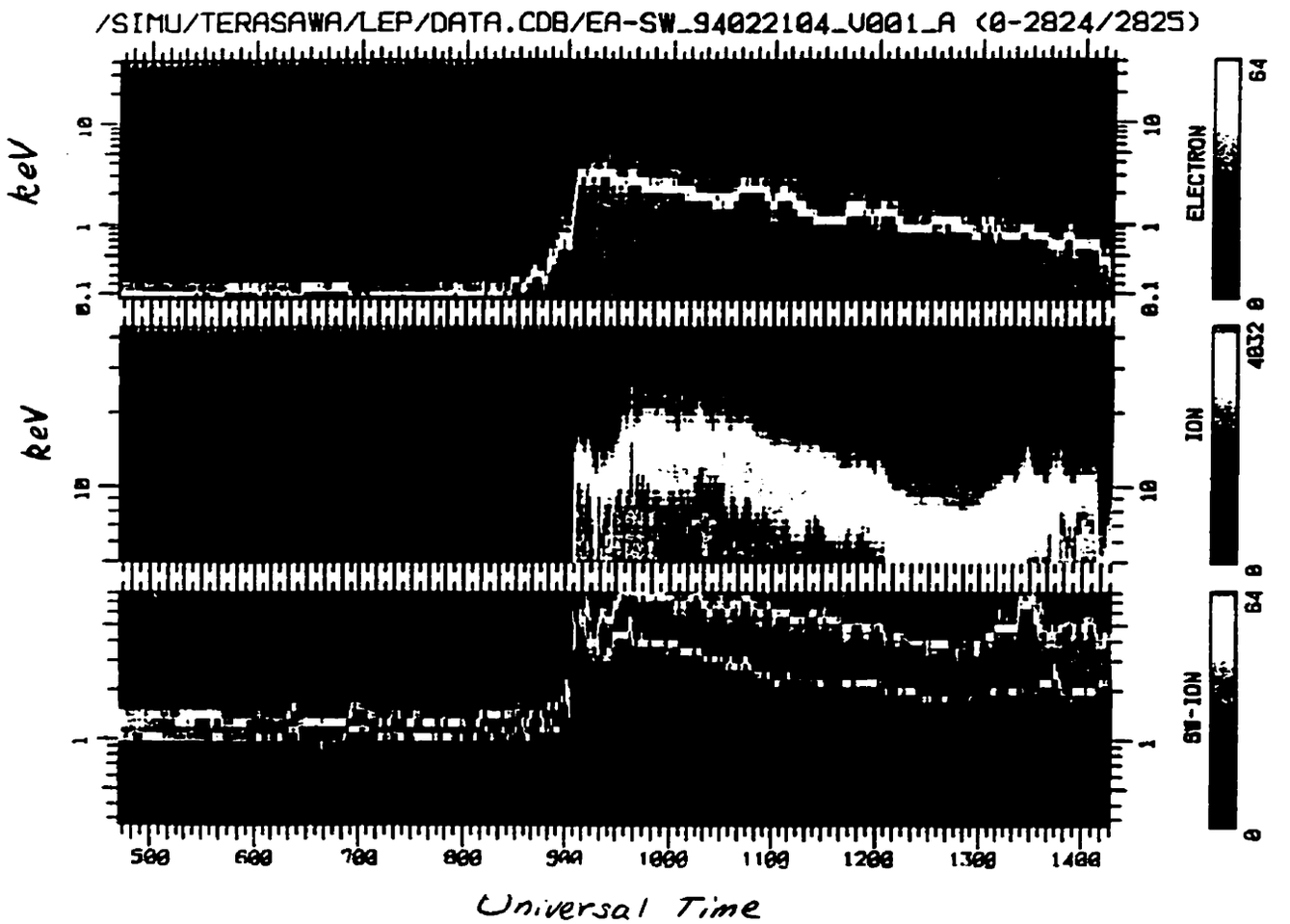

Figure 3.24: The plots of particle flux-energy by UT detected by the Geotail satellite in the solar wind on February 21, 1994, (a) electrons, (b) ions. The vertical axis is in keV and the horizontal axis is in UT hours. The flux of electrons and ions is in count-rate. (from Mukai, Tokyo University , 1994).

Chapter 4

Solar wind dynamic pressure and polar arcs

4.1 Introduction

Changing solar wind dynamic pressure causes variations of magnetospheric activities, including auroral processes. Sandholt *et al.* [1994] found that cusp/cleft auroral activity is partially governed by solar wind dynamic pressure pulses and IMF orientation. Craven *et al.*, [1986] found that when IMF B_z was southward, auroral activity in the auroral oval responded to magnetospheric compressions by shocks in the solar wind within 1-18 minutes depending on local magnetic time. When a magnetospheric compression resulted from a shock in the solar wind with northward IMF B_z, a transpolar arc was formed initially in the midnight oval and then extended to the dayside oval. Thus activities in solar wind affect auroras in both the auroral oval and polar cap.

The purpose of this chapter is to show relationships between solar wind dynamic pressure enhancements and polar arcs. The following sections will show, for the first time, arcs in the central polar cap were directly related to solar wind dynamic pressure enhancements.

4.2 Solar wind dynamic pressure enhancements

A solar wind dynamic pressure enhancement here refers to a sudden increase of solar wind dynamic pressure (P). In order to make the study of the relationship between the enhancements and polar arcs quantitative, only those enhancements above some arbitrary thresholds were considered: firstly, only cases where the solar wind dynamic pressure was at least 2.5 times the normal average solar wind dynamic pressure P_o ($\sim 0.2 \times 10^{-9} Pa$); secondly, only cases where the dynamic pressure rate of change, after smoothing of the raw data, was greater than 0.024×10^{-9} Pa/min. The smoothing used was a 5-point averaging (0.5, 0.75, 1.0, 0.75, 0.5) of each data point. The events due to single point excursions were rejected. These thresholds were established to limit the number of enhancements investigated to only the few most major ones.

$$P \geq 2.5 \times P_0 = 0.5 \times 10^{-9} Pa \tag{4.1}$$

$$\frac{dP}{dt} \geq 0.024 \times 10^{-9} Pa/min \tag{4.2}$$

A total of 25 solar wind dynamic enhancements which satisfied the above criteria were identified from IMP-8 data in the 1991-92 and 1992-93 winter periods. Polar auroras followed all of the enhancements with variable time delays [Zhang *et al.*, 1994].

Details of how polar auroras follow the dynamic pressure enhancements are discussed in the next section. The MSP data were used in this study of the relation between the enhancements and polar arcs since the MSP was more sensitive than the ASC. Some of the polar arcs which appeared were above the 300 R threshold of the Camera. Following are case studies of major events of solar wind pressure enhancements followed by polar arcs.

4.2.1 Events on November 22, 1992

Figure 4.1a is a plot of solar wind dynamic pressure versus universal time on November 22, 1992. The data were obtained from IMP-8 satellite. The data displayed here were sampled once every minute. The dynamic pressure was above $5 \times 10^{-10} Pa$ between

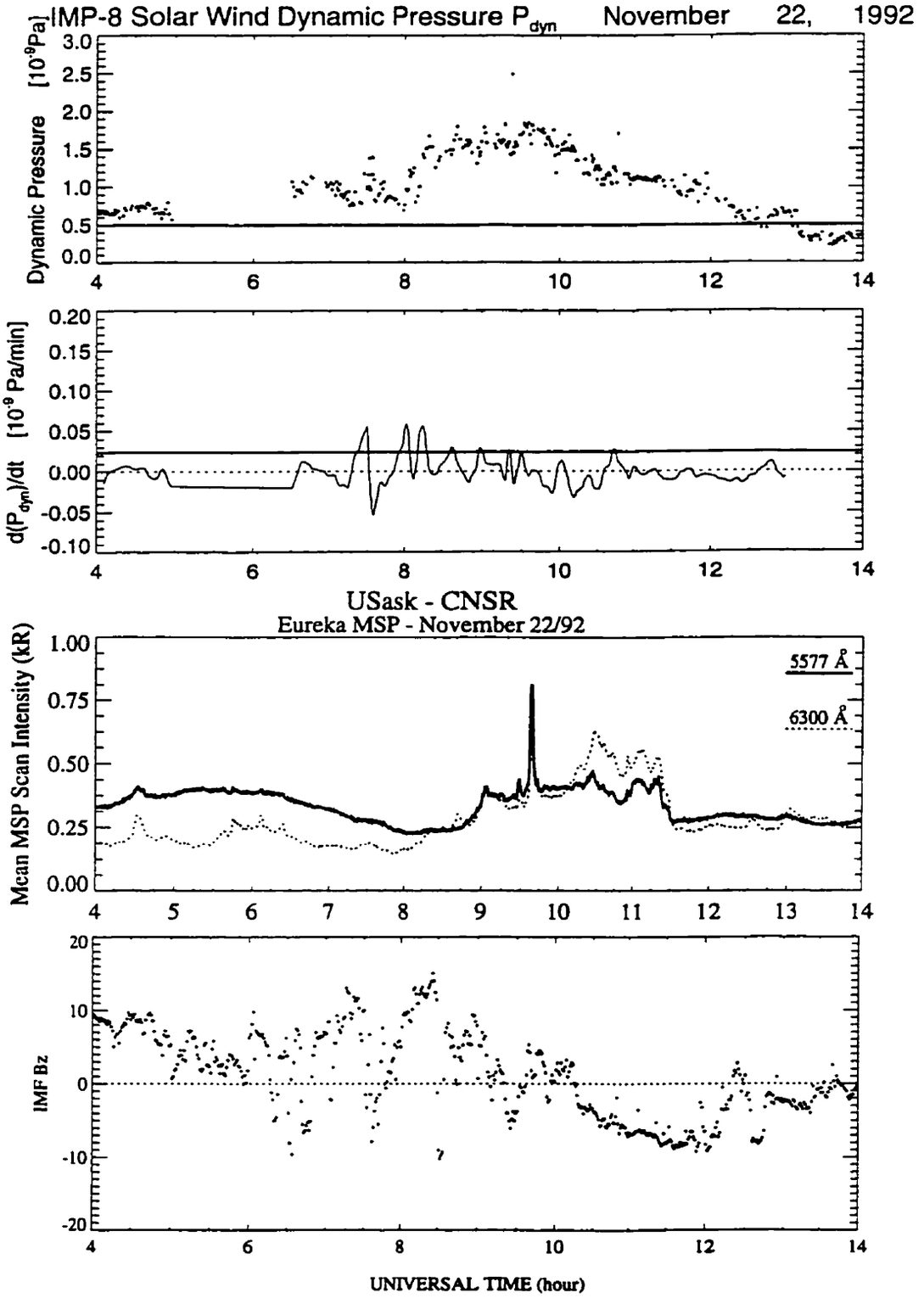

Figure 4.1: Solar wind dynamic pressure enhancements and polar arcs on November 22, 1992. (a) The solar wind dynamic pressure, (b) Gradient of the dynamic pressure, (c) The MSP mean scan intensity of polar arcs (557.7nm and 630.0 nm emissions), (d) IMF B_z.

0400 UT and 1200 UT, as shown by the solid line in Fig. 4.1a, and declined to a stable level about $2 \times 10^{-10} Pa$ after 1300 UT. There are 2 data gaps in the IMP-8 data. The solar wind speed was stable (around 420 km/s) during the day. This implies that the solar wind dynamic pressure followed the solar wind density changes. Fig. 4.1b shows a plot of the rate of change of the dynamic pressure (dP/dt). A weighted five point averaging was employed to remove high frequency oscillations. The solid line in Fig. 4.1b indicates the threshold rate of increase of $0.024 \times 10^{-9} Pa/min$. Fig. 4.1b shows that the time derivative of the dynamic pressure had eight peaks between 0700 UT and 1100 UT which were at or above the threshold. The peak at 0920 UT was due to a single point excursion so was rejected. The dynamic pressure (Fig. 4.1a) was above $5 \times 10^{-10} Pa$ during this whole period. Therefore these peaks represent solar wind dynamic pressure enhancements according to our definition in the previous section. The seven peaks at 0730, 0803, 0815, 0838, 0859, 0922 and 1045 UT are identified as solar wind dynamic pressure enhancements. These peaks are discussed in turn, and are tabulated in Table 4.1.

Table 4.1: A list of solar wind dynamic pressure enhancements and polar auroras on November 22, 1992.

Enhancement	$\frac{dP}{P_o dt}$	IMF B_z	Auroral peak	Apparent delay	corrected delay
[hr:min]	[% min^{-1}]	[nT]	[hr:min]	[min]	[min]
0730	28	9	0904	94	96
0803	30	9.5	0930	87	89
0815	29	12	0939	84	86
0838	15	8	1027	109	111
0859	14	8.5	1057	118	120
0922	14	-4	0939	17	18
1045	14	-5	1104	19	21

Fig. 4.1c shows the average MSP scan intensity from 0° to 180° degrees of elevation angle for the 557.7 nm and 630.0 nm channels. The high level of 630.0 nm intensity

between 1600 UT and 2000 UT is due to twilight. The wave structure of 557.7 nm intensity is due to atmospheric wave modification of the airglow, or sources other than auroral emissions. There are six discrete peaks between 0900 and 1200 UT on the plot of 557.7 nm intensity. The first peak is located around 0904UT. The second peak through the sixth were observed at 0930, 0939, 1027, 1057 and 1104 UT. These peaks are identified as due to auroral emissions. The dynamic pressure enhancements from the first one at 0730 UT to the sixth one at 0922 UT cover a time interval of 112 minutes. The six auroral intensity peaks from 0904 to 1104 UT cover a period of 120 minutes, which is almost the same as the 112 minute time interval for the solar wind enhancements. This suggests that the auroral emissions between 0904 UT and 1104 UT may be related to the solar wind dynamic pressure enhancements between 0730 and 0922UT. It is reasonable to assume that each of the six auroral intensity peaks followed one of the six enhancements. The time delay between the six enhancements and the auroral intensity peaks are 94, 97, 84, 109, 118, 102 minutes respectively. These time delays are the elapsed times between each enhancement recorded at the IMP-8 satellite and the times the auroras reached peak intensity.

Because of the distance between the IMP-8 and the earth, the 'apparent' time delay had to be corrected according to the position of IMP-8 and the solar wind speed. The rotation of the Sun makes the solar wind flow deviate from the sun-earth direction. A two dimensional convection effect needs to be considered due to the rotation of the Sun (see Appendix A). Table 4.2 shows the position of IMP-8 satellite at the time of the enhancements. The solar wind speed was measured at 420 km/s during the periods of those enhancements. The corrected time delays for these events are included in Table 4.1. In general the time delay corrections were between 1 and 8 minutes.

Since the IMF orientation plays a very important role in the solar wind - magnetosphere coupling it is important to check the orientation of IMF, especially the B_z component, and its effect on the auroral response to the enhancements. Fig. 4.1d is a plot of the IMF B_z component in units of nT. The B_z component was mainly positive (northward) with short periods southward between 0730 and 0930 UT. It became neg-

Table 4.2: Position (GSM) of IMP-8 satellite on November 22, 1992.

UT [hr:min]	X [R_E]	Y [R_E]	Z [R_E]
0730	13.87	-23.00	15.92
0803	14.21	-22.82	16.09
0815	14.35	-22.71	16.14
0838	14.62	-22.52	16.18
0859	14.89	-22.36	16.18
0922	15.16	-22.23	16.12
1045	16.08	-22.06	15.52

ative around 1020 UT and kept southward until 1220 UT. A close examination of the IMF B_z shows that B_z was 9.0, 9.5, 12.0, 8.0, 8.5, -4.0 and -5.0 nT at the times of the seven successive enhancements. It appears that the first three peaks of auroral intensity correspond to the first three enhancements with time delays of about 90 minutes. The IMF B_z was positive (northward) and was well above zero during this period. The last enhancement at 1045 UT was followed by the last auroral peak at 1104 UT. This gives an apparent time delay of 19 minutes. The IMF B_z was southward in this case. These four cases suggest that orientation of the IMF B_z affects the time delay, positive B_z relating to long time delays and negative B_z relating to short time delays.

The fourth and fifth enhancements are associated with positive B_z and the corresponding auroral peaks are at 1027 and 1057 UT. These give apparent time delays of 109 and 118 minutes respectively which agree with the analysis of the previous four cases.

The third aurora (peaking at 0939 UT) appears to be initiated by two separate solar wind enhancements, the one at 0815 UT and the one at 0922 UT. The apparent time delays were 84 minutes and 17 minutes respectively, but the IMF B_z had turned southward by 0922 UT. Fig. 4.1c shows that the third peak (0939 UT) of auroral intensity is well above the other peaks, which supports this conclusion. Table 4.1

gives a summary list of these enhancements recorded on November 22, 1992 with the corresponding auroras as interpreted above.

4.2.2 Events on December 17, 1992

Fig. 4.2 is a plot of solar wind dynamic pressure, gradient of the pressure, mean MSP scan intensity and IMF B_z. Its format is identical to Fig. 4.1. Following the same procedure as in the last sub-section to identify the solar wind dynamic pressure enhancements, in Fig. 4.2b one can find six peaks above the solid line (indicating a level of $0.024 \times 10^{-9} Pa/min$) . The first peak has an accompanying small peak and the two that are considered as a single peak. For the same reason, the fourth peak which consists of three closely spaced peaks is treated as a single peak also. The solar wind dynamic pressure corresponding to these peaks is above a level of $5 \times 10^{-10} Pa$. The third peak of dynamic pressure gradient at 1320 UT is due to a single point jump of data and therefore this peak is excluded from the list. All other peaks are identified as dynamic pressure enhancements. These five enhancements occurred at 0613, 0705, 1509, 1836 and 1918 UT respectively.

By checking Fig. 4.2c, the MSP scan intensities, auroral peaks following the enhancements are identified as at 0645, 0740, 1508, 1841 and 1945 UT. The auroral peak at 0645 UT actually consists of two closely spaced peaks. The auroral enhancement at 1508 UT consists of three major peaks. These multiple peaks corresponding to the multiple pressure enhancements are further evidence that the polar auroras followed the solar wind dynamic pressure enhancements. The values of the IMF B_z at time of the enhancements are shown in Table 4.3. Time delay corrections were obtained following the procedure of Appendix A. Corrected time delays for these events are shown in Table 4.3.

4.2.3 Events on December 16, 1993

Quite a few solar wind dynamic pressure enhancements were also observed on December 16, 1993. They are illustrated in Fig. 4.3.

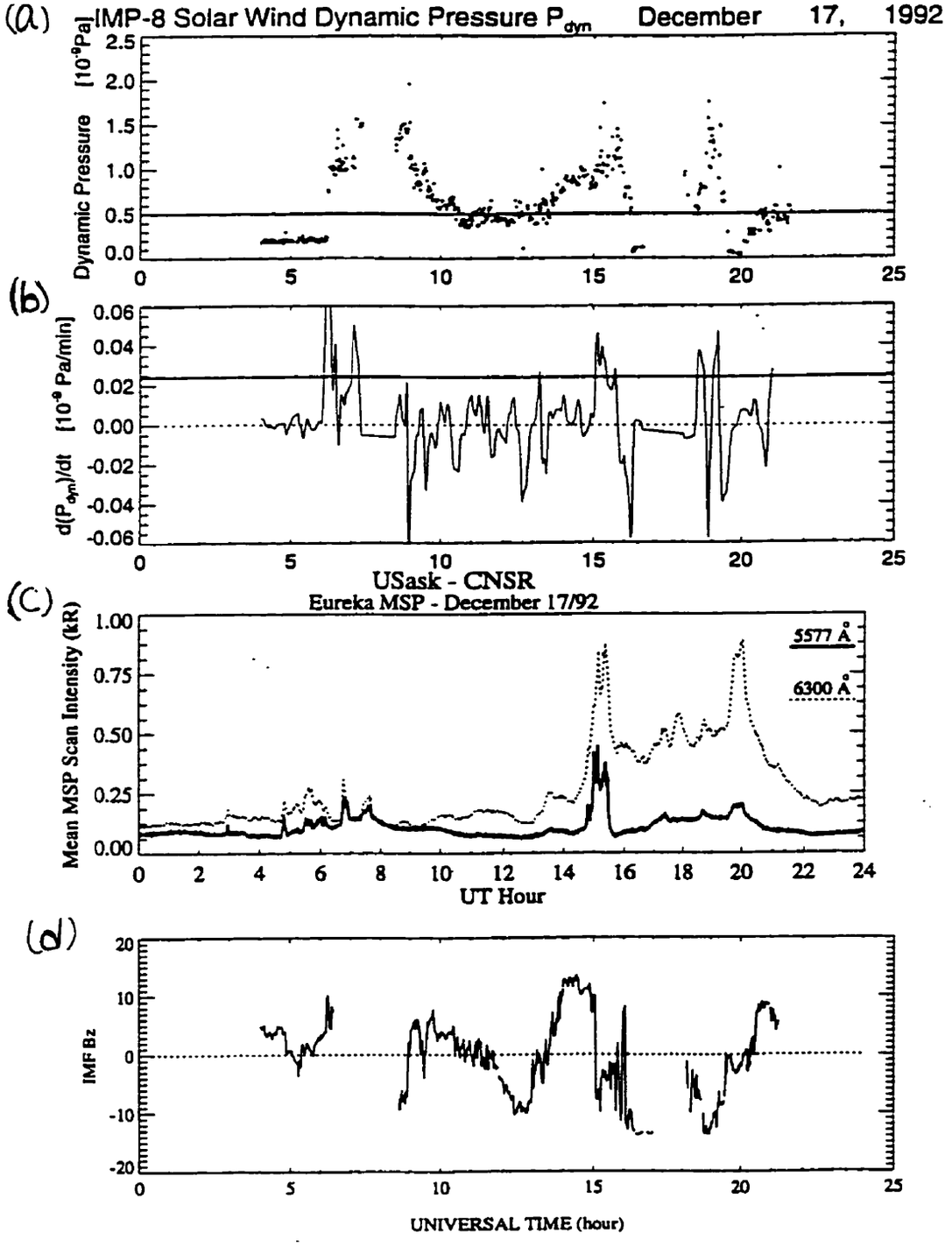

Figure 4.2: The same as Fig. 4.1, but for December 17, 1992.

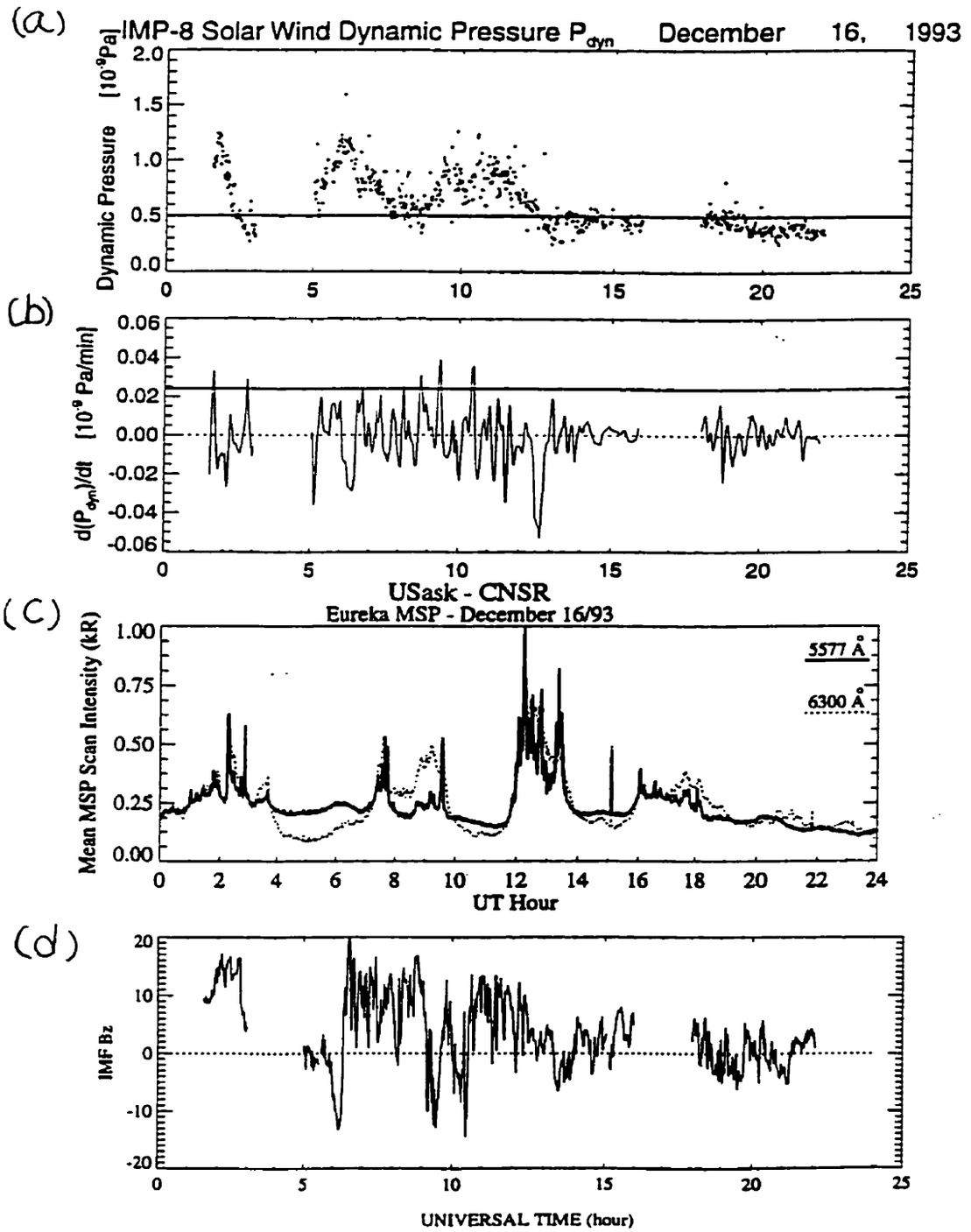

Figure 4.3: The same as Fig. 4.1, but for December 16, 1993.

Table 4.3: Solar wind dynamic pressure enhancements and polar arcs, December 17, 1992.

Enhancement	$\frac{dP}{P_o dt}$	IMF B_z	auroral peak	apparent delay	corrected delay
[hr:min]	[% min^{-1}]	[nT]	[hr:min]	[min]	[min]
0613	50	8.5	0645	32	36
0705	25		0740	35	39
1509	23	-7.5	1508	-1	1
1836	18	-6.5	1841	5	6
1918	23	-7	1945	27	28

Figure 4.3a shows the dynamic pressure is mainly above $0.5 \times 10^{-9} Pa$ between 0100 and 1200 UT. Fig. 4.3b indicates that there are seven peaks in the pressure gradient. They are located at 0140, 0248, 0646, 0810, 0845, 0923 and 1032 UT respectively. The dynamic pressures corresponding to these peaks are all above $0.5 \times 10^{-9} Pa$.

Polar arcs were identified corresponding to all the enhancements. These polar aurora peaks were observed at 0251, 0338, 0739, 0842, 0908, 0934, and 1204 UT (see Fig. 4.3c). The auroral peak at 0215 UT followed a gap in the solar wind data. The auroral information plus the IMF B_z level and the corrected time delays are listed in Table 4.4. There were multiple auroral peaks from 1210 to 1330 UT which didn't follow major pressure enhancements.

During these events, the solar wind speed increased almost linearly from 400 km/s at 0200 UT to 650 km/s at 1400 UT and then remained stable at 650 km/s level. In the previous two cases, the solar wind speed remained constant.

4.2.4 Events on Jan. 12, 1992

One more example of 5 successive solar wind enhancements on Jan. 12, 1992 is shown in Figure 4.4. These five peaks are dynamic pressure enhancements with with gradient of the dynamic pressure above the level of 0.024 $\times 10^{-9}$ Pa/min and dynamic pressure above the pressure threshold of $0.5 \times 10^{-9} Pa$. They were observed at 0641, 0911, 0935, 1025 and 1552 UT. The intensity peak of polar auroras following the enhancements

Table 4.4: Solar wind dynamic pressure enhancements and polar arcs, December 16, 1993.

Enhancement	$\frac{dP}{P_o dt}$	IMF B_z	auroral peak	apparent delay	corrected delay
[hr:min]	[% min^{-1}]	[nT]	[hr:min]	[min]	[min]
0140	17	9	0251	71	79
0248	15	8	0338	50	58
0646	12	6	0739	53	60
0810	13	-1	0843	32	39
0845	15	13	0908	23	29
0923	20	-12	0934	11	17
1032	18	6	1204	92	98

are identified at 0702, 0947, 1013, 1038 and 1621 UT. The first four auroral peaks are best seen at 630.0 nm emission. The values of the IMF B_z and the corrected time delays are listed in Table 4.5. There were auroral peaks between 1200 and 1400 UT not associated with major pressure enhancements.

Table 4.5: Solar wind dynamic pressure enhancements and polar arcs, January 12, 1992.

Enhancement	$\frac{dP}{P_o dt}$	IMF B_z	auroral peak	apparent delay	corrected delay
[hr:min]	[% min^{-1}]	[nT]	[hr:min]	[min]	[min]
0641	13	-2	0702	21	25
0911	26	10.5	0947	36	40
0935	14	10.5	1013	38	42
1025	19	-18	1038	13	16
1552	31	18	1621	29	31

4.3 Summary

The 25 major solar dynamic pressure enhancements were found to be followed by polar arcs observed at Eureka with different time delays. The time delays appeared to be

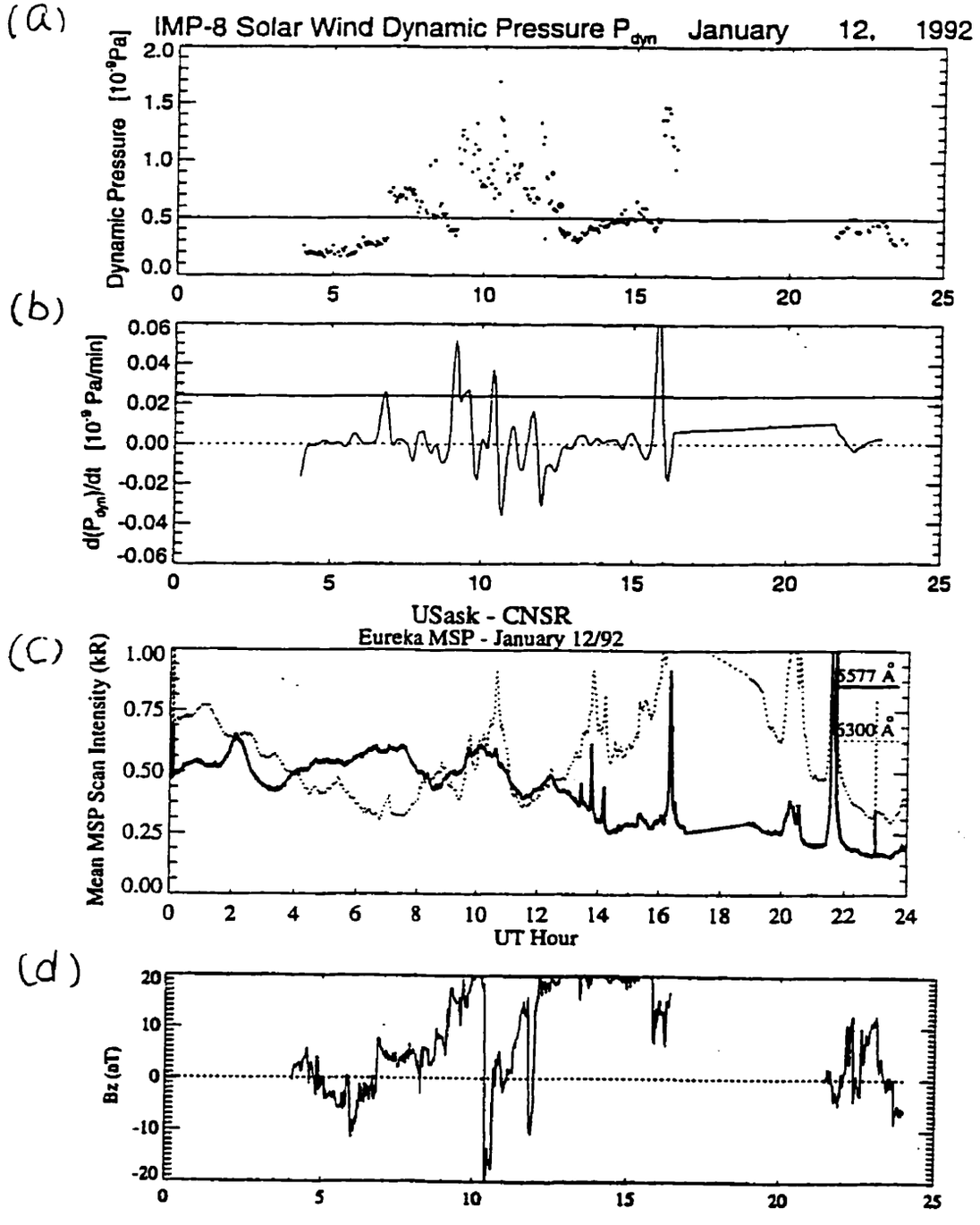

Figure 4.4: The same as Fig. 4.1, but for January 12, 1992.

controlled by the orientation of the IMF B_z. These striking cases of solar wind dynamic pressure enhancements followed by polar arcs will be discussed in Chapter 6.

Chapter 5

Mapping of polar arcs

5.1 Introduction

The source of the electrons which cause polar arcs is one of the most important problems in auroral study. Motions of electrons are guided by the geomagnetic field lines in the magnetosphere. Therefore, precipitated electrons causing auroras can be traced (mapped) back to their source regions along magnetic field lines. Mapping of polar arcs is actually to find the magnetic field lines which connect the area where polar arcs occurred and the region in the magnetotail (see a 3-D structure of the magnetosphere shown in Fig. 1.3). A magnetic field line configuration must be assumed before the mapping can be done. The magnetic field in the near earth environment has contributions from a number of different current sources. The simplest model describing the magnetic field around the earth is the dipole model which was developed many centuries ago. The dipole model just includes currents inside the Earth. The discovery of the ionosphere more than half a century ago opened a new world of space plasma studies. Currents in the ionosphere contribute to most of the daily variations in the magnetic field observed on the surface of the Earth. A magnetic field model called the International Geomagnetic Reference Field (IGRF) was developed to represent the magnetic field in near earth space. The IGRF is much better than the simple dipole model in describing the magnetic field around the Earth. However, the IGRF is still not sufficient to represent the magnetic field in the magnetosphere. An ideal model

should meet two main requirements [Stern and Tsyganenko, 1992; Stern 1994]: (1) It should faithfully represent the effects of five main sources of the magnetospheric field: The Earth's internal field, magnetopause currents, ring currents, tail currents, and the system of Birkeland currents. (2) It should be flexible, taking into account various factors that affect the magnetosphere. One is the tilt angle. Other factors are indices, such as auroral electrojet index (AE), Dst, the solar wind pressure (P), IMF and area of the polar cap. Recently, global magnetic field models which include the contributions of currents in the magnetosphere as well as the effects of IMF were developed. The Tsyganenko series models, Rice University model and modified Tsyganenko model are among those global magnetic field models.

Tsyganenko models are empirical models based on a large satellite data set. The most recent model T89 [Tsyganenko, 1989a] is selected here for mapping polar arcs to their source region. The T89 model takes into account the effect of warping the tail current sheet in two dimensions due to the geodipole tilt, as well as spatial variations of the current sheet thickness along the sun-earth and dawn-dusk directions. Therefore, it improves the quantitative representation of the magnetic field in the magnetosphere comparing to the earlier T87 model [Tsyganenko, 1989a, 1990].

5.2 T89 global magnetic field model

The T89 model includes the contribution of currents in the magnetosphere, such as the ring current, the magnetotail current, tilt angle and K_p level effects are inputs to the model. But the field-aligned, or Birkeland, currents and the effect of the IMF were not included [Tsyganenko, 1989a]. All effects of the currents are represented by an all-purpose "polynomial" in the model. It is used in conjunction with the IGRF. As the model is an averaged model, it does not properly describe fast variations. It is claimed to be valid only out to X= -70 R_E [Tsyganenko, 1989a]. Fig. 5.1 shows an example of a cross-section of geomagnetic field lines in X-Z plane using Geocentric Solar Magnetospheric (GSM) coordinates (with K_p = 2, at 1200 UT, December 14, 1990). The magnetic field near the earth is mainly a dipole field but the magnetic field

in the magnetosphere takes form of a 'Comet tail' as it represents the average field in the tail region. Fig. 5.1 also shows the magnetic field lines are not symmetric about the X-axis due to the effect of the tilt angle of geomagnetic dipole axis.

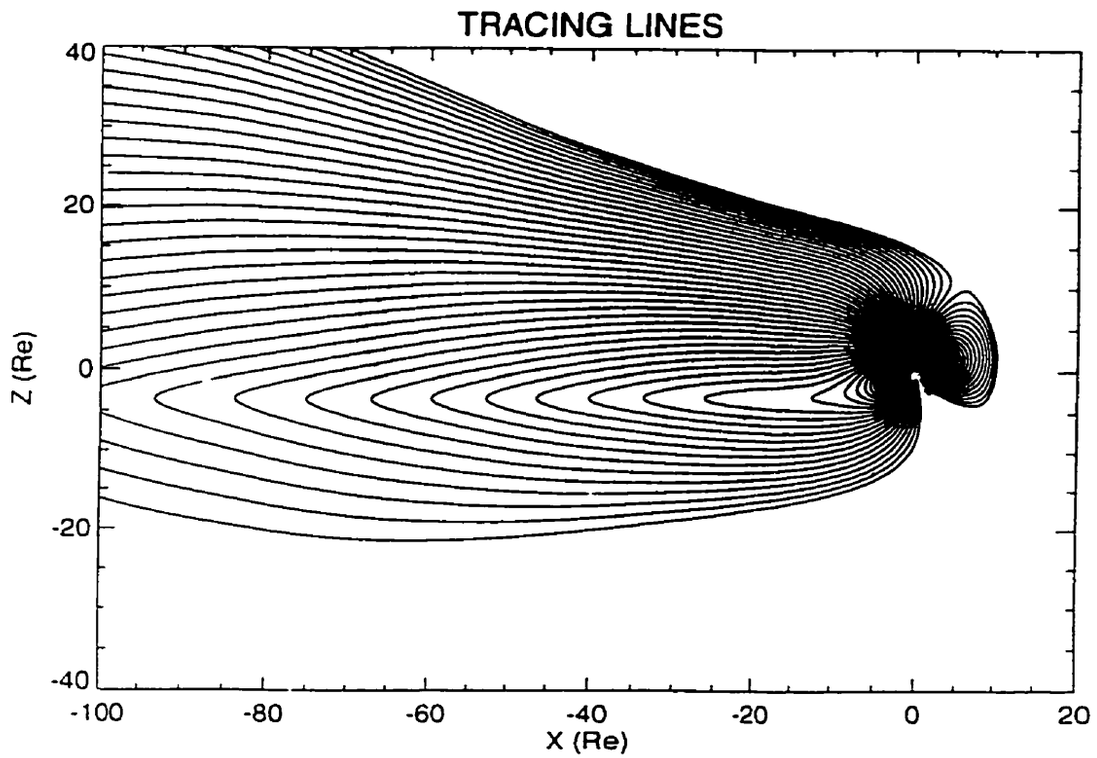

Figure 5.1: Magnetic field lines in X-Z (GSM) plane from Tsyganenko magnetic field model (T89).

5.3 Mapping of individual polar arcs

5.3.1 Field view of the ASC in the magnetotail

For mapping the particles exciting polar arcs back to their source regions, it is useful to find where the entire ASC field of view maps to in the distant magnetosphere. If an auroral height of 150 km is assumed, then the radius of the ASC viewing area in the ionosphere is about 9 degree of latitude. A simple way is to map the edge of the ASC

viewing area in the ionosphere into the magnetotail along the magnetic field lines. Such mapping was performed for December 14, 1990 at different UT values with $K_p = 0$. Fig. 5.2a is the edge of the ASC field view mapped in the Y-Z plane (GSM) of the magnetotail at X=-20 R_E at 0000, 0600, 1200 and 1800 UT. As the tilt angle changes with UT, Fig. 5.2a indicates the effect of the tilt angle on the viewing area of the ASC in the magnetotail. It shows the ASC was mainly viewing the northern magnetotail lobe. The ASC viewing area located around the middle of the northern magnetotail lobe at 0000 and 1200 UT. The viewing area shifted to the right-lower side of the lobe at 0600 UT and left side of the lobe at 1800 UT. Fig. 5.2b is similar to Fig. 5.2a, but at X=-40 R_E. The ASC viewing area at 0000 and 1200 UT is very similar to that at X=-20 R_E. However, the 'tear drop' shape indicates that the ASC viewing area at 0600 and 1800 UT extends to a region below Z=0 R_E. Overall, the ASC viewing area mainly maps to the northern magnetotail lobe most of the time.

In addition to the effect of tilt angle, the K_p level also affects the viewing area of the ASC in the magnetotail. Fig. 5.3 and Fig. 5.4 are the same plots to Fig. 5.2, but the K_p levels selected were at 2 and 4 respectively. Compared to Fig. 5.2a, Fig. 5.3a shows that the ASC viewing area is reduced and shifted down toward Z=0 R_E. Fig. 5.3b also shows the ASC viewing area is compressed and the 'tear drop' shape disappears. Fig. 5.4, with K_p=4, indicates that the ASC viewing area is further compressed and shifted toward Z=0 R_E. A higher K_p indicates larger magnetospheric currents and therefore a greater compression of the magnetotail. So, the mapped area of the ASC will be smaller than that for lower K_p level although the particle flux density may be larger.

5.3.2 December 14, 1990

A bright sun-aligned arc was observed on December 14, 1990 from 1058 UT to 1230 UT [Huang *et al.*, 1995]. It occurred first in the midnight sector and then extended toward the dayside. Fig. 5.5 is a sequence of the ASC images (557.7 nm) of the polar arc from 1124 to 1225 UT. The sunward direction is to the right of the images. The sequence of the images is selected to show the growth and time history of the event.

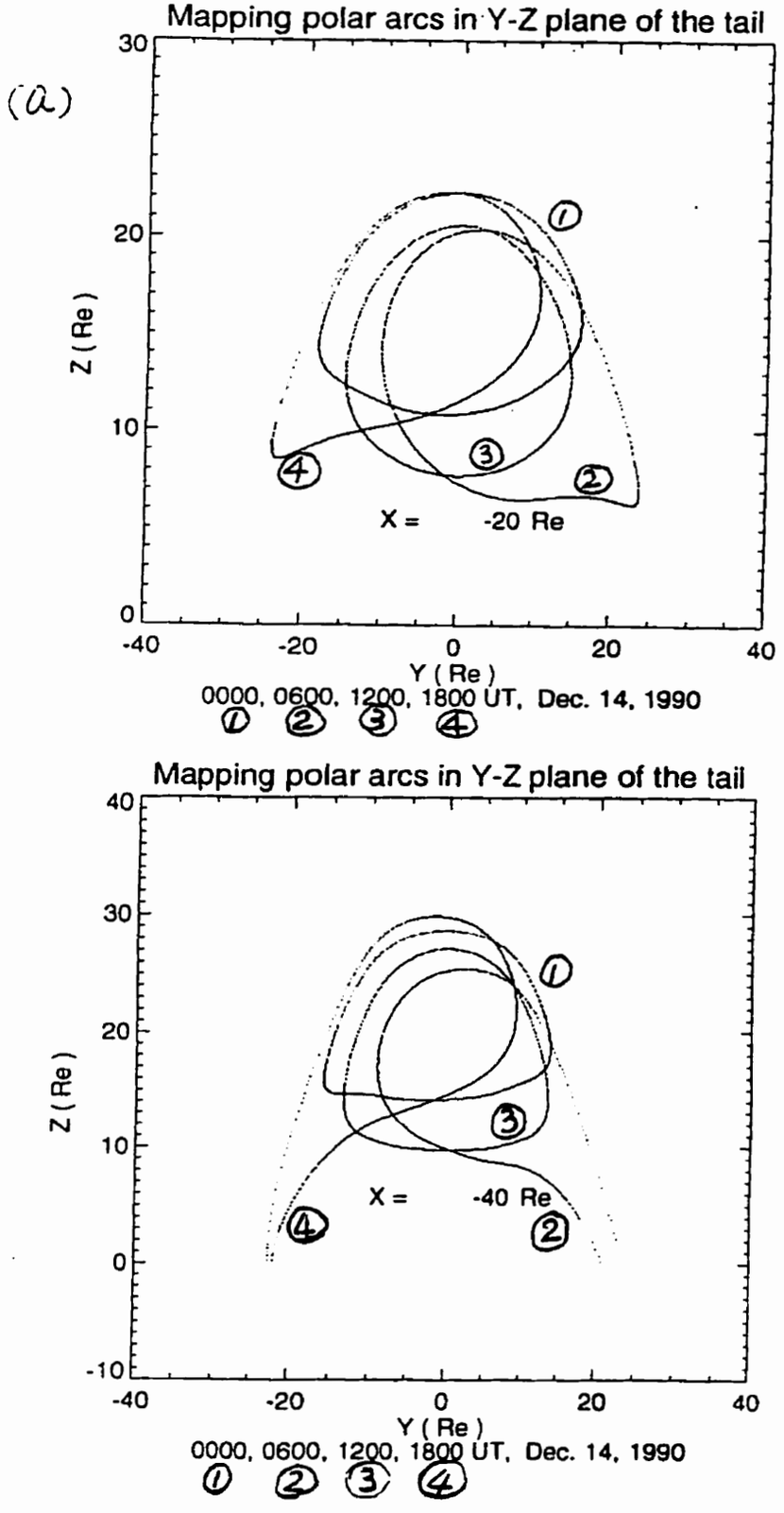

Figure 5.2: ASC field view in the magnetotail at different times (0000, 0600, 1200, and 1800 UT) on December 14, 1990. (a) X=-20 R_E, (b) X=-40 R_E. $K_p = 0$.

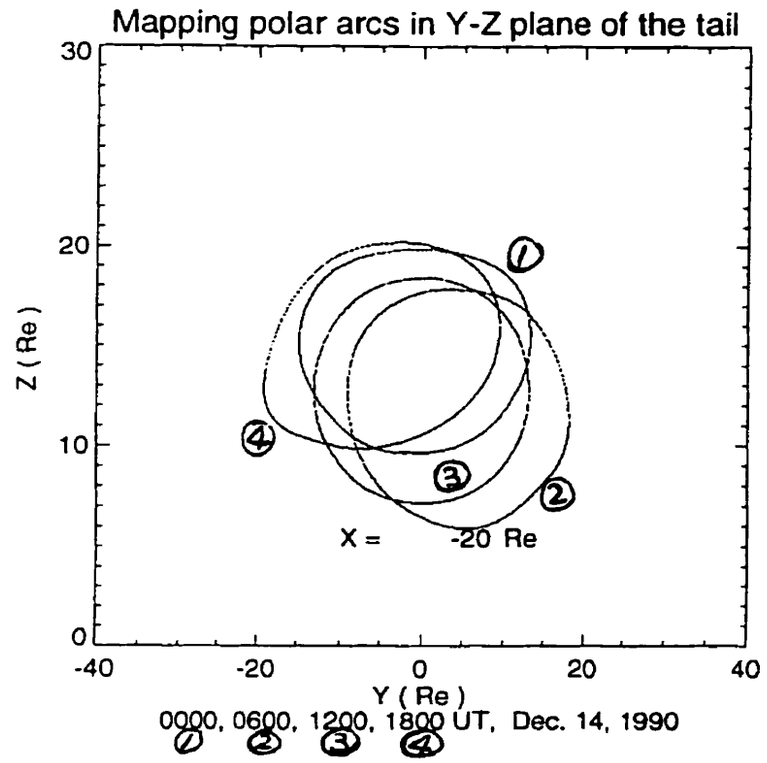

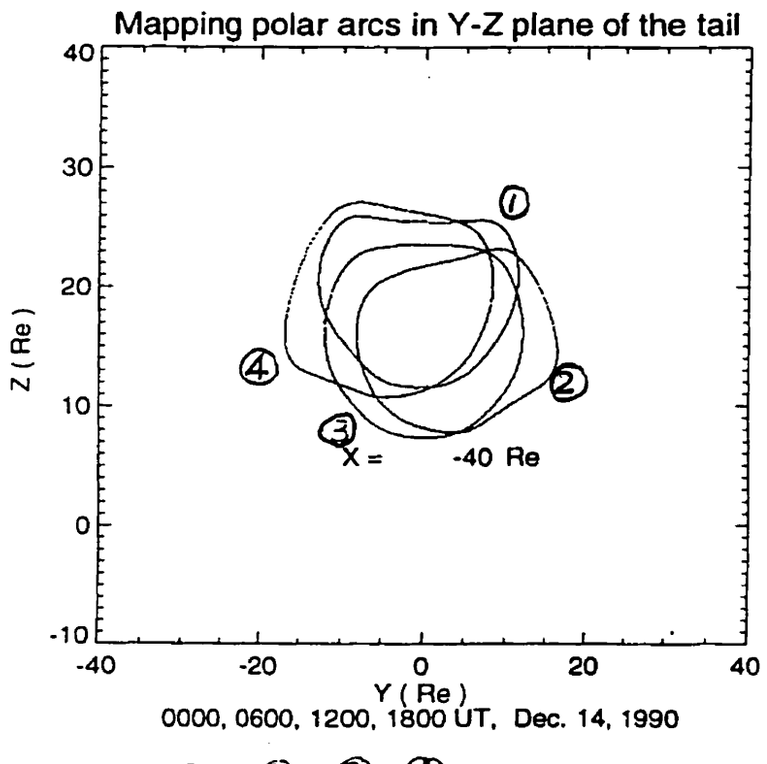

Figure 5.3: The same as Fig. 5.2, but $K_p = 2$.

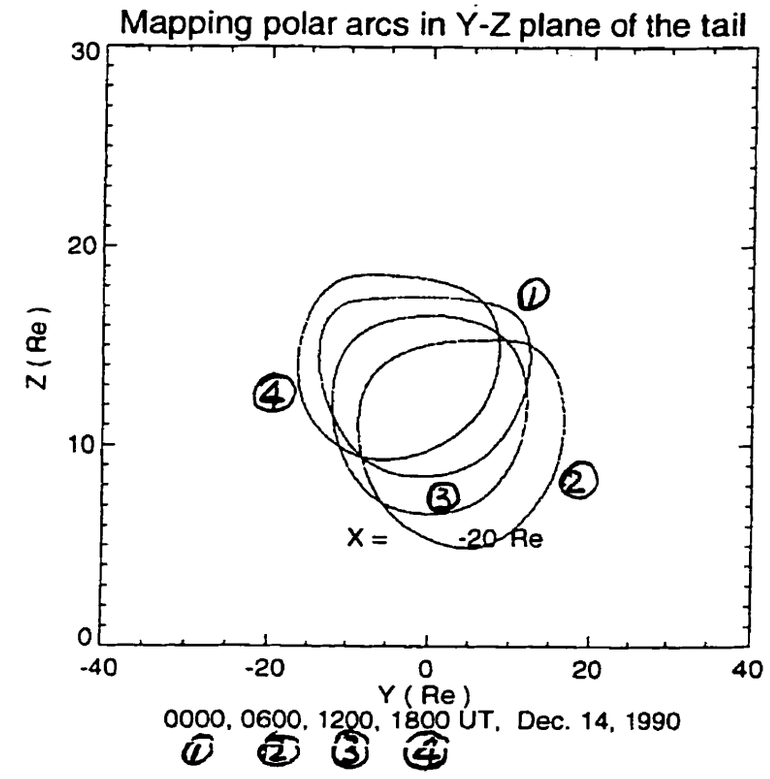

Figure 5.4: The same as Fig. 5.2, but $K_p = 4$.

The arc segment appeared about 1058 UT in the left (midnight) sector of the field of view. By 1126 UT the arc had extended through half the field of view of the ASC in the sunward direction and by 1130 UT it stretched across the whole field of the ASC. Structures were evident in the arc by 1138 UT and these showed as periodic folds in the arc by 1140 UT. The arc moved slowly south (from dusk to dawn) during this 15 minute period. The arc returned to a stable form by 1144UT, moved back toward the dusk sector during the following 20 minutes, and disappeared by 1230 UT. A second short-lived arc appeared in the midnight sector around 1216 UT and extended to the dayside crossing the zenith at 1217 UT. It disappeared before 1225 UT. The images of the polar arc at 1124:20 (t_1), 1125:13 (t_2) and 1129:33 (t_3) UT were selected to map the precipitated electrons causing the polar arc into the magnetotail.

The polar arc mapped to the Y-Z plane in the magnetotail at X=-20 and -40 R_E at t_1 as shown in Fig. 5.6. Fig. 5.6a shows that the source of the arc is parallel to the Z-axis at X=-20 R_E and covered from Z=10 R_E to Z=12.5 R_E and from Y=1 R_E to 1.5 R_E. The closed line was the mapped edge of the ASC viewing field at the ionospheric height of 150 km. Fig. 5.6b shows the electron source of the polar arcs located between Z=11.5 and 15 R_E ; Y=1 and 1.5R_E at X=-40 R_E of the magnetotail.

Fig. 5.7 is a mapped image of the polar arc at t_2. Fig. 5.7a shows the source of the polar arc was still parallel to the Z axis and extended from Z=10 R_E to Z=12.5 R_E. In Y direction, it covered from Y=0.7 R_E to Y=1.3 R_E. It was very close to the central line Y=0. Fig. 5.7b is similar to Fig. 5.7a, but at X=-40 R_E. The difference is that the mapped image of the polar arc was located between Z=11.5 R_E and Z=16.5 R_E. The Y range is from 1 R_E to 1.6 R_E.

The mapped image of the polar arc at t_3 is indicated in Fig. 5.8. Fig. 5.8a shows the mapped image at X=-20 R_E in the magnetotail. The source of the polar arc covered from Z=9 R_E to Z=16 R_E and from Y=0.3 R_E to 1.2 R_E. In addition to the electron source for the original arc, a new electron source for a new arc appeared on the right side of the original one. Fig. 5.8b shows the source of the arc at X=-40 R_E located from Z=10.2 to 19.8 R_E and from Y=0.3 to 1.5 R_E.

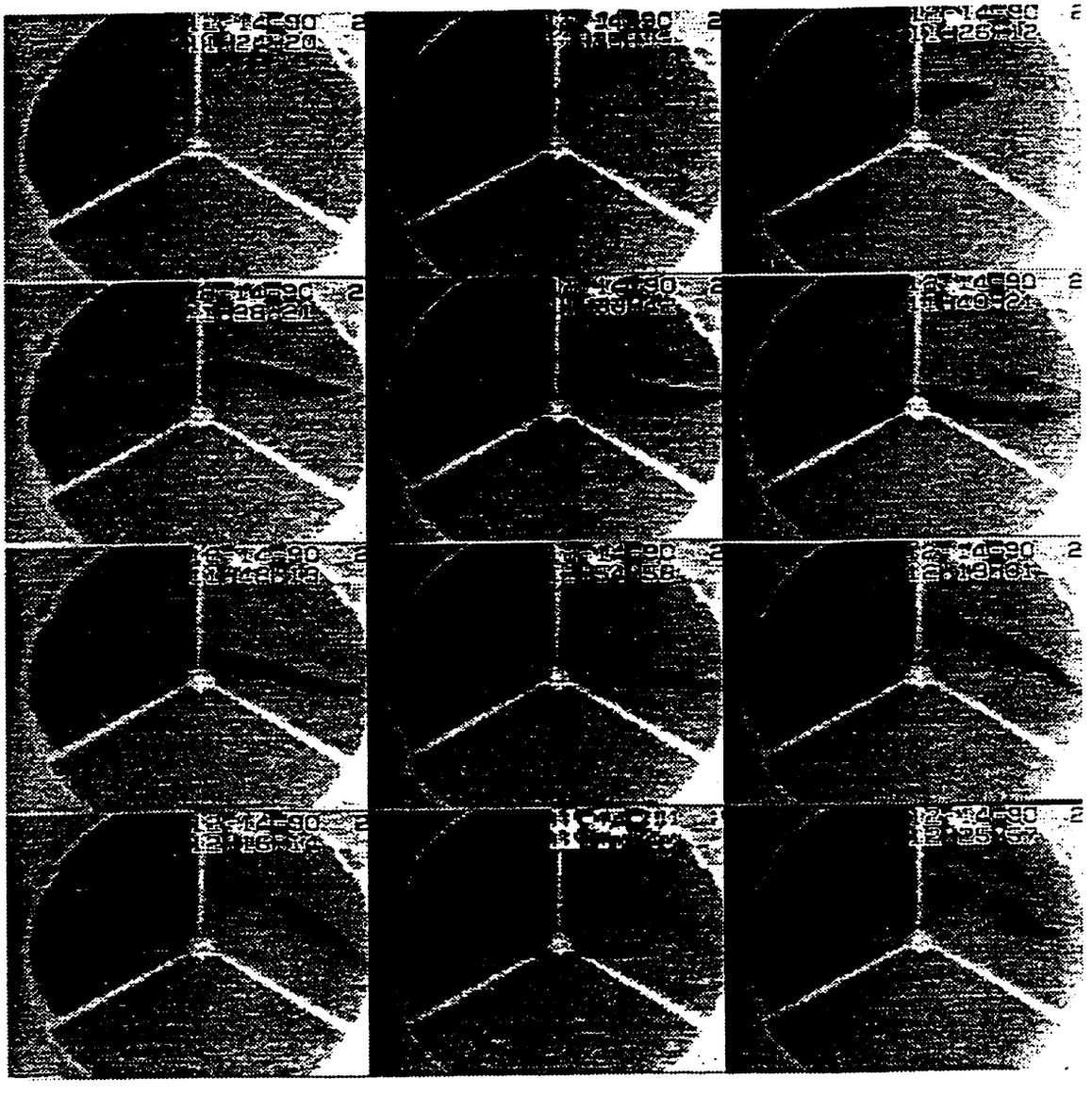

Figure 5.5: A sequence of the ASC images of a polar arc observed on December 14, 1990 at Eureka from 1124 to 1225 UT.

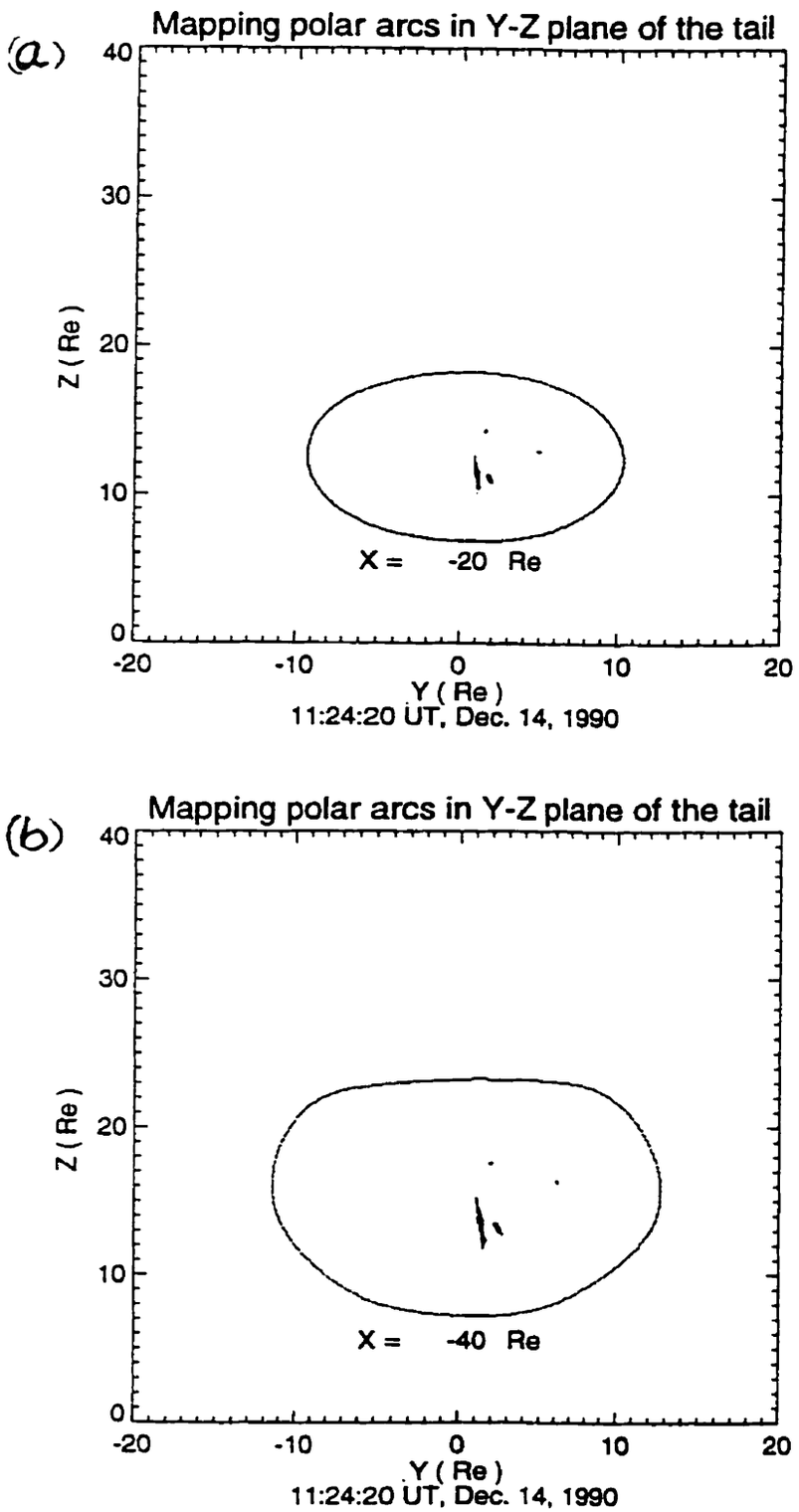

Figure 5.6: The polar arc observed at 1124 UT on December 14, 1990 mapped into two Y-Z cross sections: (a) X=-20 R_E, (b) X=-40 R_E)

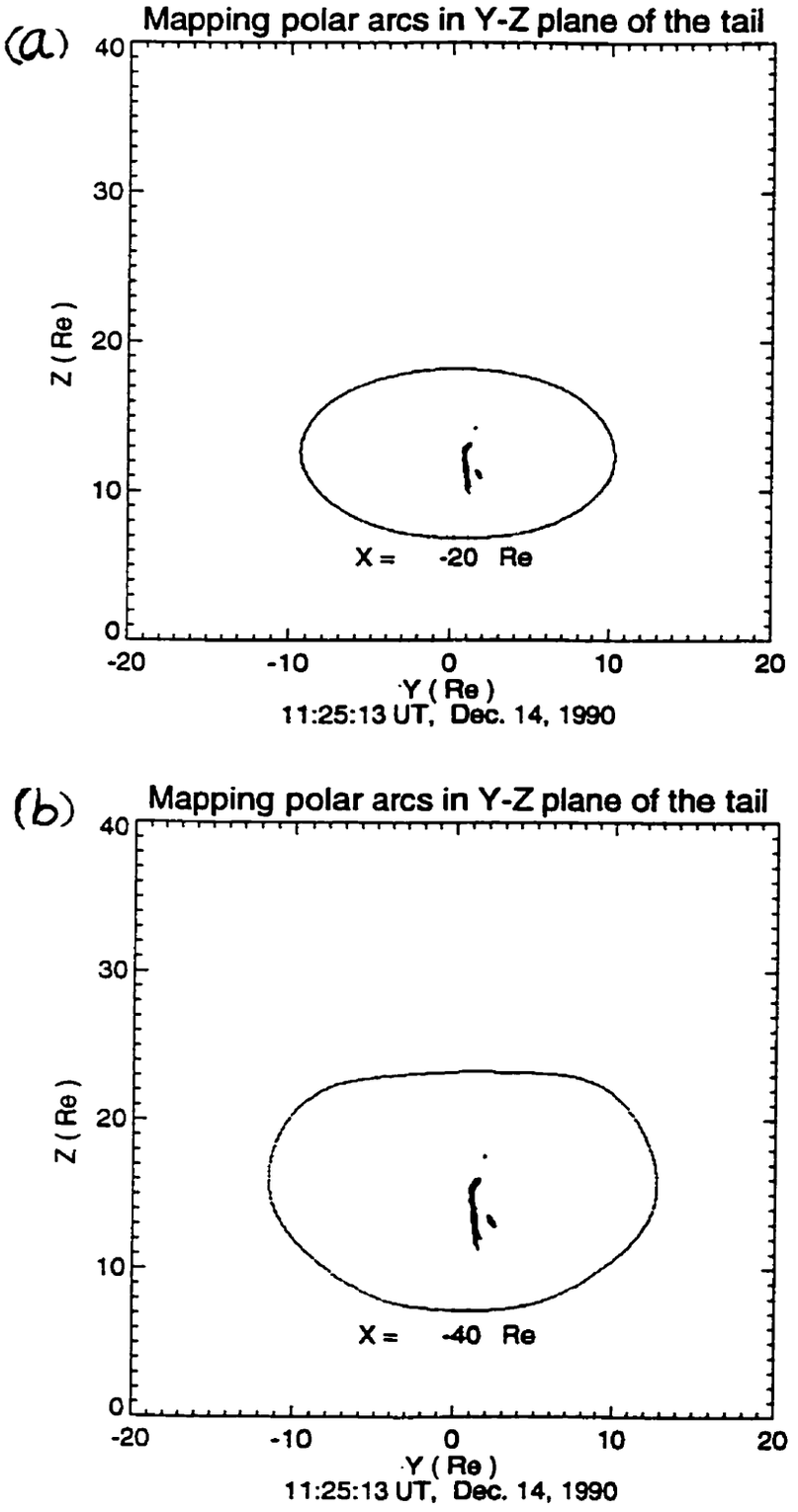

Figure 5.7: The polar arc observed at 1125 UT on December 14, 1990 mapped into two Y-Z cross sections: (a) X=-20 R_E, (b) X= -40 R_E)

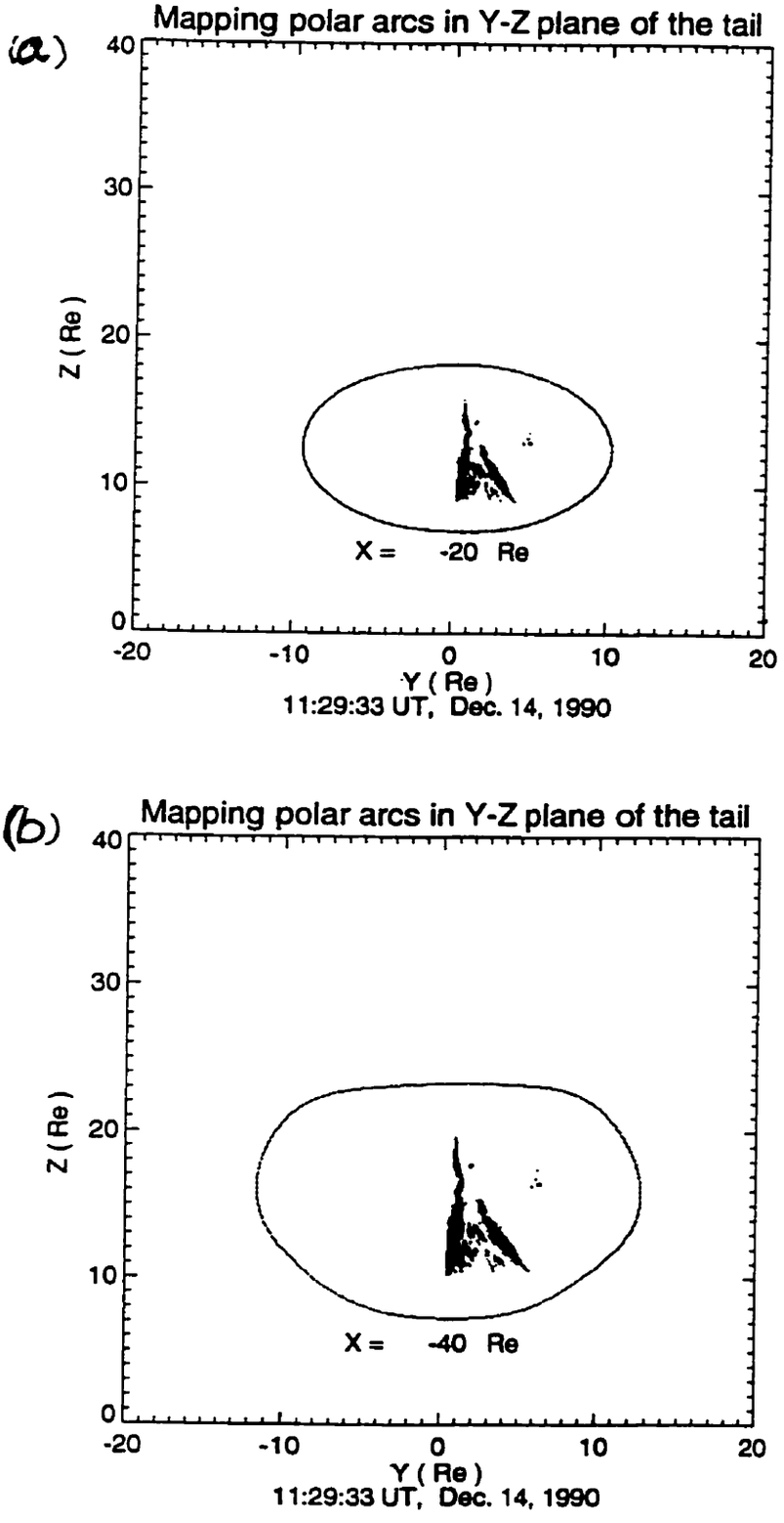

Figure 5.8: The polar arc observed at 1129 UT on December 14, 1990 mapped into two Y-Z cross sections: (a) X=-20 R_E, (b) X= -40 R_E)

5.3.3 November 1, 1991

A bifurcated polar arc was observed on November 1, 1991 (see Fig. 3.12). One of the ASC images (at 0442 UT) was used for the mapping. Fig. 5.9a shows how the bifurcated sun-aligned arc was mapped into the Y-Z plane in the magnetotail at X=-20 R_E. Similar to the figures in subsection 5.3.2, the mapped image of the polar arc was nearly parallel to the Z axis and was located between 13 and 16 R_E from the equatorial plane. The mapped image of the polar arc covered about 1 R_E in the Y direction (Y=2 to 3 R_E). Fig. 5.9b shows a mapped image of the polar arc at X=-50 R_E. The mapped image covered a region from Z=18 to 23 R_E and Y=3 to 4.5 R_E. The mapped polar arc was near parallel to the Z axis but with a 1.5 R_E extension in the Y direction. The T89 model indicates that the field lines from the polar arc traversed the magnetotail lobe, well above the central plasma sheet as shown by Fig. 5.9a. The bifurcation occurred in the Y direction.

5.3.4 November 15, 1993

An especially bright and long-lived polar arc occurred on November 15, 1993. It first appeared around 0730 UT in the dawn sector of the central polar cap, and lasted for about 10 hours. Fig. 3.1 shows a sequence of the ASC images of the polar arc from 0742 to 1218 UT. In these images geographic north is at the top and the sun direction is to the right-upper corner around 0900 UT (the arc shown is sun-aligned). The arc was weak, diffuse and stable (about 500 R at 557.7 nm emission) from 0730 UT to about 0900 UT, remaining in the dawn sector. Its intensity then increased to 2-3 kR by 0921 UT and it moved duskward to the zenith at Eureka by 1100 UT. It reversed its motion up to 1143 UT. It began to move duskward again after 1143 UT and reached the maximum intensity of 20 kR (557.7 nm) at 1148 UT. The arc co-rotated with the Sun during its lifetime, retaining sun-alignment. The IMF B_z remained northward during the whole lifetime of the arc. Fig. 5.10 is a plot of the 3 components of the IMF on November 15, 1993 from 0000 UT to 2000 UT.

The arc was also recorded by all-sky imagers at Resolute Bay ($74.7°N, 265.1°E$)

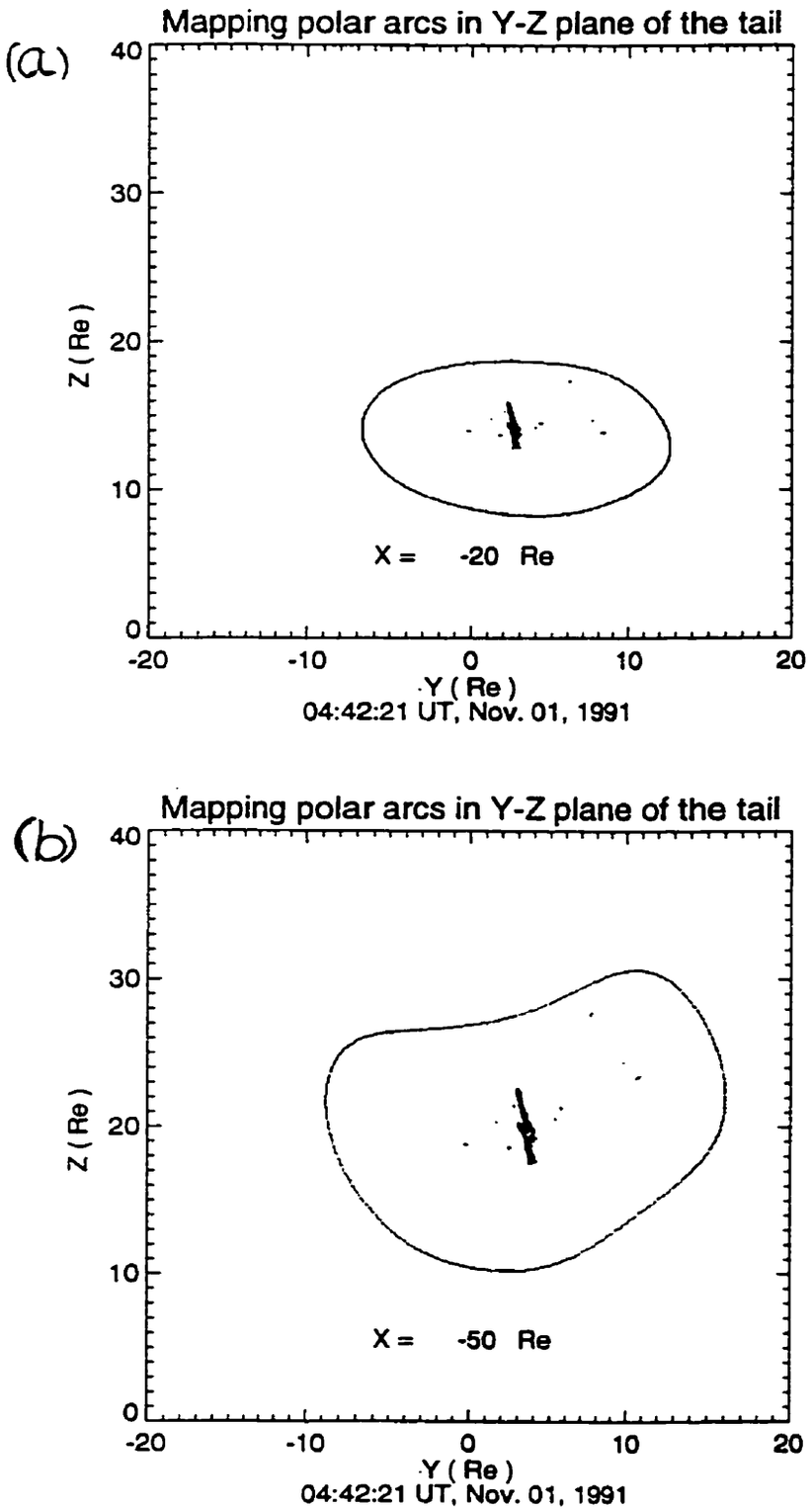

Figure 5.9: The bifurcated polar arc observed on November 1, 1991 at 0442 UT was mapped into the Y-Z cross sections in the magnetotail at (a) X=-20R_E, (b) X=-50 R_E.

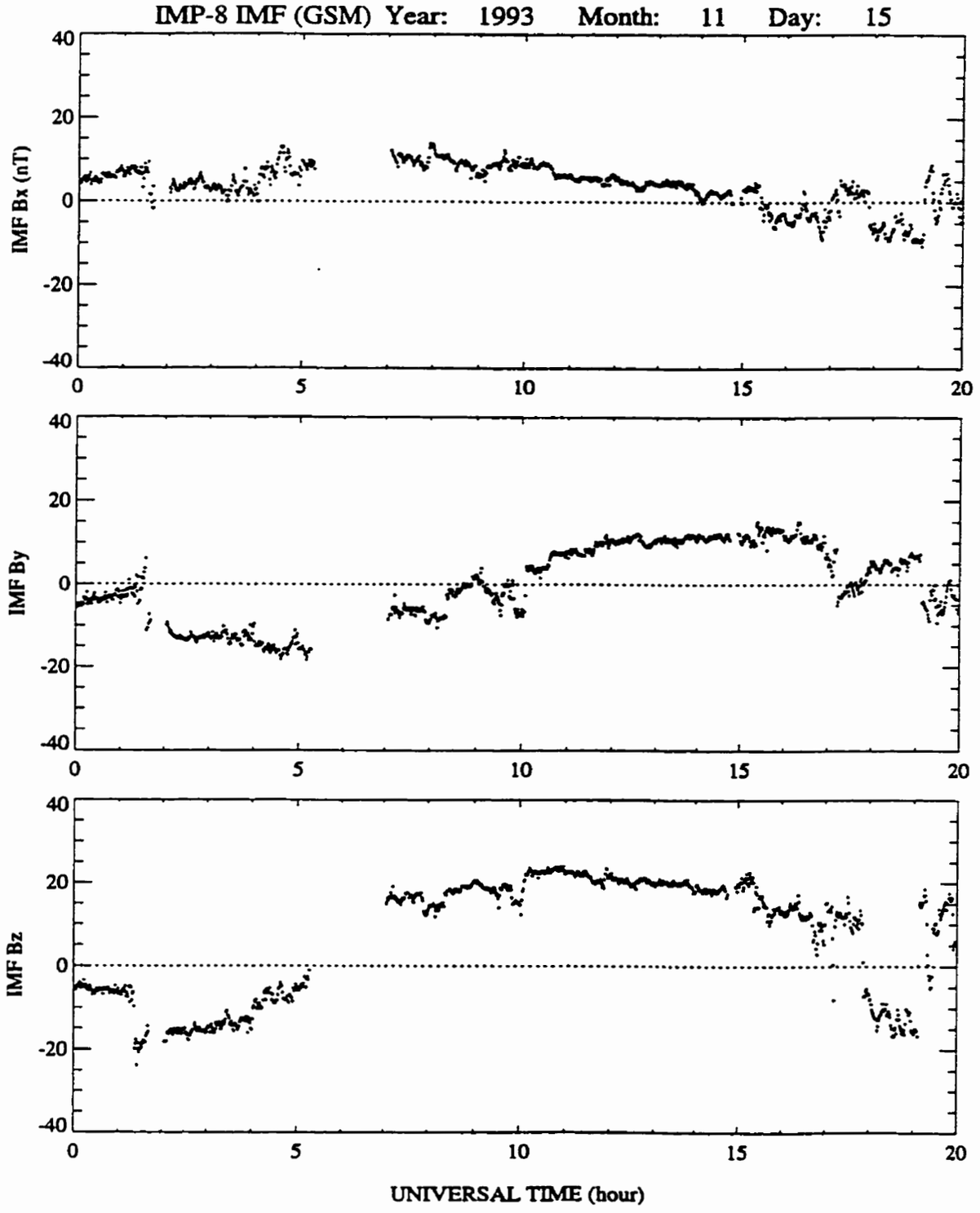

Figure 5.10: A plot of IMF B_x, B_y and B_z components (GSM) from 0000 UT to 2000 UT on November 15, 1993.

and Cambridge Bay ($69.1°N, 255.0°E$). These imagers had overlapping fields of view with a latitude coverage extending from the central polar cap to the auroral oval. Fig. 5.11 shows the polar arc as recorded by all three imagers at 0921 UT, projected into geographic coordinates. Here the sunward direction is toward the upper right corner. The arc extended over both Resolute Bay and Cambridge Bay to the proximity of the poleward edge of the nightside auroral oval. This polar arc was also seen by an ASC at Thule, Greenland. It was identified as a transpolar arc. The transpolar arc and the poleward edge of the auroral oval were mapped into the magnetotail. Fig. 5.12a and b show the location in the Y-Z plane when the transpolar arc and the part of poleward edge of nightside auroral oval were mapped into the magnetotail. Fig. 5.12a indicated auroras at the poleward edge of the nightside auroral oval were mapped into region of Z $\leq$ 4 R_E at X=-50 R_E, where the plasma sheet is located. On the other hand, the transpolar arc was mapped into the region above Z=4 R_E, where the plasma sheet boundary and the magnetotail lobe are located. Fig. 5.12b indicated the cross section of the mapped transpolar arc at X=-60 R_E expanded compared to that in Fig. 5.12a. The auroras at the poleward edge of the midnight auroral oval and part of the transpolar arc could be mapped into the negative Z region at a tail distance larger than 60 R_E. This implies the aurora was on closed field lines.

5.3.5 February 21, 1994

A major magnetic storm ($K_p = 7+$) was observed on February 21, 1994. It followed a sudden commencement (SSC) at 0900 UT and was related to a magnetic compression caused by a coronal mass ejection (CME) which resulted in a fast (1300 km/s) shock which reached the magnetopause. A very bright (up to 80 kR, 557.7 nm) polar aurora was recorded almost at the same time with the storm. The auroral onset at the magnetic pole was at 0920 UT [McEwen, 1994]. Fig. 5.13 is a sequence of the ASC images of the polar aurora from 0924 UT to 0938 UT. The aurora moves in both from the midnight sector and from the noon sector and by 0937 UT the whole central polar cap was filled with aurora. The forms are not sun-aligned as the Sun was in the upper right direction around 9:30 UT. The aurora at 0930:44 UT was selected for mapping

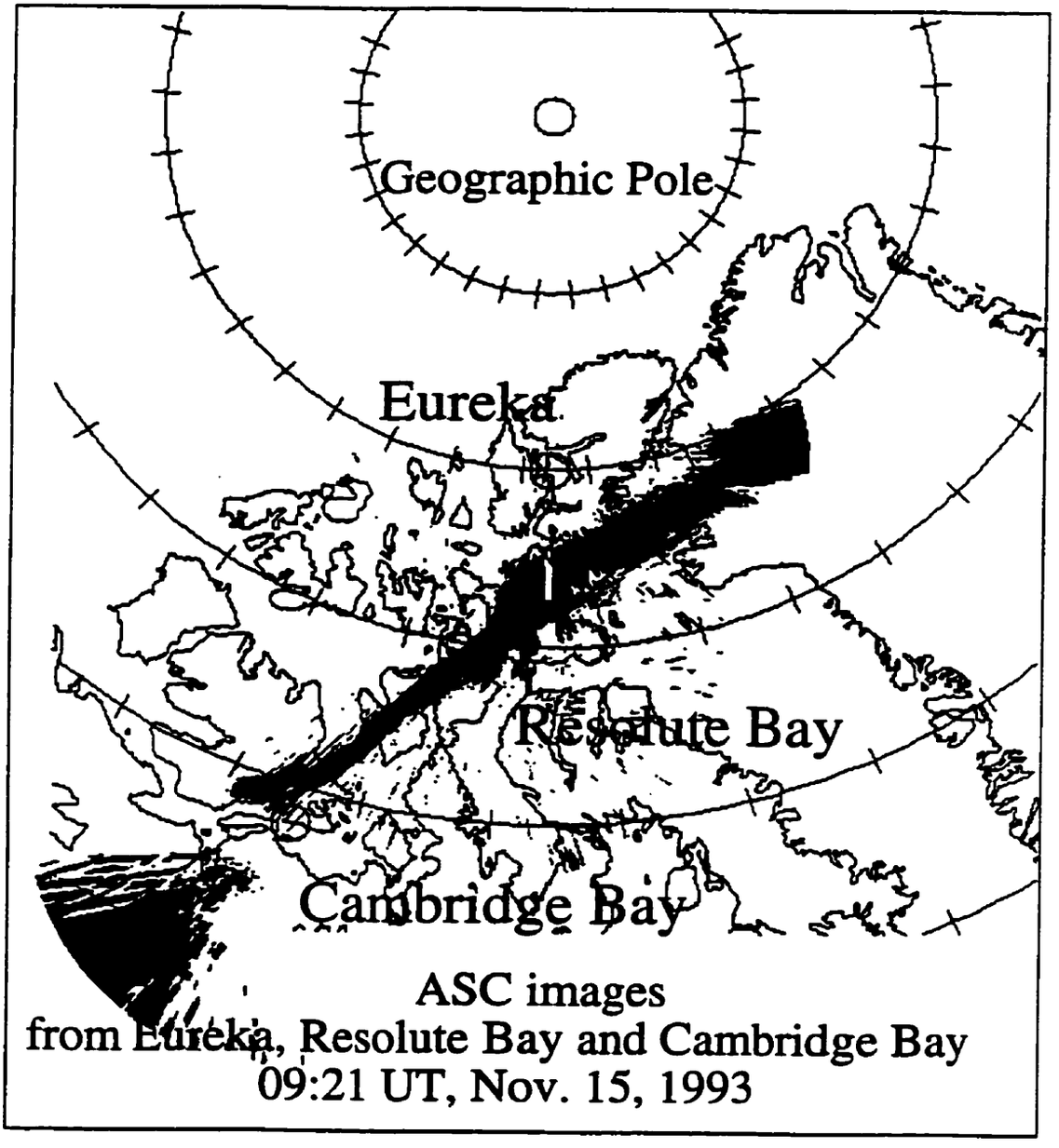

Figure 5.11: A transpolar arc observed on November 15, 1993. It was seen by ASCs at Eureka, Resolute Bay and Cambridge Bay. The diagram shown here is the transpolar arc after it is projected into geographic coordinates. The luminosity in the lower left corner is the poleward edge of the auroral oval.

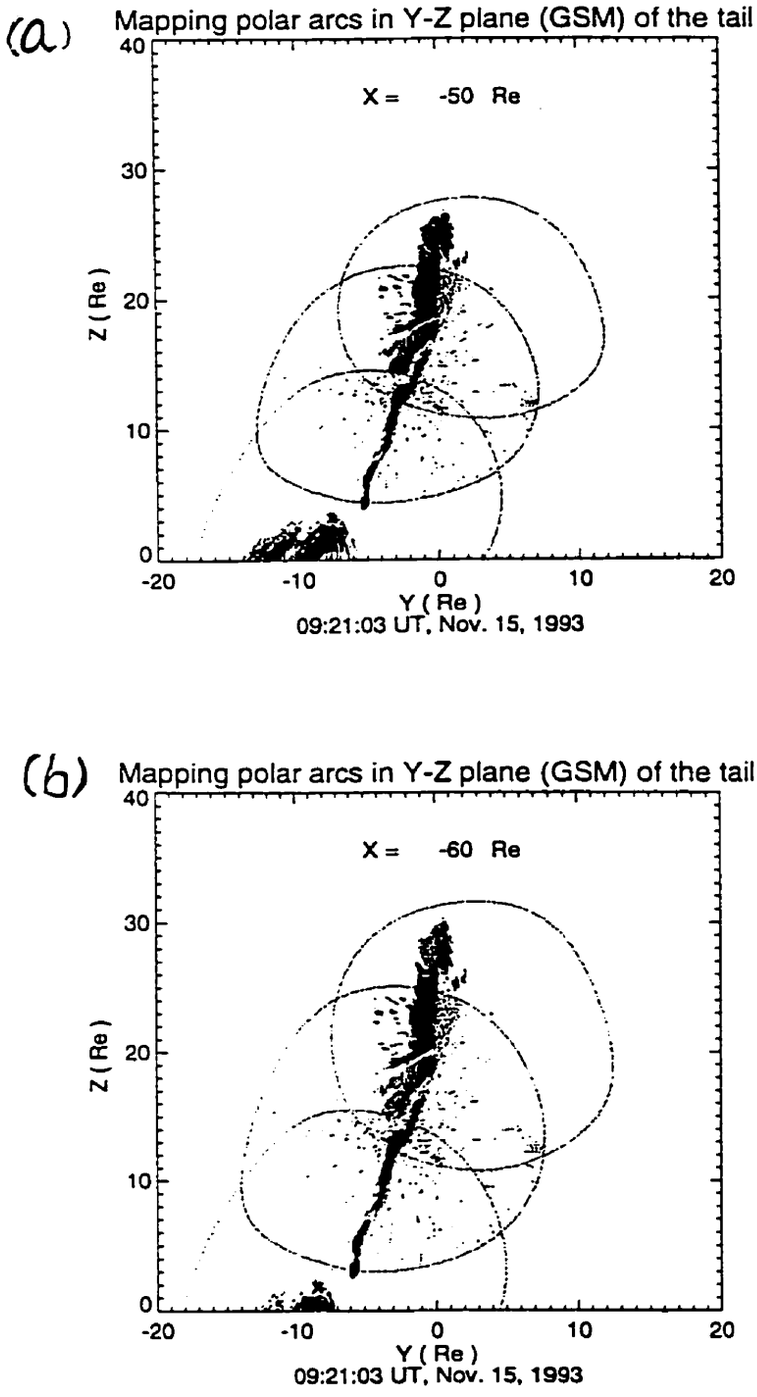

Figure 5.12: The transpolar arc observed on November 15, 1993 mapped into the Y-Z cross sections in the magnetotail. (a) X=-50R_E, (b) X=-60 R_E.

into the magnetotail. The ASC sequence also shows the polar arc came from the midnight side auroral oval and moved into central polar cap. Fig. 5.14a is the cross section of mapping lines in Y-Z plane at X=-30 R_E. The figure shows that the polar arcs was almost parallel to the Y axis (equatorial plane). This is also the evidence that the original polar arc was midnight auroral oval aligned. As the polar arc was near the poleward edge of the auroral oval, the mapping indicated that the upper boundary of the plasma sheet expanded to up to Z= 16 R_E from its normal position of Z= 3 $\sim$ 5R_E. Fig. 5.14b is a similar plot to Fig. 5.14b, but at X=-60 R_E. This figure shows the polar arc tilted anti-clockwise. The field of view of the ASC was compressed near Y=0 due to the strong cross-tail current during the magnetic storm.

Mapping of the arc was also viewed in the X-Z plane (see Fig. 5.15). The shaded area in the figure indicates the extension of the plasma sheet into the deep magnetotail in the equatorial plane. The dotted vertical lines are the X positions where the arc was mapped in the Y-Z cross sections as shown in Fig. 5.14 for X=-30 and -60 R_E. The mapped positions of the arc for X =-40, -50, -70, -100 and -120 R_E are also shown with dotted vertical lines. The dashed lines show the upper and lower limits (in the Z direction) of the magnetic field tracing lines from the arc. The traversed region is well above the equatorial plane ($Z > 10R_E$) with ($-70R_E < X < -30R_E$). The lower two dashed lines correspond to the mapping of the small arc (see Fig. 5.14). As the boundary of the normal plasma sheet is about 3-5 R_E from the equatorial plane, the plasma sheet or plasma sheet boundary appears to have expanded into the magnetotail lobe region during the magnetic storm of February 21, 1994.

5.4 Possible source regions of polar arcs

The mapping of different polar arcs in the last section showed that different polar arcs were mapped into different regions in the magnetotail. Typical polar arcs were mapped into the northern magnetotail lobe. Transpolar arcs were mapped into plasma sheet boundary layer and the magnetotail lobe regions. Those auroras near the poleward edge of the auroral oval were mapped into the plasma sheet or expanded plasma sheet.

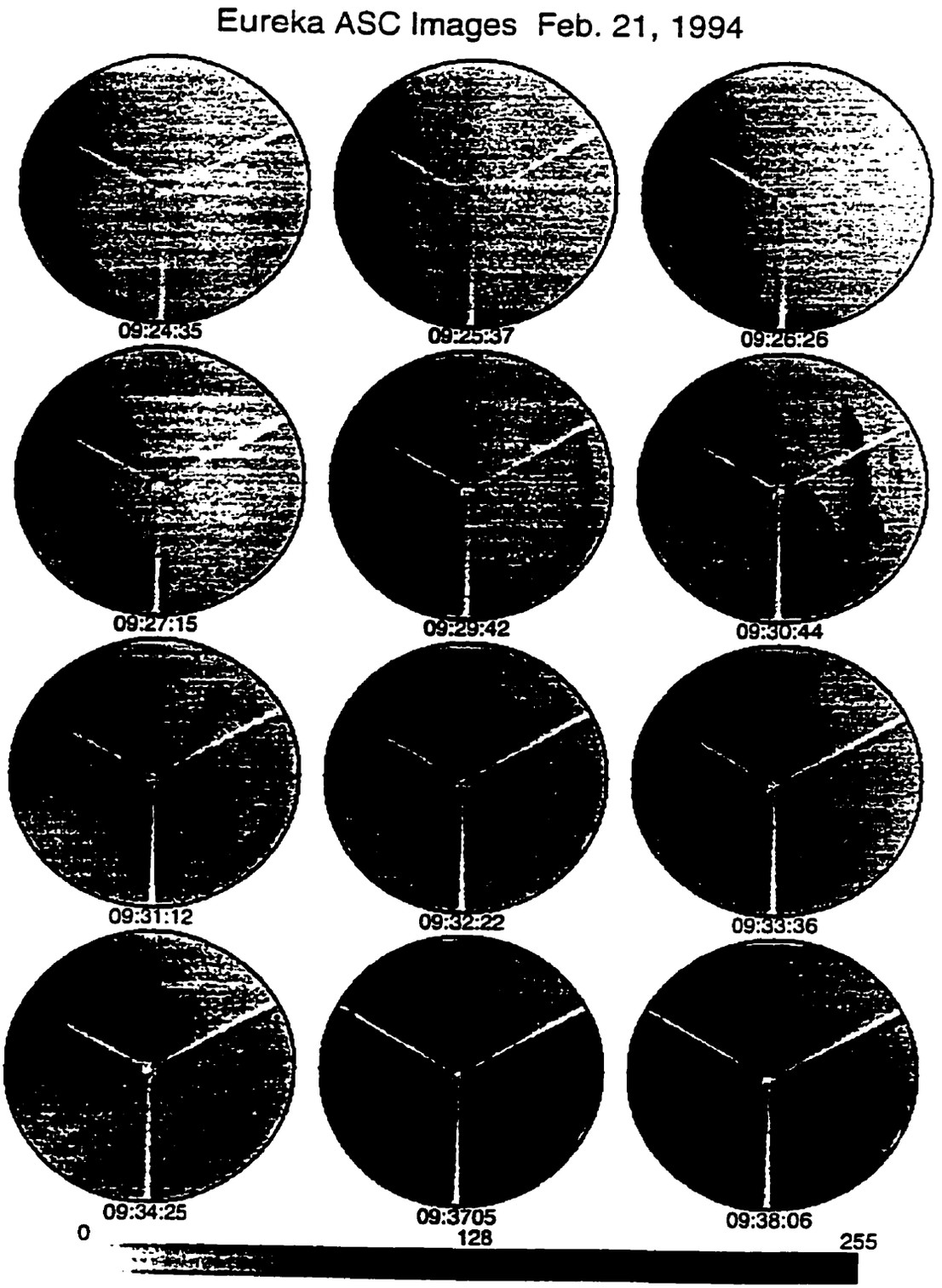

Figure 5.13: A selected sequence of ASC images of polar arcs observed on February 21, 1994.

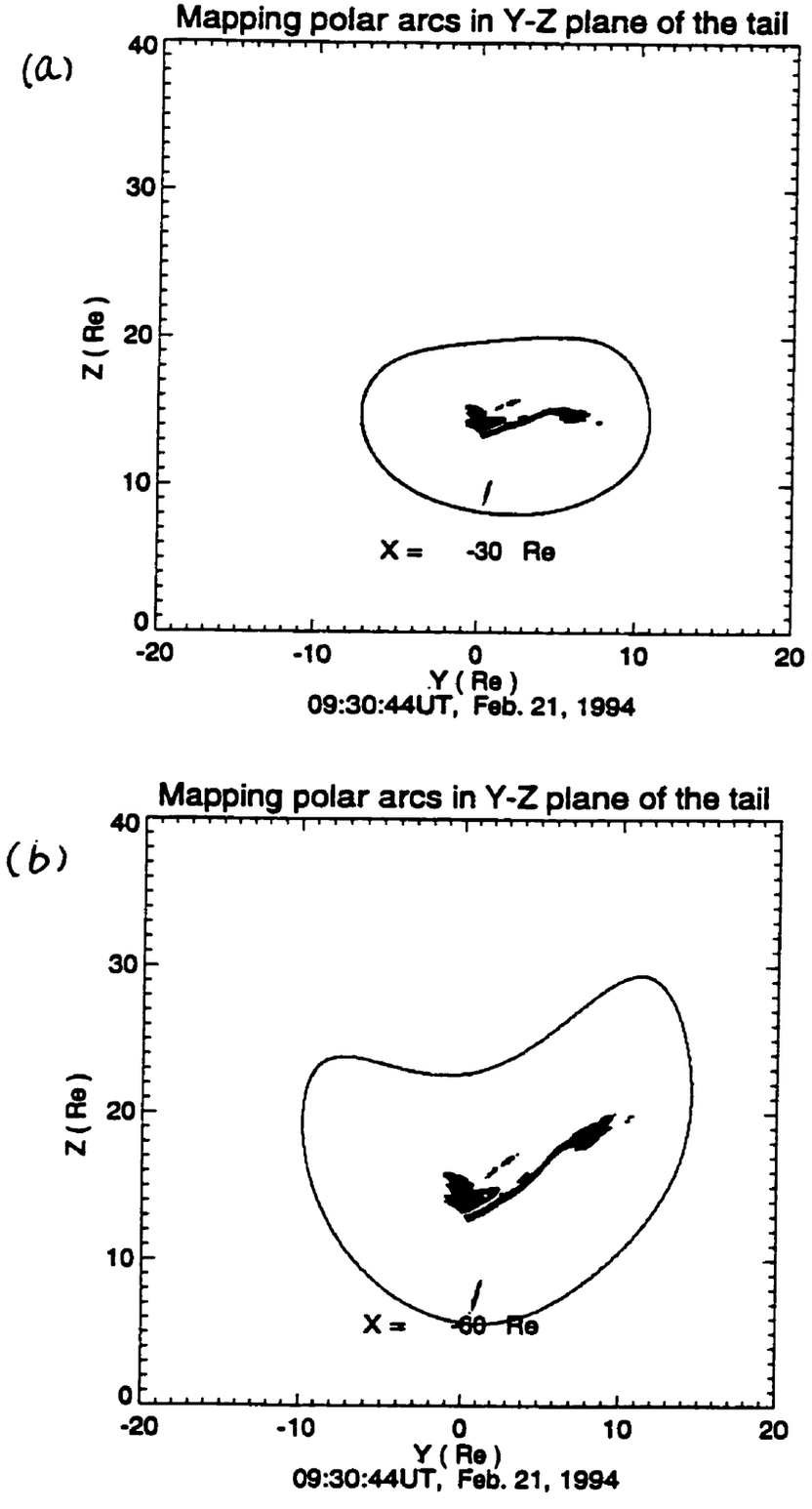

Figure 5.14: The polar arcs observed at 0930 UT, February 21, 1994 mapped into the Y-Z plane in the magnetotail: (a) X=-30 R_E, (b) X=-60 R_E.

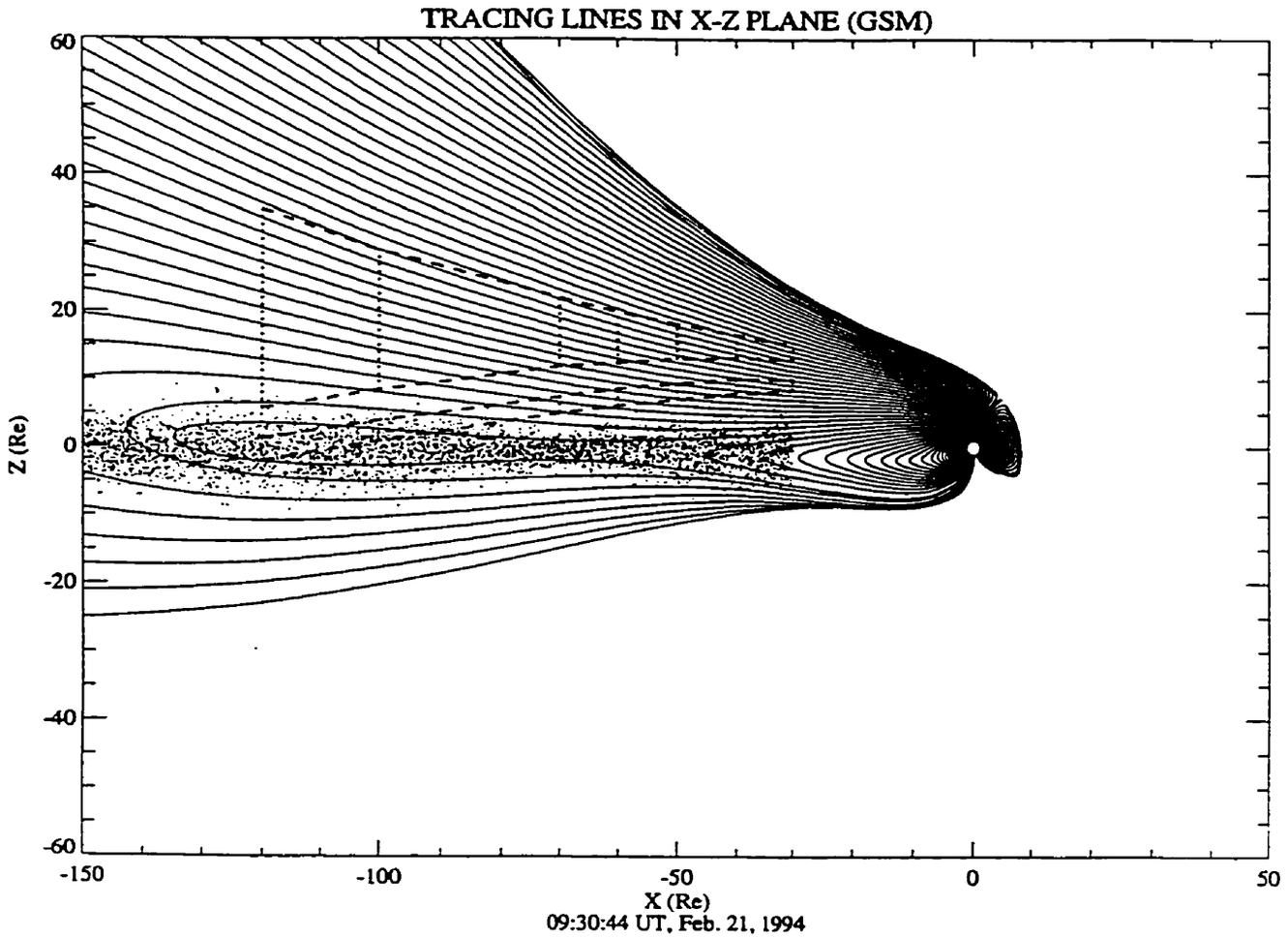

Figure 5.15: A sketch of mapping regions in the X-Z plane (GSM) for the arcs observed at 0930 UT on February 21, 1994. The shaded region shows the extension of the plasma sheet into the deep tail in the equatorial plane. The dotted vertical lines show the X positions where the arcs were mapped in the Y-Z plane. The dashed lines show the upper and lower limits of the tracing lines from the arc. The lower dashed lines show the mapping of the faint arc equatorward of the main arcs.

Chapter 6

Discussion of results

6.1 Introduction

This thesis involves a detailed study of the occurrence and characteristics of polar auroras, the influence of the solar wind on initiation of polar arcs and the mapping of these arcs to their source regions in the magnetosphere and beyond. The detailed results were shown in Chapters 3, 4 and 5 respectively. The special location of Eureka enables one to view all 24-hr local magnetic sectors at any time. The data set formed a firm base for a statistical study of polar arcs and their relation to activity in the interplanetary medium. Details of statistical results and their relations to solar wind, IMF and geophysical indices are interpreted. Their applications are discussed.

It was found that there is a diurnal variation in the occurrence pattern of polar arcs. Polar arcs occurred under either northward or southward IMF B_z conditions but the major number were associated with northward IMF B_z. Most polar arcs have a short lifetime. It is also found that polar arcs generally occurred uncorrelated with K_p levels. High solar wind dynamic pressure, especially solar wind dynamic pressure enhancements appear to play a crucial role in inducing polar arcs. The time delay between the enhancements and the polar arcs was much longer for northward IMF B_z than for southward IMF B_z. Mapping of the polar arcs by using the T89 magnetic model predicts that the electron source region for polar arcs is mainly in the magnetotail lobe.

6.2 Occurrence patterns of polar arcs

The occurrence patterns of polar auroras were studied using optical data from an ASC located at Eureka during the 4 winter periods since 1990-91. The ASC had a sensitivity threshold of 300 R (557.7 nm), so the data from the ASC to be discussed here pertain to all auroras recorded at Eureka having intensities above about 300 R (557.7 nm). From the location near the magnetic pole, the region observed extended down to about 80° CGM and covered all magnetic local time sectors. The dawn-dusk scans of the MSP with sensitivity threshold of 50 R (557.7 nm) enable one to detect weaker polar arcs.

6.2.1 Frequency of occurrence

Polar arcs with intensity above 300 R (557.7 nm) were observed in the central polar cap (above 80° CGM) from images recorded by the ASC about 8 % of the time on average. The frequency of occurrence declined from 8.7 % and 9.3 % of the time during the 90-91 and 91-92 winter periods to about 6.5 % of the time during the 93-94 winter period. Early satellite observations of polar arcs showed that sun-aligned arcs with intensity above 500 R (557.7 nm) were observed on 6 % of northern polar cap passes above 80° CGM latitude during winter seasons [Ismail *et al.*, 1977]. This is consistent with the ASC measurements. Polar arcs with intensity above thresholds of approximately 50 R (557.7 nm) and 50 R (630.0 nm) were observed 30 % and 49 % of the time respectively from meridian scans recorded by the MSP operating at Eureka during a 38 day test period in the 1993-94 winter. This shows that polar arcs are present almost all the time when the IMF B_z is northward, as most polar arcs were detected with northward IMF (which appears almost half of the time). The higher frequency of detection of auroral 630.0 nm emissions compared to 557.7 nm emissions suggests that the precipitated electrons which caused the polar arcs were often soft (much less than 1 keV of energy). This disagrees with the preliminary study of electron energies inferred for several arcs (Fig. 3.21 to 3.23) which gave average energies well above 700 eV. In general, polar arcs are very faint. Fully three quarters of them have intensity below 300 R. This places them below the threshold of most satellite imagers. Of the more intense arcs, the brightening was only transient (lasting a few minutes) and when

that occurred the arc usually became unstable, with accompanying motion or splitting into 2 or more arcs. Observation of polar arcs with an ASC (50 R sensitivity at 630.0 nm) at Qaanaaq ($77°N, 69°W$ geographic) showed that polar arcs occurred at least 40 % of the time [Valladares *et al.*, 1994]. This is similar to Eureka MSP results. The frequency of occurrence of 49 % of the time (630.0 nm emission) at Eureka supports the prediction of Carlson [1990] that polar arcs occurred one-half of the time or whenever the IMF B_z is northward. All these results show that polar arcs occur very often, not only occasionally as earlier studies suggested. If instruments with higher sensitivity are used to detect polar auroral emission over the whole polar cap , then polar auroral emissions may be found to occur quasi-continuously.

6.2.2 Temporal effects

Polar arcs were observed more frequently during and following the midnight hours (0400 - 1500 hrs UT) than during the daytime hours (see Fig. 3.5). This diurnal variation was fitted by a sinusoidal curve with an amplitude of nearly 40 % of the mean occurrence (8 % of the time). The maximum of the distribution in Fig. 3.5 locates around 1000 UT and the minimum around 2200 UT. This diurnal variation could be explained by the region in the magnetotail which was magnetically connected with the ASC field of view in the ionosphere. This magnetotail region changes with time of day as illustrated in Fig. 6.1 for the Y-Z plane (GSM). Fig. 6.1 shows that the region in the magnetotail between 0600 UT and 1200 UT located at the lower part (which is nearer to the line of Z=0 R_E) in the Y-Z plane, in comparison with the other three areas at 0000 and 1800 UT. It also covers the larger area in the Y-Z cross section. Thus, between 0600 and 1200 UT the central polar cap maps to the region closer to the central plasma sheet which at the equator (Z=0 R_E) has a thickness of only about 6 R_E. Also, it maps to the larger cross-sectional area during the hours between 0600 and 1200 UT (0000 and 0600 local time at EUreka). Satellite observations indicate that the plasma in the central plasma sheet and the adjacent plasma sheet boundary layers are usually energetic and are the source of precipitated electrons in the auroral oval. Those energetic plasmas sometimes intrude into the magnetotail lobe region [Huang

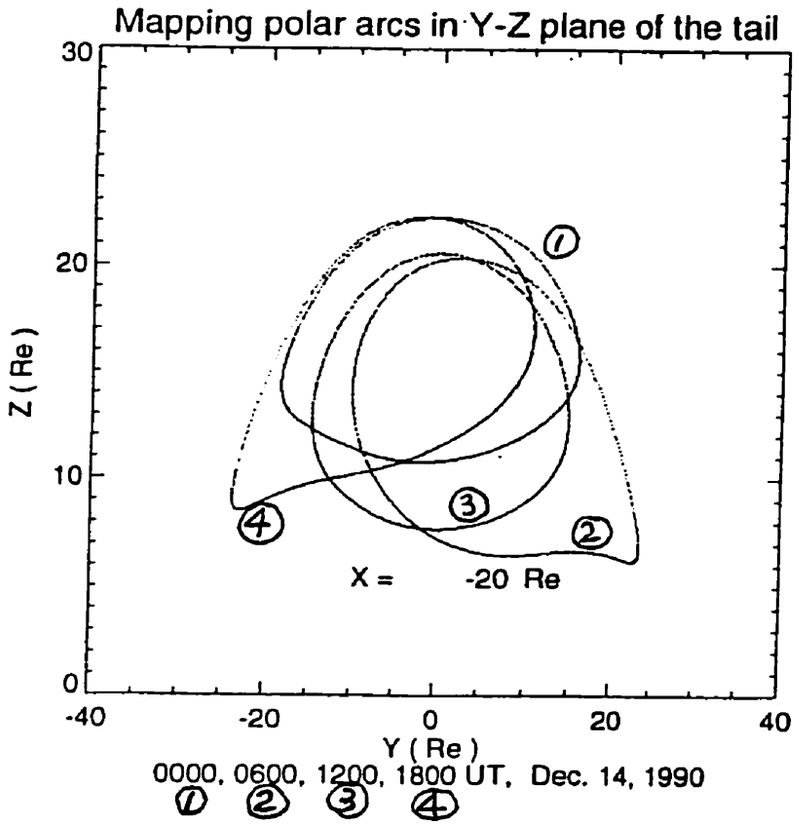

Figure 6.1: The Eureka ASC viewing area in the magnetotail (Y-Z plane at X=-20 R_E) variations with UT or local magnetic time during winter season in northern hemisphere. The closed lines numbered 1,2 3 and 4 correspond to 00, 06, 12 and 18 UT, Dec. 14, 1990.

et al., 1987, 1989] where the Eureka ASC viewing area links, to in the magnetotail. Therefore, the closer to the central plasma sheet the ASC viewing area is, the higher the probability of observing energetic electron precipitation and polar arcs. As well, the larger viewing area at local midnight provides a higher probability of observing electron precipitation and polar arcs. This may explain why the occurrence pattern of polar arcs has a diurnal variation.

6.2.3 Lifetime and characteristic time scale

The distribution of lifetimes of polar arcs (Fig. 3.7a) indicates that more than half of the observed 656 polar arcs with intensity above the threshold of 300 R have lifetimes less than 20 minutes. This suggests polar arcs are mostly transient phenomena and the magnetosphere is quite dynamic. However, there are several cases of polar arcs lasting 1-2 hours or more. The transpolar arc observed on November 15, 1993 lasted for 10 hours and it is one good example of a very stable polar arc [Zhang *et al.*, 1994]. The IMF B_z was positive and stable during the period of this transpolar arc (see Fig. 5.10). This suggests that the magnetosphere is stable during the periods of long lifetime polar arcs. Pudovkin [1977] found that all modes of convections in the polar cap due to a change of IMF (southward, northward or in azimuthal components) are formed within 15-25 minutes. A study of the correlation between solar wind , IMF parameters (observed by ISEE 3) and magnetospheric activity (AE, D_{st}) shows a typical, intrinsic 25 to 40 min time delay between the variations of interplanetary parameters and magnetospheric response during quiet periods and $\leq$ 15 min during disturbed times [Baker, et al., 1983]. These studies indicate that the time scale of the magnetospheric activities covers from 15 minutes to 40 minutes. The lifetime distribution (Fig. 3.7a) indicates that 50 % of the 656 polar arcs have lifetime less than 20 minutes and 75 % of the 656 polar arcs have lifetime less than 40 minutes. These facts suggest that the lifetime of polar arcs probably is influenced by the intrinsic time scale of the magnetosphere. This observed distribution of lifetimes is instrument-dependent. With greater instrument sensitivity arcs are seen much more frequently and last longer. In fact they may be quasi-continuous during all periods when the IMF B_z is northward. They then can be a useful means of diagnostic studies of polar cap processes.

6.2.4 Special features of polar arcs

Wave structure, bifurcation and other special features of polar arcs were observed, though not very often. Fig. 3.9 shows the development of a straight arc into an arc with wave structure. It took a long time (75 minutes) to form a half-wave structure (within the field view of the ASC) and a short time (5 minutes) to form a full-wave structure.

Finally the arc took multi-wave structure. This process represents a typical nonlinear development of waves due to an instability. The development of wave structure of the arc suggests that the magnetosphere, or the coupling with the magnetosphere, is unstable in this case. The bifurcation of polar arcs when they brighten (Fig. 3.12, Fig. 3.13) further confirms that there is a kind of plasma instability which is related to the development of the features. The fast changing of IMF B_z and IMF B_y during the period of bifurcation of polar arcs suggests the process of bifurcation appeared to be controlled by the variation of the IMF. Other observed special features such as polar arcs changing shape (Fig. 3.10, Fig. 3.11) indicates the process may be very complicated. There is a common point in observations, that is the changing of shapes of the polar arcs takes place within a few minutes. This is a further evidence that those special features of polar arcs were developed from instabilities in the magnetosphere or ionosphere.

6.2.5 K_p level and polar arcs

The study of the relation between polar arcs and magnetic activity (K_p levels) indicates that they are at most, only weakly correlated. The similarity of the distributions of polar arcs and K_p level suggests they are independent of each other. Polar arcs occur not only with low level of K_p, but also high level of K_p. This is consistent with the fact that polar arcs occur under both northward and southward IMF conditions, as a high K_p level usually associated with southward IMF and a low K_p with northward IMF. Early studies in literature (e.g. Ismail *et al.*, 1977) showed that polar arcs were usually associated with low K_p levels. There are also some reports that polar arcs were observed with middle and high K_p levels [Elphinstone and Hearn, 1993]. These studies were based on short periods of observations or non-continuous observations (such as satellite observations). Polar arcs occurred most frequently at $K_p = 2$, but the most frequent K_p level is also at $K_p = 2$. This is why earlier reports (e.g. Lassen and Danielsen, 1978) found polar arcs usually occurred with low K_p levels. This also agrees with a conclusion that polar arcs are associated mainly with northward IMF B_z, which implies a low level of K_p. The polar arc distribution also shows that 10 % of the polar

arcs were observed under extremely high K_p level, from 5 to 7. Very large K_p levels are usually associated with southward IMF B_z which implies that polar arcs can occur with southward IMF B_z [Gussenhoven, 1990].

6.2.6 Solar activity and frequency of occurrence of arcs

With the four-winter polar auroral data, it is possible to investigate how solar activity affects occurrence of polar arcs. The solar activity level is usually presented by the solar 10.7 cm flux and sun-spot number. The continuous observations at Eureka through four winters indicate that the occurrence of polar arcs is positively correlated with the solar 10.7 cm flux and the sun-spot number. Fig. 6.2 shows details of the relation between the mean frequency of polar arc occurrence, the mean solar 10.7 flux and the mean sun-spot number of each winter period from 1990 to 1995. The diagram illustrates that polar arc occurrence shows the same general trend of decrease as the solar 10.7 cm flux and the sun-spot number. The mean frequency of polar arcs during the 1994-95 winter period is estimated from a preliminary analysis [Zhang, 1995]. The solar 10.7 cm flux and sun-spot number are just indicators of solar activity level. High solar activity suggests high solar wind activity (pressure, density, velocity etc.). This is a further evidence that the solar wind controls polar auroral activity on a large time scale.

6.2.7 Solar wind parameters and polar arcs

The distribution of the 208 polar arcs in relation to solar wind dynamic pressure (Fig. 3.20b) shows that most of the polar arcs occurred with low solar wind dynamic pressure. Those polar arcs appearing with low level of solar wind dynamic pressure evidently occurred due to release of stored energy in the magnetosphere. A fraction of the polar arcs associated with high solar wind dynamic pressure was most likely due to the extra energy the high pressure solar wind brought to the magnetosphere. Ionospheric projections of the magnetospheric regions under low and high solar wind dynamic pressure conditions suggest that solar wind dynamic pressure plays a crucial role in the interactions between the solar wind and the magnetosphere [Newell and Meng, 1994].

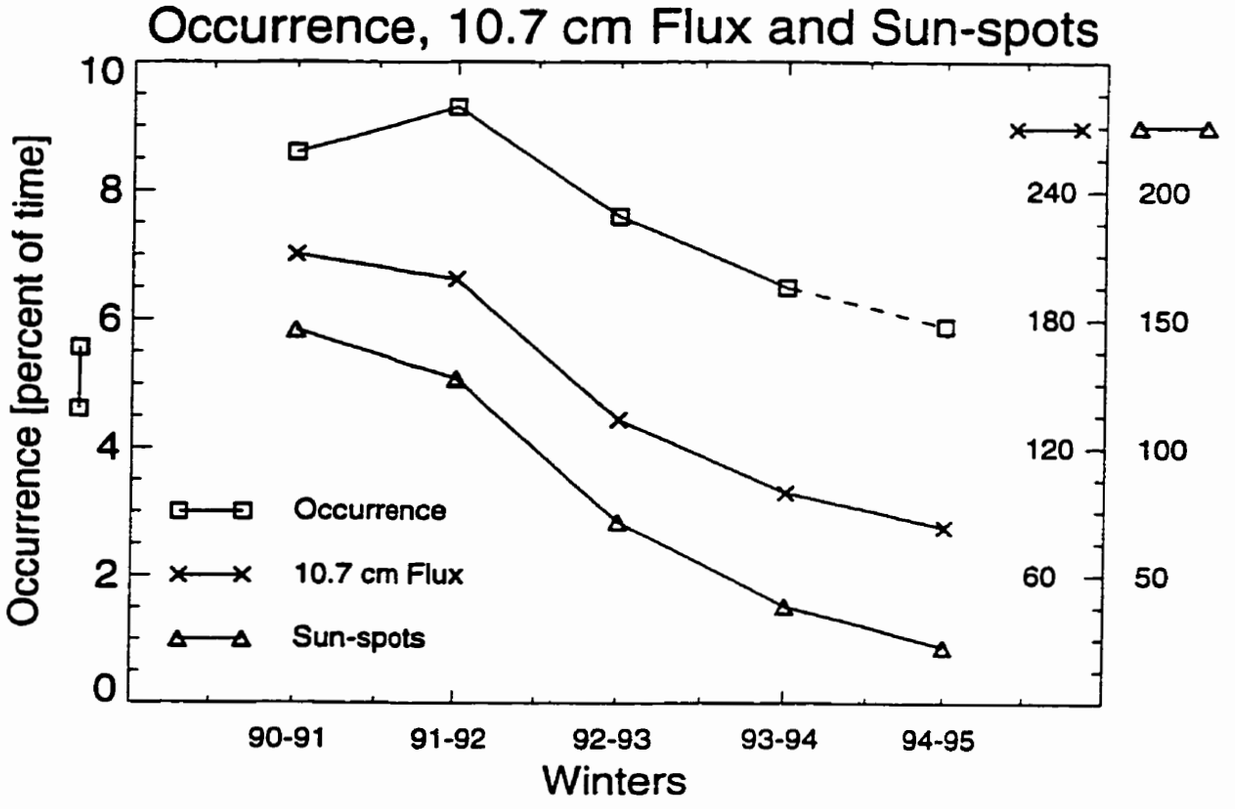

Figure 6.2: A comparison between mean percentage of the time with polar arcs, mean solar 10.7 cm flux and mean sun-spots number over each of the five winter periods from 1990 to 1995.

However, solar wind dynamic pressure does not appear to have a significant effect (see Fig. 3.20b) on occurrence of the polar arcs which resulted from the coupling of the magnetosphere and the ionosphere. A study of the relation between solar wind speed and polar arcs (Fig. 3.19a) suggests that solar wind speed does not have a significant effect on occurrence of polar arcs either. These results imply that most of the polar arcs occurred due to precipitated electrons which were accelerated on closed magnetic field lines by release of stored energy in the magnetosphere.

Our data set of 208 polar arcs show that they occurred mostly with northward B_z (78 %). However, 16 % of the polar arcs occurred with southward IMF. Many of these

polar arcs occurred during relatively long (> 1 hour) periods of southward IMF B_z. This result differs with earlier studies that polar arcs occur under northward IMF condition [Berkey et al., 1976; Lassen and Danielsen, 1978; Hardy et al., 1986]. Polar arc formation following solar wind dynamic pressure enhancements under stable southward IMF B_z confirms the occurrence of the southward IMF polar arcs. These results do not agree with Valladares *et al.* [1994] who suggested that the southward IMF polar arcs are formed under earlier northward IMF condition. Our results show that polar arcs can occur either with northward IMF (closed magnetosphere) or southward IMF (open magnetosphere).

Polar arcs also tended to occur with IMF B_x near zero and IMF B_y slightly positive. The IMF B_x affects the symmetry of the magnetic configurations in the south and north polar cap regions. This implies that the most favoured orientation of the IMF vector for polar arc generation is that the IMF vector locates in the Y-Z (GSM) plane with θ (measured clockwise from the vertical) in the range of 0 to 90°.

6.3 Enhancements and polar arc source regions

Polar arcs were observed following all the identified solar wind dynamic pressure enhancements during the 1991-92 and 1992-93 winters (see Chapter 4). Polar auroral response to solar wind dynamic pressure enhancements depends on the configuration of the magnetosphere, which is predominantly controlled by the state of the interplanetary medium, especially solar wind dynamic pressure and IMF B_z [Roelof and Sibeck, 1993]. Changing of solar wind dynamic pressure causes displacement of the magnetopause and compression of the magnetosphere. The orientation of the IMF appears to determine the fraction of the solar wind dynamic pressure applied to the magnetosphere [Fairfield et al., 1990] as well as the fraction of solar wind energy transferred to the magnetosphere and the depth of solar wind penetration into the magnetosphere. Therefore, it is instructive to study the difference of responses of polar auroras to the solar wind dynamic pressure changes under southward and northward IMF orientations.

A summary plot of the corrected time delay between the solar wind dynamic pressure enhancements and the polar arcs as a function of the IMF B_z levels is shown in Fig. 6.3. The diagram indicates that there are two categories of time delay, the first is a short time delay (< 30 minutes) and the second is a long time delay (> 30 minutes). The cases with short time delays were associated with southward IMF B_z ($B_z < 0$). The cases with long time delays were associated with northward IMF B_z ($B_z > 0$).

6.3.1 Auroral response with southward IMF

The ionospheric response to the enhancements of solar wind dynamic pressure when the IMF was southward was characterized by the appearance of polar aurora arcs with a short time delay following the enhancements. Among the 25 cases of solar wind dynamic pressure enhancements observed during 1991-93 winter periods, 10 of them occurred with IMF B_z southward. IMF. Table 6.1 is a summary list of the enhancements with southward IMF. It shows that the time delay is less than 28 minutes in all except one case. For that case there was a weak southward IMF (B_z=-1 nT) and the time delay was 39 minutes. The average time delay was 17.5 minutes.

These short time delays (17.5 minutes on average) suggest solar wind particles had direct access to the polar ionosphere with auroral arcs resulting. There was a positive correlation between the magnitude of the enhancements and polar arc intensities as illustrated in Fig. 6.4. This shows that maximum intensity of 630.0 nm emission in proportional to the magnitude of dynamic pressure enhancements (increasing rate $dP/(P_0 dt)$) with southward IMF B_z. The solid line is obtained by a least-squares fit. As a higher dynamic pressure suggests a larger particle flux, then this is further evidence to support the idea of direct access of solar wind particles to the polar ionosphere. When the IMF B_z turns southward, the auroral oval moves to lower magnetic latitude. Then polar cap may be magnetically connected to the solar wind directly on open field lines.

In general when B_z turns southward, polar arcs disappear and F-layer patches appear in the polar cap [McEwen and Harris, 1995]. This is further evidence that the

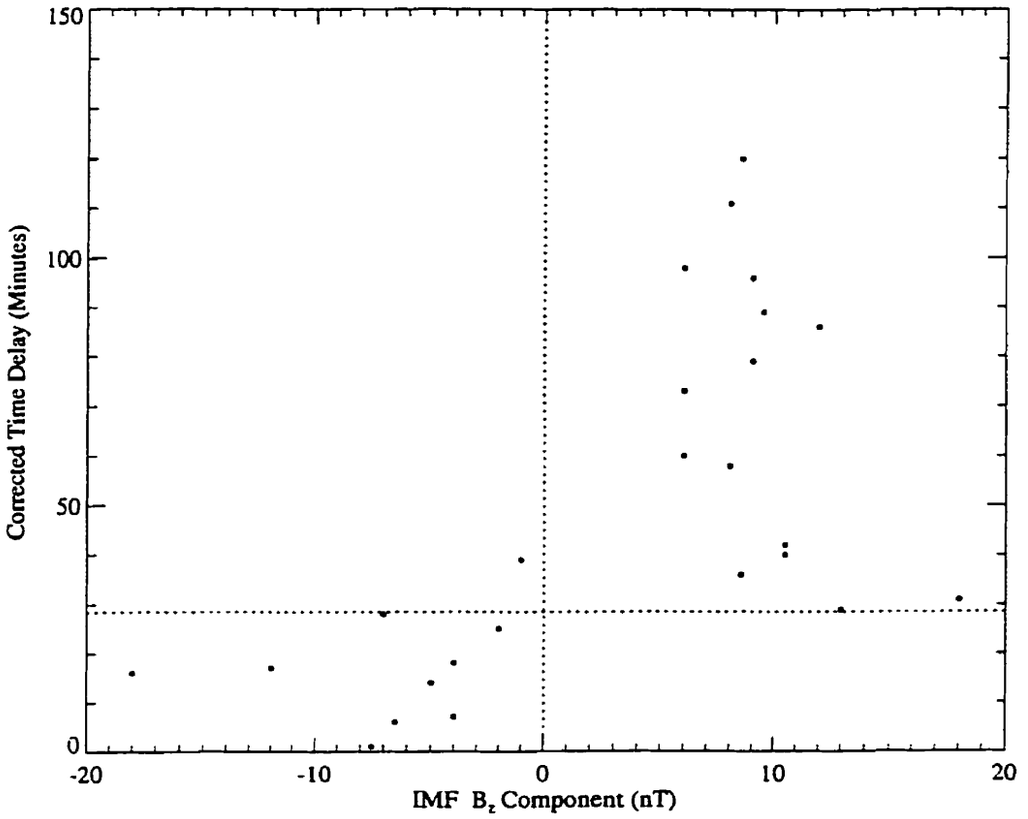

Figure 6.3: Time delay between solar wind dynamic pressure enhancements and the polar auroral peaks as a function of IMF B_z.

magnetic configuration of the magnetosphere is open in the polar cap region with southward IMF. Satellite observations of polar rain during southward IMF support

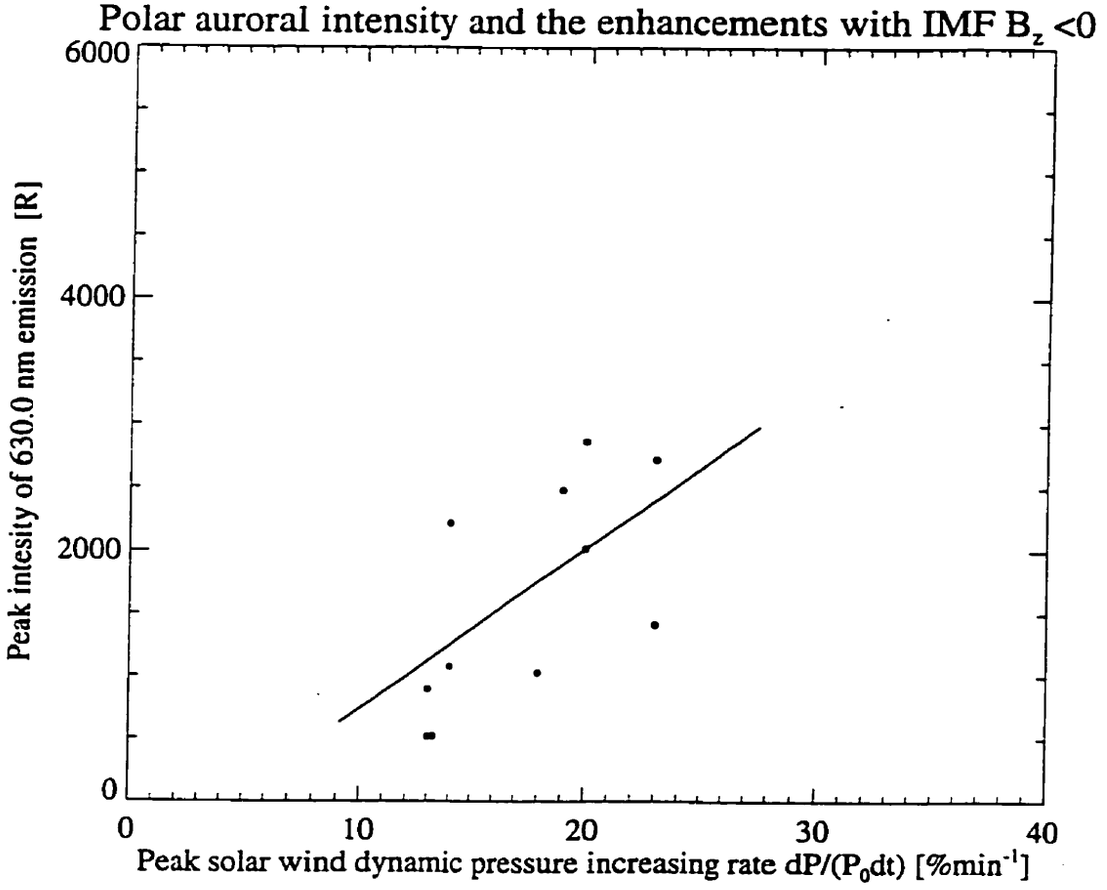

Figure 6.4: The relation between the peak 630.0 emission and amplitude of solar wind dynamic pressure increasing rate. IMF B_z is southward.

the theory that the polar rain originates in the solar wind and gains access to the polar cap along open field lines connecting through the lobes to the solar wind [Hardy *et al.*,, 1986]. Relativistic solar wind electrons observed in the polar cap and non-conjugate polar arcs suggested that they occurred on open field lines [Gussenhoven, 1990]. Stauning et al. [1994] reported frequent observations of poleward progression of polar convection during IMF $B_z < 0$ which supported the concept of an open magnetosphere. These

Table 6.1: Summary list of solar wind dynamic pressure enhancements and polar arcs with southward IMF B_z.

Date	Enhancement	$\frac{dP}{P_o dt}$	IMF B_z	corrected delay
	[hr:min]	$[\%min^{-1}]$	[nT]	[min]
Dec. 16, 93	0810	13	-1	39
	0923	20	-12	17
Dec. 17, 92	1509	23	-7.5	1
	1518	20	-4	7
	1836	18	-6.5	6
	1918	23	-7	28
Nov. 22, 92	0922	14	-4	18
	1045	14	-5	21
Jan. 12, 92	0641	13	-2	25
	1025	19	-18	16
Mean		**18**	**-6.7**	**17.5**

results are consistent with the short time delay between the enhancements and polar arcs under southward IMF B_z.

Sandholt et al. [1994] found cusp/cleft auroral activity to be partially governed by IMF orientation and solar wind dynamic pressure pulses. The time delays between solar wind density peaks and peaks in cleft auroral intensities were from 5 min to 10 min with southward IMF B_z. This short time delay is evidence of direct access of solar wind particles to the cusp/cleft region through open field lines. All this evidence supports the view that the magnetosphere is open from the cusp to the central polar cap region under IMF $B_z < 0$.

6.3.2 Auroral response with northward IMF

A long time delay is a common feature for those polar arcs following the enhancements under northward IMF. Among the 25 solar wind enhancement events, 15 of them

occurred with northward IMF B_z. Table 6.2 is a summary list of these events with magnitude of IMF B_z and corrected time delays. It shows that the time delay is from 29 minutes to 120 minutes with $B_z > 0$. The average time delay is 70 minutes. This long time delay evidently indicates that sources, or acceleration, of electrons for the polar arcs are located in the distant magnetotail. In this case, there should be little correlation between the magnitude of the solar wind dynamic pressure enhancements and the intensities of either 630.0 nm or 557.7 nm emissions. This was found to be true. The maximum intensities of 630.0 nm and 557.7 nm emissions show no correlation with the magnitude of the dynamic pressure enhancements (see Fig. 6.5 and Fig. 6.6).

Table 6.2: A summary list of solar wind enhancements and polar arcs with the IMF B_z northward.

Date	Enhancement	$\frac{dP}{P_o dt}$	IMF B_z	corrected delay
	[hr:min]	$[\%min^{-1}]$	[nT]	[min]
Dec. 16, 93	0140	17	9	79
	0248	15	8	58
	0646	12	6	60
	0845	15	13	29
	1032	18	6	98
Dec. 17, 92	0613	50	8.5	36
	0630	21	6	73
Nov. 22, 92	0730	28	9	96
	0803	30	9.5	89
	0815	29	12	86
	0838	15	8	111
	0859	14	8.5	120
Jan. 12, 92	0911	26	10.5	40
	0935	14	10.5	42
	1552	31	18	31
Mean		**22**	**9.5**	**70**

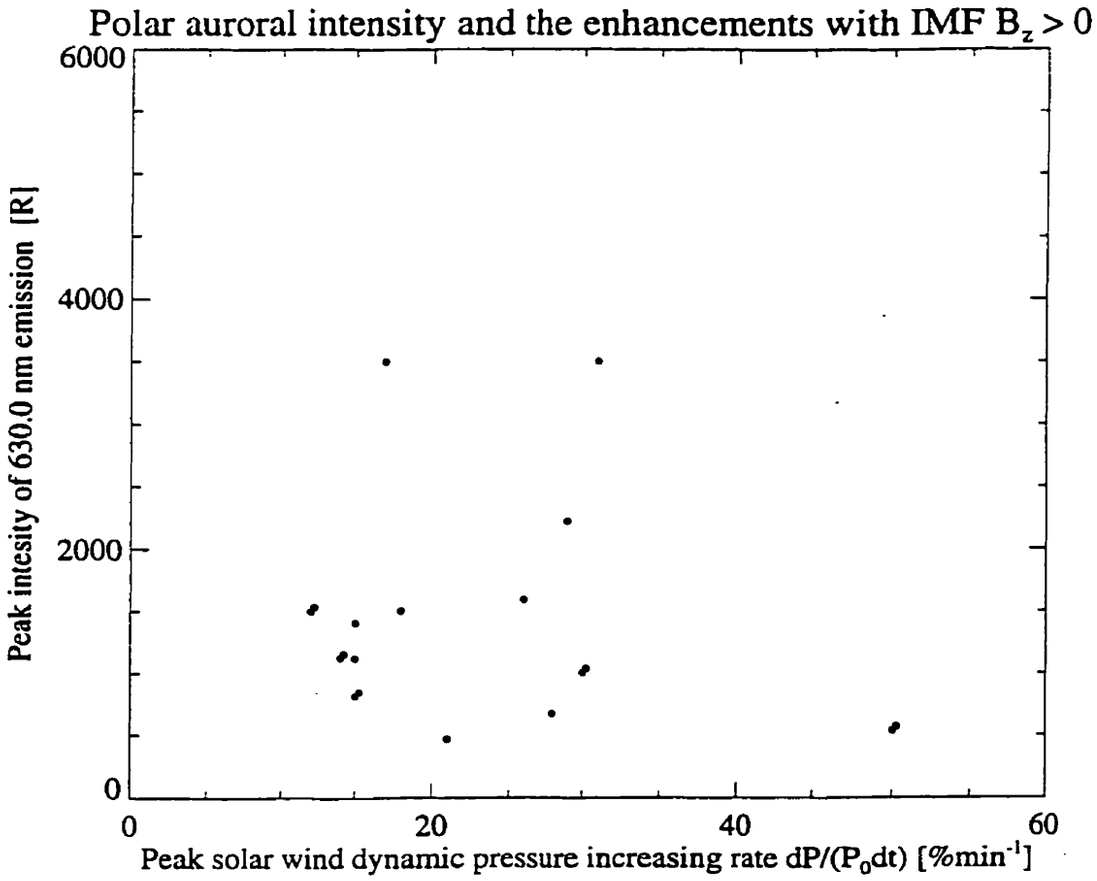

Figure 6.5: Similar to Fig. 6.4, but for northward IMF B_z.

It is believed that the magnetic field lines in the magnetosphere are mainly closed under northward IMF. When IMF B_z changes from southward to northward, the auroral oval moves to higher latitude. The polar cap shrinks. This implies that the open field lines in the polar cap under southward IMF are reconnected and become closed field lines when the IMF turns northward. A closed magnetic field configuration is a good model to describe the magnetosphere in this case (see Fig. 6.7). Recent observations of keV electrons in the polar cap under northward IMF and low energy electrons ($\leq$ 200 eV) during southward IMF condition (open field lines) suggest a closed magnetic field

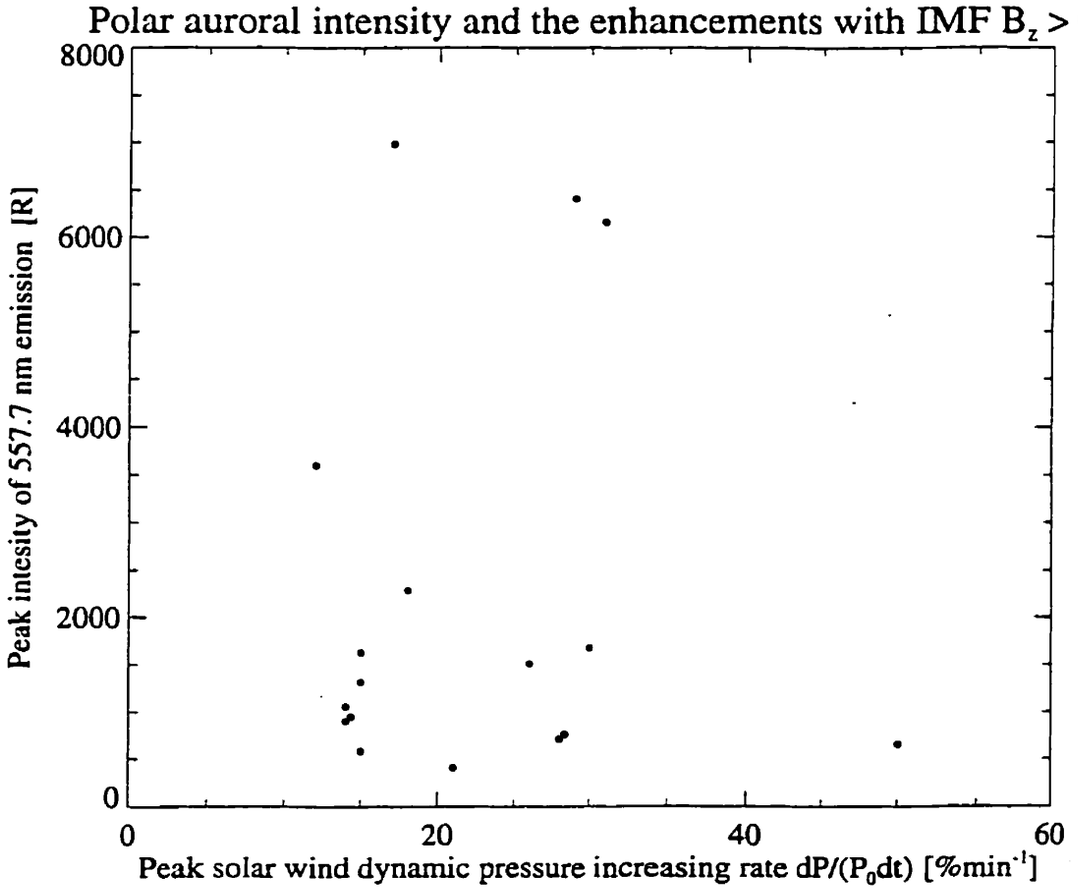

Figure 6.6: The same as Fig. 6.6, but for 557.7 nm emission.

configuration with IMF $B_z > 0$ [Xu and Kivelson, 1994]. The closed magnetic field configuration under northward IMF condition prevents the solar wind particles from accessing the polar ionosphere directly. The long time delay between the enhancements and the polar arcs under northward IMF conditions suggests that the electron source for the polar arcs was located in the deep magnetotail.

6.3.3 Mechanism

Those two degrees (long and short) of time delay were also observed based on a study of the relation between solar wind parameters of solar wind velocity and magnetic field

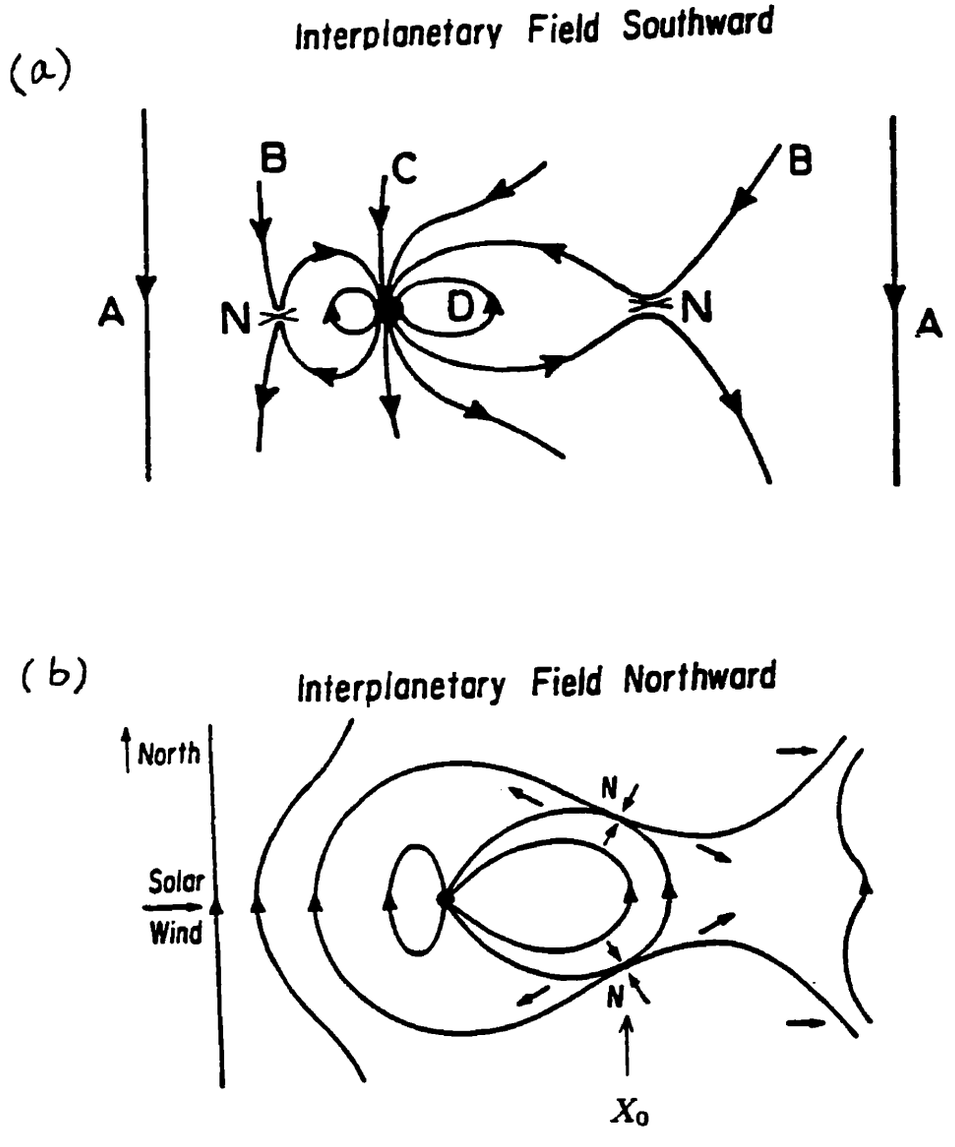

Figure 6.7: A sketch of geomagnetic field configuration in X-Z (GSM) plane. (a) IMF B_z is southward, (b) IMF B_z is northward. (after J.W. Dungey, 1963).

($V_{sw} \times B_s$, observed by IMP-8) and AL index [Bargatze *et al.*, 1986]. The short time delay (about 20 min) shows a direct effect of interaction between the solar wind and the magnetopause. The long time delay (about 60 min) demonstrates an effect due to release of stored energy from the magnetotail. A study of the correlation between solar wind , IMF parameters (observed by ISEE 3) and magnetospheric activity (AE, D_{st}) shows a typical intrinsic time delay, 25 to 40 min between the variations of interplanetary parameters and magnetospheric response during quiet periods and less than 15 min during disturbed times [Baker, et al., 1983]. Quiet periods usually accompany northward IMF, and disturbed times are usually associated with southward IMF. Troshichev et al., [1988] from studies of polar arcs at Vostok station, Antarctica found that the mean time delay of appearance of the sun-aligned arcs after the northward turning of IMF was 55 minutes, while the typical time delay of the disappearance of the polar arcs after the southward turning of IMF was only about 20 min. These are consistent with our results of polar arc appearance following the enhancements after a long time delay with IMF B_z northward and a short time delay with southward IMF B_z. Therefore, the solar wind dynamic pressure enhancements induced polar arcs directly with a southward IMF B_z or indirectly (through the magnetotail) with a northward IMF B_z.

Different time delays of the polar arcs following the enhancements suggest the different electron sources which cause the polar arcs. The average time delay with northward and southward IMF, the mean value of IMF B_z and the average magnitude of dynamic pressure enhancements are listed in Table 6.3. There is no significant difference between the mean magnitudes of the enhancements and the B_z for northward and southward IMF, but the time delay shows a big difference (17.5 and 70 minutes). It is clear that the sign (polarity) of B_z controlled the time delay. That is the positive IMF B_z leads to a long time delay (70 minutes on average) and negative IMF B_z leads to a short time delay (17.5 minutes on average).

A mechanism was proposed to explain the different time delays polar auroras to solar wind dynamic pressure enhancements. Enhanced solar wind dynamic pressure has two effects: (1) to compress the magnetosphere and enhance the convection in the magnetosphere, (2) to provide higher particle flux. Zhu [1995] suggested that convec-

Table 6.3: Average time delay and sign of IMF B_z.

	$\frac{dP}{P_o dt}[\%min^{-1}]$	IMF $B_z[nT]$	corrected delay [min]
Average	18	-6.7	17.5
Average	22	+9.5	70

tion in the magnetosphere can generate field aligned electric fields which accelerate electrons and the produce auroras.

Under southward IMF conditions, the central polar cap is connected to the interplanetary medium directly by the open magnetic field lines. Solar wind particles can precipitate into the polar ionosphere directly and cause polar auroras (mainly red auroras due to low energy of precipitated electrons). With this open magnetosphere, (see Fig. 6.7a, a sketch of magnetic field configuration under IMF $B_z < 0$), the solar wind provides energy to the magnetosphere by continuous merging between the interplanetary magnetic field and the front magnetospheric field [Jacquey and Sauvaud, 1994; Stauning, 1994]. The solar wind dynamic pressure enhancements cause the compression of the magnetosphere, and enhance the convection in the magnetosphere. The enhanced convection intensifies shears of the magnetic field in the magnetosphere. Field-aligned electric fields can suddenly switch on when the shear reaches a critical value [Zhu, 1995]. When the field-aligned electric field is strong enough, it can accelerate the electrons (polar rain?) to a few hundred eV or keV and then cause polar auroras. The short time delay between the dynamic pressure enhancements and polar auroras supports the idea of direct access of solar wind particles and an 'open' magnetosphere configuration.

Under northward IMF conditions, the magnetic field of the magnetosphere is more closed. The efficiency for the solar wind to penetrate the magnetosphere and deposit energy in the magnetosphere is greatly reduced (30 - 100 times less, [Bruce et al., 1995] based on a 'viscous' mechanism) compared to the case of southward IMF B_z condition. Fig. 6.7b shows a magnetic field configuration of the magnetotail under northward

IMF. It also shows that solar wind compresses the deep magnetotail much more than the front magnetosphere. If one assumes the strongest compression of the magnetotail is at $X = X_0$ due to a solar wind dynamic pressure enhancement, then particles in region of $X > X_0$ will move tailward. Those particles in region of $X < X_0$ will move earthward. These particles moving earthward, if accelerated, have the possibility to precipitate in very high latitude ionosphere and cause polar auroras. This is supported by the long time delay between the solar wind dynamic pressure enhancements and the polar auroras. If one assumes 250 km/s is the speed of the solar wind traveling just outside of the magnetotail and electrons in the magnetotail moves with the same speed on most of their way toward polar region, for a time delay from 30 minutes to 120 minutes, the corresponding position of the X_0 is from -35 R_E to -140 R_E in the magnetotail.

6.3.4 Acceleration of electrons in the magnetosphere and ionosphere

Field-aligned acceleration of electrons due to parallel electric fields was observed many years ago. So-called double layers are often observed. Similar phenomena are reported by recent observations of electrostatic solitary waves in the plasma sheet boundary layer of the magnetotail by Geotail satellite. Computer simulations shows those solitary waves are due to high speed electron beams [Matsumoto et al., 1994; Omura et al., 1994]. Therefore high speed electron beams and parallel electric fields are related to each other. However, it is still not clear which is the cause and which is the effect.

Solar wind is the major energy source to the magnetosphere. Solar wind dynamic pressure enhancements provide extra energy and particles above normal levels. They are responsible for some of the polar auroras observed at Eureka. This extra energy drives the convection in the magnetosphere to a higher level. When the flow of plasma of the magnetosphere cuts across geomagnetic field lines, it can create field aligned electric field [Zhu, 1995]. From the Ohm's law, we have:

$$\vec{E} + \vec{V} \times \vec{B} = \eta \vec{J} \tag{6.1}$$

Where $\vec{E}$ is electric field, $\vec{B}$ is magnetic field and $\vec{V}$ is velocity of the plasma in the magnetosphere. Two sources contribute to the magnetic field: (1) background geomagnetic field $\vec{B_0}$, and (2) $\vec{B_1}$ which is due to the enhanced plasma convection in the magnetosphere. Therefore, $\vec{B} = \vec{B_0} + \vec{B_1}$. The parallel component of the electric field along the background magnetic field $\vec{B_0}$ can be written as:

$$\vec{E_{||}} = -[\vec{V} \times \vec{B_1}]_{||} + \eta \vec{J_{||}} \tag{6.2}$$

$[\vec{V} \times \vec{B_1}]_{||}$ can be not zero as the magnetic field B_1 may be not parallel to B_0. If following condition is satisfied:

$$[\vec{V} \times \vec{B_1}]_{||} > \eta \vec{J_{||}} \tag{6.3}$$

then, an upward parallel electric field will result. Such a parallel electric field can accelerate electrons downward and cause polar arcs. A complete study on the generation of field aligned electric field requires both theoretical analysis and computer simulations.

6.4 Mapping and source regions of polar arcs

Mapping of auroras is to link the ionosphere where auroras occur to particle sources of the auroras in the magnetosphere. There are two ways to do this: (1) using magnetic field models (2) using particle data above the auroras and in the deep magnetosphere. Both of the methods can be used in trying to find source regions of auroras. The second method requires two satellites to be located in different parts of the magnetosphere which are connected by magnetic field lines. This satellite configuration does not occur very often. The first method simply depends on magnetic field models and is commonly used for the mapping. Among the magnetic field models, the Tsyganenko magnetic field model (T87, T89) [Tsyganenko, 1989a,b,c, 1990] is widely used in auroral mapping. The T87 model is an empirical model based on large magnetic field data set measured by

satellites. T89 is an improved version of T87 model, as the T89 used a warped current to represent the cross tail current in the magnetotail. Pulkkinen *et al.* [1992] modified the T89 model by enhancing the near -Earth currents and thinning the current sheet from the values given by the T89 model during a substorm growth phase. Elphinstone *et al.* [1991] mapped auroral oval and polar cap regions into the magnetotail using the T87 model. Mapping of the nightside auroral oval into the magnetotail was investigated using DE-1 and DE-2 plasma data in combination with the T89 and Hilmer-Voigt 91 (H-V91) magnetic field models [Weiss *et al.* 1992]. The H-V91 model is a theoretical model depending on four external physical parameters, (1) the dipole tilt angle, (2) the magnetopause stand-off distance, (3) the midnight equatorward boundary of the diffuse aurora, and (4) the geomagnetic index D_{st} [Hilmer and Voigt, 1993]. Our mapping of polar auroras observed at Eureka is based on the T89 model.

Mapping of polar arcs observed at Eureka shows that the source of the precipitated energetic electrons which caused polar arcs was mainly located in the magnetotail lobe region (Chapter 5). This supports the model of a bifurcated magnetosphere presented by Frank *et al.* [1986] and Weiss *et al.* [1994]. They discussed five different magnetotail models as shown in Fig. 6.8. They are the (a) open magnetosphere that the magnetosphere is magnetically connected to the solar wind directly, (b) bifurcated tail that the magnetotail is divided into two parts (left and right) by a region with energetic particles, (c) expanded plasma sheet that the thickness of the plasma sheet is larger than normal one, (d) expanded low latitude boundary layer that the low latitude boundary extends to the lobe region, and (e) rotated x-line (plasma sheet) models that the plasma sheet is rotated either clockwise or anti-clockwise. The mapping of the transpolar arc observed on November 15, 1993 indicates that the electron source of the transpolar arc extended from Z=4 R_E to Z=26 R_E in the Y-Z cross section in the magnetotail at X=-50 R_E while the poleward auroral oval was mapped into the central plasma sheet. The extension of the source region from Z=4 R_E to Z=26 R_E shows that the plasma sheet boundary layer contributed to the occurrence of the transpolar arc. It also supports a model of bifurcated magnetotail. Overall, the mapping suggests that the electron source region for arcs in the central polar cap is in the magnetotail lobe. This is consistent with the work of Elphinstone *et al.* [1991] which showed that the

(tear-drop shaped) polar cap maps into the magnetotail lobe region and the auroral oval maps into the central plasma sheet, by using T87 magnetic field model.

For auroral oval aligned arcs expanding into the polar cap, their source regions are parallel to Y axis (Y-Z plane) in the magnetotail. The aurora observed on February 21, 1994 at Eureka following a Coronal Mass Ejection event and a major magnetic storm is an example of auroral oval-aligned arcs. The oval-aligned arc was identified as a poleward expansion of the auroral oval [McEwen, 1994]. Mapping of this aurora suggests the plasma sheet expanded to Z=15 R_E at X=-30 R_E. This event appears to support the expanded plasma sheet model (see Fig. 6.8c).

The mapping of polar auroras using the T89 magnetic field model suggests the particle source region is in the magnetotail lobe on the average. Those typical sun-aligned arcs in the central polar cap have their electron sources in the magnetotail lobe (northern) and well above the central plasma sheet. The transpolar arc had its particle source located from the plasma sheet boundary layer to the northern lobe region. Particles in the plasma sheet boundary layer were linked to the auroral oval aligned arcs.

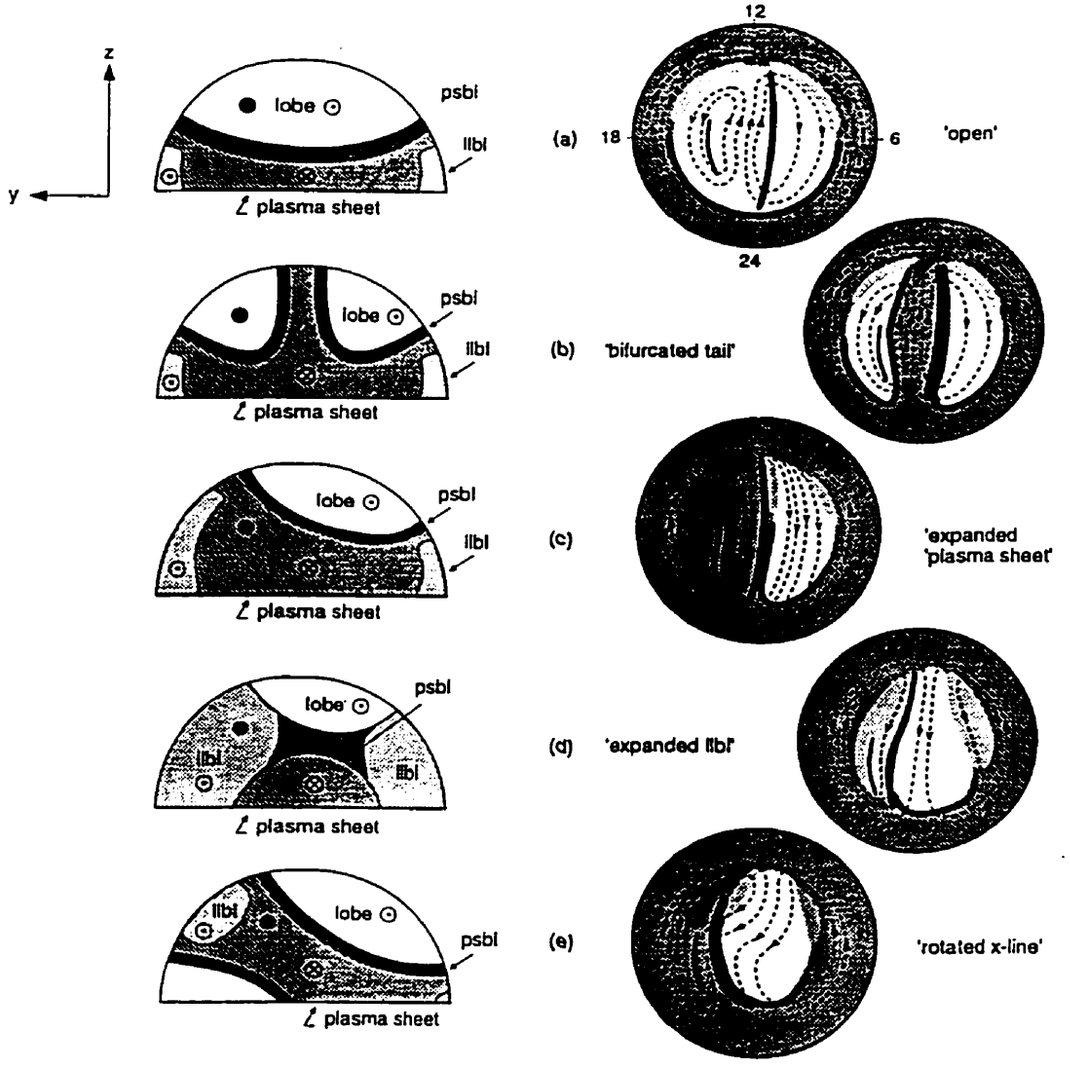

Figure 6.8: Schematic diagram of the mapping of the high-latitude ionosphere to the distant magnetotail for the (a) 'open', (b) 'bifurcated tail', (c) 'expanded plasma sheet', (d) 'expanded LLBL', (e) 'rotated x-line' midels of polar cap morphology. A cross-section of the northern magnetotail lobe (y-z plane, looking from the tail sunward) is shown on the left, and the corresponding ionospheric convection pattern (dotted lines) and location of the sun-aligned and theta arc (solid lines), is shown on the right. Closed field line regions are shown in light gray (LLBL), medium gray (plasma sheet), and dark gray (PSBL), while open field line regions are shown in while. The solid dot in each figure on the left represents a field line threading the weak, sun-aligned arc at 22 MLT. (after L.A. Weiss, et al., 1994).

Chapter 7

Summary and conclusions

Characteristics of auroras in the central polar cap and some ideas on their source regions were obtained from the studies of the large data set of polar arcs which were recorded by the ASC and the MSP near the north magnetic pole during the four winter periods (1990-1994). Polar arcs were also investigated in related to the IMF polarity and solar wind dynamic pressure, especially solar wind dynamic pressure enhancements. Major results and conclusions are given in following sections.

7.1 Occurrence patterns of polar arcs

Polar arcs were recorded 8 % of the time by an ASC with a 300 R threshold at 557.7 nm at Eureka over the four winter periods from 1990 to 1994. There was a diurnal variation in the occurrence pattern of polar arcs. The amplitude of the diurnal variation was about 37 % of the mean occurrence. The maximum was observed around the Eureka local midnight and the minimum was observed at noon. This diurnal variation is possibly due to two facts: (1) the ASC viewing area in the polar ionosphere was magnetically connected to a region in the magnetotail closer to the central plasma sheet in the magnetotail around local (Eureka) midnight, (2) the region in the magnetotail also is the larger. Therefore, the region (around midnight) has the higher probability to observe energetic electrons and the ASC has the higher possibility to detect polar auroras around local midnight hours. The observability of polar arcs depends on sensitivity of the instrument. The MSP operated at higher sensitivity with a 50 R threshold

at 557.7 nm and 630.0 nm. Polar auroral emissions were detected by the MSP 30 % of the time (557.7 nm) and 49 % of the time (630.0 nm) on average over a 38 day test period during the 1993-94 winter. The difference in occurrence frquency of polar arcs at 557.7 nm and 630.0 nm suggests that the precipitated electrons exciting the polar arcs are often very soft. It was also found that the mean frequencies of polar arcs over the winter periods positively correlated with solar activity (10.7 cm flux or sunspot number).

Our results show that the lifetimes of polar arcs with intensity above 300 R vary from two minutes to up to 10 hours. Their mean lifetime is 36 minutes, but 50 % of the polar arcs observed had lifetimes less than 20 minutes. This shows that the appearance of the brighter polar arcs is transient. This suggests the intrinsic time constant of the magnetosphere for activity of these polar arcs is around or below 20 minutes. The bifurcation of some polar arcs suggests that their development may be due to instabilities in the magnetosphere or ionosphere with time constant of about a few minutes.

The observed lifetimes of polar arcs depend on sensitivity of instruments. With higher instrument sensitivity, polar arcs can be seen much more frequently and with longer lifetimes. In fact, polar arcs may be present quasi-continuously whenever the IMF B_z is northward. They can be a useful diagnostic tool for study of polar cap processes and for remote sensing of activities in the magnetosphere and the solar wind.

7.2 Magnetic activity, IMF polarity, solar wind and polar arcs

No specific relation was found between the occurrence patterns of polar arcs and global magnetic activity as depicted by K_p level. Polar arcs were seen to occur at all levels of K_p. This finding is somewhat at variance with the commonly held view that polar arcs tend to occur only under quiet magnetic conditions [Lassen and Danielsen, 1978]. While the orientation of the IMF has a significant effect on the occurrence of polar arcs, most polar arcs (78 %) occurred with the IMF B_z northward. There were significant numbers (16%) of polar arcs appeared with the IMF B_z stably southward. For those

latter arcs, the B_z had been southward for at least 30 minutes and in some cases for hours. In relation to the IMF B_x and B_y, the polar arcs tended to occur preferentially with IMF B_x near 0 nT and IMF B_y positive. In addition to the important effect of IMF orientation, solar wind dynamic pressure was found to be another key parameter affecting occurrence of polar arcs.

7.3 Solar wind dynamic pressure enhancements and polar arcs

Solar wind dynamic pressure enhancements play a significant role in the occurrence of polar arcs. Of 25 enhancements detected by the IMP-8 satellite during good observing periods in the 1991-92 and 1992-93 winters, all were followed by polar arcs. The short time delay (18 min on average) between the enhancements and the polar arcs under southward IMF suggests a direct access of solar wind particles into the polar ionosphere and an open magnetospheric configuration in the polar cap region. A positive correlation between the intensity of 630.0 nm emission and the magnitude of the enhancements with southward IMF confirmed the direct access of the solar wind particles. When the IMF is southward, the precipitating electrons connected directly with the solar wind For northward IMF, the time delay for polar arc appearance was much longer (70 minutes on average). This suggests the particle source for the polar arcs in this cases was located in the magnetotail. This finding shows the solar wind dynamic pressure enhancements do generate or induce energetic electron precipitation with either northward or southward IMF. It also indicates that the magnetosphere response to changes in the solar wind is much more direct with southward IMF than northward IMF.

7.4 Mapping and source regions of precipitated electrons

Mapping of polar arcs by using the T89 magnetic field model shows locations of electron sources of polar arcs. Typical sun-aligned arcs in the central polar cap may have their electron sources located in the magnetotail lobe region. Precipitated electrons for

transpolar arcs are magnetically connected to a region from the plasma sheet boundary to the magnetotail lobe. This supports the bifurcated magnetotail model. The auroras in the poleward edge of the auroral oval were mapped into the plasma sheet. Expansion of the nightside auroral oval during a major magnetic storm (February 21, 1994) indicates that the plasma sheet or the plasma sheet boundary layer expanded into the magnetotail lobe region well beyond the normal location . An expansion of either the plasma sheet or the plasma sheet boundary layer must represent a dynamic state of the magnetotail during a magnetic storm.

7.5 Future work

The long period observations at Eureka provide a unique opportunity for the study of the central polar cap auroras. The new satellite measurements becoming available (WIND and CLUSTER particularly) both in the solar wind (particle and IMF) and in the magnetosphere, especially in the deep magnetotail and over the polar cap regions, will enable researchers to better define the relationship between dynamical changes in the solar wind, the magnetosphere and polar arcs. Once such a relationship or mechanism is established, ground observations of polar arcs provide a way for the remote sensing of the magnetosphere and contributing to space weather forecasts. Before the polar arcs can be completely understood, it is important to carry out following studies:

- The generation of upward field-aligned electric fields by the magnetospheric convection under different solar wind and IMF conditions via theoretical analysis and computer simulations.
- Relation between the energy of precipitated electrons and the polarity of the IMF, solar wind dynamic pressure and magnetospheric conditions.
- The relationship between lifetimes of polar arcs and : (a) intrinsic time scales or time constants for energetic particle precipitation and magnetotail reconfiguration ; (b) the stability of the northward IMF B_z and solar wind dynamic pressure.
- Conditions under which polar arcs can extend from the midnight oval or mid-noon oval to the central polar cap and their relationship to the source of the precipitated

electrons.

- Studies of the development of fine structure of the polar arcs and their relation to plasma instabilities in the magnetosphere or the ionosphere.
- Analysis of 630.0nm/557.7 nm intensity ratios to deduce the softness/hardness of precipitated electrons.

Appendix A

Plasma propagation time from satellite to earth

A simple, first order correction (ΔT_x) for the time delay between solar wind dynamic pressure enhancements and polar arcs involved a time interval between the time that solar wind is detected at IMP 8 and the time this plasma reaches the earth's orbit. The ΔT_x is given by

$$\Delta T_x = \frac{\Delta X}{V_{sw}} \tag{A.1}$$

where ΔX is the distance in X direction (GSM) between the satellite and the earth, and V_{sw} is the solar wind speed. This assumes the solar wind flow is along the sun-earth line. A more refined calculation of the expected propagation time between IMP 8 and the earth takes into account convection in the Y direction also [Baker *et al.*, 1983; Zwickl *et al.*, 1980]. Letting Ω be the angular frequency of rotation of the Sun, R_{au} be the radial distance to the Sun for the plasma in question and ΔY_E, the motion of the earth during the propagation interval, ΔT_x, as measured in (A.1). We have a time correction (ΔT_y) due to plasma convection in the Y direction:

$$\Delta T_y = \frac{1}{\Omega} tan^{-1}\left(\frac{\Delta Y - \Delta Y_E}{R_{au} - \Delta X}\right) \tag{A.2}$$

$$\Delta Y_E = V_E * \Delta T_x \tag{A.3}$$

where ΔY is the distance in the Y direction between the satellite and the earth at the time the measurement is taken, and V_E is the speed of the earth traveling around

the Sun. Thus taking into account convection in both X and Y directions, a two-dimensional convection propagation time interval (ΔT) is given by

$$\Delta T = \Delta T_x + \Delta T_y \tag{A.4}$$

The following parameters were used in calculations :
$R_{au} = 1.5 \times 10^8 km$, $\Omega = 2\pi/27 days$, $R_E = 6400 km$, $V_E = 30 km/s$. A corrected time delay between solar wind dynamic pressure enhancements and polar arcs (Chapter 4) is obtained by subtracting the ΔT from an apparent time delay.

Bibliography

[1] Ashour-Abdalla, M., J.P. Berchem, J. Buchner and L.M. Zelenyi, Shaping of the magnetotail from the mantle: Global and local structure. *J. Geophys. Res.*, **98**, No.A4, 5651-76, 1993.

[2] Austin, J.B., J.S. Murphree and J. Woch, Polar arcs: New results from Viking UV images, *J. Geophys. Res.*, **98**, No. A8, 13545-55, 1993.

[3] Axford, W.I., Observation of the interplanetary Plasma, *Space Sci. Rev.* , **8**, 331-65, 1968.

[4] Baker, D.N., R.D. Zwickl, S.J. Bame, E.W. Hones, B.T. Tsurutani, E.J. Smith and S.-I. Akasofu, An ISEE 3 high time resolution study of interplanetary parameter correlations with magnetospheric activity, *J. Geophys. Res.*, **88**, No. A8, 6230-42, 1983.

[5] Bargatze, L.F., D.N. Baker, and R.L. McPherron, Magnetospheric response to solar wind variations, *Solar wind-magnetosphere coupling*, edited by Y. Kamide and J.A. Slavin, Terra Scientific Publishing Company, Tokyo, 93-100, 1986.

[6] Berkey, F.T., L.L. Cogger, and S. Ismail. Evidence for a correlation between sun-aligned arcs and the interplanetary magnetic field direction. *Geophys. Res. Lett.*, **3**, No.3, 145-7, 1976.

[7] Burch, J.L., Low energy electron fluxes at latitudes above the auroral zone, *J. Geophys. Res.*, **73**, 3585-91, 1968.

[8] Burch, J.L., S.A. Fields and R.A. Heelis, Polar cap electron acceleration regions, *J. Geophys. Res.*, **84**, No.A10, 5863-74, 1979.

[9] Carlson, H.C., Dynamics of the quiet polar cap, *J. Geoelectr. Geomag.*, **42**, 697-710, 1990.

[10] Carlson, H.C. Jr., The dark polar ionosphere: progress and future challenges, *Radio Science*, **29**, No. 1, 157-65, 1994.

[11] Carpenter, D.L., Remote sensing of the magnetospheric plasma by means of whistler mode signals, *Review of Geophysics*, **26**, No.3, 535-49, 1988.

[12] Chamberlain, J.W., Physics of the aurora and airglow, *Academic Press*, New York and London, 1961.

[13] Chiu, Y.T., N.V. Crooker and D.J. Gorney, Model of oval and polar cap arc configurations, *J. Geophys. Res.*, **90**, No.A6, 5153-7, 1985.

[14] Chiu, Y.T, Formation of polar cap arcs, *J. Geophys. Res.*, **94**, No.7, 743-46, 1989.

[15] Craven, J.D., L.A. Frank, C.T. Russell, E.J. Smith, and R.P. Lepping, Global auroral response to the magnetospheric compressions by shocks in the solar wind: Two case studies, *Solar wind-magnetosphere coupling*, edited by Y. Kamide and J.A. Slavin, 367-380, *Terra Scientific Publishing Company, Tokyo,* 1986.

[16] Craven, J.D., J.S. Murphree, L.A. Frank, and L.L. Cogger, Simultaneous optical observations of transpolar arcs in the two polar caps. *Geophys. Res. Lett.*, **18**, No.12, 2297-300, 1991.

[17] Davis, N., *The aurora watcher's handbook*, 109-16, University of Alaska Press, 1992.

[18] Dungey, J.W., The structure of the exosphere or adventures in velocity space, in *The Earth's environment*, edited by C. Dewitt, J. Hieblot, and A. Lebeau, Gordon and Breach, 505, New York, 1963.

[19] Eather, R.H. and S.-T. Akasofu, Characteristics of polar cap auroras, *J. Geophys. Res.*, **74**, *No.19, 4794-98, 1969.*

[20] Elphinstone, R.D., D.J. Hearn, J.S. Murphree, and L.L. Cogger, Mapping using the Tsyganenko long magnetospheric model and its relationship to Viking auroral images, *J. Geophys. Res.*, **96**, No. A2, 1467-80, 1991.

[21] Elphinstone, R.D., J.S. Murphree, D.J. Hearn, L.L. Cogger, P.T. Newell, and H. Vo, Viking observations of the UV dayside aurora and their relationship to DMSP particle boundary definitions. *Ann. Geophysicae*, **10**, 815-26, 1992.

[22] Elphinstone, R.D. and D.J. Hearn, The auroral distribution and its relation to magnetospheric processes, *Adv. Space Res.*, **13**, No.4, 417-27, 1993.

[23] Engebretson, M.J, J.L. Alford, W.J. Hughes, E. Zesta, R.L. Arnoldy and C.G. Maclennan, Conjugate studies of broadband ULF magnetic pulsations at Cusp/cleft latitudes, *Eos Trans. AGU*, **76**, S254, 1995.

[24] Fairfield, D.H., An evaluation of the Tsyganenko magnetic field model, *J. Geophys. Res.*, **96**, 1481-94, 1991.

[25] Fairfield, D.H., W. Baumjohann, G. Paschmann, H. Luhr and D.G. Sibeck, Upstream pressure variations associated with the bow shock and their effects on the magnetosphere, *J. Geophys. Res.*, **95**, No.A4, 3773-86, 1990.

[26] Fairfield, D.H., Solar wind control of the distant magnetotail: ISEE3, *J. Geophys. Res.*, **98**, No.A12, 21265-76, 1993.

[27] Feldstein, Y.I. and Galperin Yu. I., The auroral luminosity structure in the high-latitude upper atmosphere: its dynamics and relationship to the large-scale structure of the Earth's magnetosphere. *Rev. Geophys.*, **23**, No.3, 217-75, 1985.

[28] Fasel, G.J., J.I. Minow, R.W. Smith, C.S. Deehr, and L.C. Lee, Multiple brightening of transient dayside auroral forms during oval expansions. *Geophys. Res. Lett.*, **12**, No. 24, 2429-32, 1992.

[29] Foster, J.G. and J.R. Burrows, Electron fluxes over the polar cap 1. Intense keV fluxes during poststorm quieting, *J. Geophys. Res.*, **81**, No.34, 6016-28, 1976.

[30] Foster, J.G. and J.R. Burrows, Electron fluxes over the polar cap 2. Electron trapping and energization on open field lines, *J. Geophys. Res.*, **82**, No.32, 5165-70, 1977.

[31] Frank, L.A., J.D. Craven, D.A. Gurnett, S.D. Shawhan, D.R. Weimer, J.L. Burch, J.D. Winningham, C.R. Chapell, J.H. Waite, R.A. Heelis, N.C. Maynard, M. Sugiura, W.K. Peterson and E.G. Shelley, The theta aurora, *J. Geophys. Res.*, **91**, No.A3, 3177-224, 1986.

[32] Gosling, J.T., *Solar activity observations and predictions*, Editors: McIntosh and Tryer, MIT Press, 1972.

[33] Gusev, M.G. and O.A. Troshichev, Hook-shaped arcs in the dayside polar cap and their relation to the IMF. *Planet. Space Sci.*, **34**, No.6, 489-96, 1986.

[34] Gusev, M.G. and O.A. Troshichev, Relation of sun-aligned arcs to polar cap convection and magnetic disturbances, *Planet. Space Sci.*, **38**, No.1, 1-11, 1990.

[35] Gusev, M.G. and O.A. Troshichev, Simultaneous ground observations of polar cap arcs and spacecraft measurements of particle precipitation. *J. Atmos. and Terr. Phys.*, **54**, No.11/12, 1573-91, 1992.

[36] Gussenhoven, M.S., Extremely high latitude auroras, *J. Geophys. Res.*, **87**, No. A4, 2401-12, 1982.

[37] Gussenhoven, M.S., D.A. Hardy, N. Heinemann and R.K. Burkhardt, Morphology of the polar rain, *J. Geophys. Res.*, **89**, No.A11, 9785-800, 1984.

[38] Gussenhoven, M.S., D.A. HArdy, F.J. Rich, E.G. Mullen, and R. Redus, Evidence that polar cap arcs occur on open field lines, *J. Geoelectr. and Geomag.*, **42**, 737-51, 1990.

[39] Hardy, D.A., W.J. Burke and M.S. Gussenhoven, DMSP optical and electron measurements in the vicinity of polar cap arcs, *J. Geophys. Res.*, **87**, 2413-30, 1982.

[40] Hardy, D.A., M.S. Gussenhoven, K. Riehl, R. Burkhardt, N. Heinemann and T. Schumaker, The characteristics of polar cap precipitation and their dependence on the interplanetary magnetic field and solar wind, *Solar wind-magnetosphere coupling*, edited by Y. Kamide and J.A. Slavin, 575-604, Terra Scientific Publishing Company, Tokyo, 1986.

[41] Hargreaves, J.K., The solar-terrestrial environment, Cambridge University Press, 1992.

[42] Hilmer, R.V. and R.G. Voigt, A magnetospheric magnetic field model with flexible current systems driven by independent physical parameters, Submitted to *J. Geophys. Res.*, 1993.

[43] Huang, C.Y., J.D. Craven and L.A. Frank, Simultaneous observations of a theta aurora and associated magnetospheric plasmas, *J. Geophys. Res.*, **94**, No.A8, 10137-43, 1989.

[44] Huang, K., D.J. McEwen and I. Oznovich, Analysis of a polar auroral arc observed from Eureka ($89°N$) and by DMSP satellites on December 14, 1990, *J. Geophys. Res.*, **99**, 21353-59, 1994.

[45] Ismail, S. and C.-I. Meng, A classification of polar cap arcs, *Planet. Space Sci.*, **30**, No.4, 319-30, 1982.

[46] Ismail,, S., D.D. Wallis, and L.L. Cogger, Characteristics of the polar cap sun-aligned arcs, *J. Geophys. Res.*, **82**, No.29, 4741-49, 1977.

[47] Jacquey, C. and J.-A. Sauvaud, Magnetosphere-ionosphere response to an enhanced energetic coupling with the solar wind, *J. Geophys. Res.*, **99**, No. A6, 11331-9, 1994.

[48] Kaymaz, Z., G.L. Siscoe, J.G. Luhmann, R.P. Lepping and C.T. Russell, Interplanetary magnetic field control of magnetotail magnetic geometry: IMP 8 observations, *J. Geophys. Res.*, **99**, No.A6, 11113-26, 1994.

[49] Kletzing, C.A., Electron acceleration by kinetic Alfven waves, *J. Geophys. Res.*, **99**, No.A6, 11095-103, 1994.

[50] Lassen, K. and C. Danielsen, Quiet time pattern of auroral arcs for different directions of the interplanetary magnetic field in the Y-Z plane, *J. Geophys. Res.*, **83**, No.A11, 5277-84, 1978.

[51] Lennartsson, W., A scenario for solar wind penetration of the Earth's magnetic tail based on ion composition data from the ISEE 1 spacecraft, *J. Geophys. Res.*, **97**, No. A12, 19221-38, 1992.

[52] Lockwood, M., The excitation of ionospheric convection, *J. Atmos. Terr. Phys.*, **53**, 177-99, 1991.

[53] Lockwood, M., S.W.H. Cowley, P.E. Sandholt, and R.P. Lepping, The ionospheric signature of flux transfer events and solar wind dynamic pressure changes. *J. Geophys. Res.*, **95**, 17113-35, 1990.

[54] Mawson, D., Auroral observations at the the Cape Royds Station, Antarctica, *Trans. Proc. S. Aust., XL,* 151, 1916.

[55] Matsumoto, H., H. Kojima, T. Miyatake, Y. Omura, M. Okada, I. Nagano and M. Tsutsui, Electrostatic Solitary Waves (ESW) in the magnetotail: BEN wave form observed by Geotail, *Geophys. Res. Lett.*, **21**, No.25, 2915-8, 1994.

[56] Mawson, D., Australasian Antarctic expedition 1911-1914, *Sci. Rep., Ser.* B. vol. II, part I, records of the Aurora Polaris, Sydney, Australia, 1925.

[57] McEwen, D.J., and D.A. Harrington, Polar airglow and aurora, *Canadian Journal of Physics*, **69**, 1055-58, 1991.

[58] McEwen, D.J., Polar aurora and F-layer dynamics at Eureka, Canada. *Proceedings of the International Society for Optical Engineering*, **2266**, 92-100, 1994.

[59] McEwen, D.J. and D. Harris, Optical characteristics of F-layer patches, submitted to *Radio Science*, 1995.

[60] Meng, C.-I, Polar cap arcs and the plasma sheet, *Geophys. Res. Lett.*, **8**, 273-76, 1981a.

[61] Meng, C.-I, The auroral electron precipitation during extremely quiet geomagnetic conditions, *J. Geophys. Res.*, **86**, 4607-27, 1981b.

[62] Meng, C.-I. and K. Makita, Dynamic variations of the polar cap, in *Solar wind-magnetosphere coupling*, edited by Y. Kamide and J.A. Slavin, 605-31, Terra Scientific publishing company, Tokyo, 1986.

[63] Mitchell, D.G., F. Kutchko, D.J. Williams, T.E. Eastman, L.A. Frank and C.T. Russell, An extended study of the low-latitude boundary layer on the dawn and dusk flanks of the magnetosphere. *J. Geophys. Res.*, **92**, 7394-404, 1987.

[64] Moses, J.J. and P.H. Reiff, Polar cap convection: Steady state and dynamic effects, in *Magnetospheric Substorms*, edited by J.K. Kan, T.A. Potemra, S. Kokubun and T. Iijima, 375-85, American Geophysical Union, 1991.

[65] Mozer, F.S., H. Hayakawa, S. Kokubun, M. Nakamura, T. Okada, T. Yamamoto and K. Tsuruda, Direct entry of dense flowing plasma into the distant tail lobes, *Geophys. Res. Lett.*, **21**, No.25, 2959-62, 1994.

[66] Murphree, J.S. and L.L. Cogger, Observations between apparent polar cap features and the instaneous diffuse auroral oval, *Planet. Space Sci.*, **29**, No.11, 1143-9, 1981.

[67] Murphree, J.S., L.L. Cogger, C.D. Anger, D.D. Wallis and G.G. Shepherd, Oval intensifications associated with polar arcs. *Geophysical Res. Lett.*, **14**, No.4, 403-6, 1987.

[68] Newell, P. T. and C.-I Meng, Ionospheric projections of magnetospheric regions under low and high solar wind pressure conditions. *J. Geophys. Res.*, **99**, A1, 293-, 1994.

[69] Ness, N.F., C.S. Scearce, and J.B. Seek, Initial results of the IMP 1 magnetic field experiment, *J. Geophys. Res.*, **69**, 3531-69, 1964.

[70] Obara, T.M., M. Kitayama, T. Mukai, N. Kaya, J.S. Murphree, and L.L. Cogger, Simultaneous observations of sun-aligned polar cap arcs in both hemispheres by EXOS-C and Viking , *Geophys. Res. Lett.*, **15**, 713-6, 1988.

[71] Omura, Y., H. Kojima, and H. Matsumoto, Computer simulation of electrostatic solitary waves: a nonlinear model of Broadband Electrostatic Noise, *Geophys. Res. Lett.*, **21**, No.25, 2923-6, 1994.

[72] Oznovich, I. and D.J. McEwen, Auroral emissions at the north magnetic pole - A February 17, 1993 case study, *J. Geomag. Geoelectr.*, **46**, 861-71, 1994.

[73] Oznovich, I., R. Yee, A. Schiffler, D.J. McEwen and G.J. Sofko, The all-sky camera revitalized, *Applied Optics* , **33**, No. 30, 7141-50, 1994.

[74] Oznovich, I., D.J. McEwen, R.P. Lepping and Y. Zhang, Evidence that some polar cap arcs are threaded by open field lines, *Eos Trans. AGU*, **75**, 567, 1994.

[75] Pellinen, R.J., H.E.J. Koskinen, T.I. Pulkkinen, J.S. Murphree, G. Rostoker, and H.J. Opgenoorth, Satellite and ground-based observations of a fading transpolar arc, *J. Geophys. Res.*, **95**, No.A5, 5817-24, 1990.

[76] Potemra, T.A., *Johns Hopkins APL Tech. Digest*, **4**, 276, 1983.

[77] Pudovkin, M.I., V.P. Kozelov, L.L. Lazutin, O.A. Troshichev and A.D. Chertkov, Physical principles of the magnetosphere disturbance forecasting, Nauka, Lenningrad, 1977, (in Russian).

[78] Pudovkin, M.I. and V.S. Semenov, Magnetic reconnection theory and the solar wind magnetosphere interaction: a review, *Space Science Reviews*, **41**, 1-89, 1985.

[79] Pulkkinen, T.I., D.N. Baker, R.J. Pellinen, J. Buchner, H.E.J. Koskinen, R.E. Lopez, R.L. Dyson, and L.A. Frank, Particle scattering and current sheet stability in the geomagnetic tail during the substorm growth phase, *J. Geophys. Res.*, **97**, No.A12, 19283-97, 1992.

[80] Riehl, K.B., and D.A. Hardy, Average characteristics of the polar rain and their relationship to the solar wind and the interplanetary magnetic field, *J. Geophys. Res.*, **91**, No.A2, 1557-71, 1986.

[81] Roelof, E.C. and D.G. Sibeck, Magnetopause shape as a bivariate function of interplanetary magnetic field B_z and solar wind dynamic pressure, *J. Geophys. Res.*, **98**, No. A12, 21421-50, 1993.

[82] Rosenbauer, H., *Solar system plasma and fields*, (eds. J. Lemaire and M.J. Rycroft), in *Advances in Space Research*, **2**, No.1, 47-50, Pergamon Press PLC, 1982.

[83] Russell, C.T., Solar wind control of magnetospheric configuration. in *Solar wind-Magnetosphere Coupling*, Edited by Y. Kamide and J.A. Slavin, Terra Scientific Publishing Company, Tokyo, 209-31, 1986.

[84] Sandholt, P.E., J. Moen and D. Opsvik, Periodic auroral events at the midday polar cap boundary: implications for solar wind-magnetosphere coupling, *Geophys. Res. Lett.*, **19**, No.12, 1223-26, 1992.

[85] Sandholt, P.E., C.J. Farrugia, L.F. Burlaga, J.A. Holtet, J. Moen, B. Lybekk, B. Jacobsen, D. Opsvik, A. Egeland, R. Lepping, A.J. Lazarus, T. Hansen, A. Brekke, E. Friis-Christensen, Cusp/cleft auroral activity in relation to solar wind dynamic pressure, interplanetary magnetic field B_z and B_y, *J. Geophys. Res.*, **99**, No. A9, 17323-42, 1994.

[86] Scurry, L. and C.T. Russell, Proxy studies of energy transfer to the magnetosphere. *J. Geophys. Res.*, **96**, 9541-8, 1991.

[87] Southwood, P.J., Ionospheric signatures of magnetospheric boundary phenomena, *J. Geoelect. and Geomag.*, **42**, 789-99, 1990.

[88] Stauning, P., E. Friis-Christensen, O. Rasmussen, and S. Vennerstrom, Progressing polar convection disturbances: Signature of an open magnetosphere, *J. Geophys. Res.*, **99**, No. A6, 11303-17, 1994.

[89] Stauning, P., Coupling of IMF B_y variations into the polar ionosphere through interplanetary field-aligned currents, *J. Geophys. Res.*, **99**, No. A9, 17309-22, 1994.

[90] Steele, D.P. and D. J. McEwen, Electron auroral excitation efficiencies and intensity ratios, *J. Geophys. Res.*, **95**, No. A7, 10321-36, 1990.

[91] Stern, D. P., The art of mapping the magnetosphere, *J. Geophys. Res.*, **99**, No. A9, 17169-98, 1994.

[92] Stern, D. P. and N. A. Tsyganenko, Uses and limitations of the Tsyganenko magnetic field models, *Eos Trans. AGU*, **73**, 489, 1992.

[93] Stormer, C., The polar aurora, Oxford at the Clarendon Press, 1955.

[94] Tascione. T.F., *Introduction to the space environment*, Orbit Book Company, Inc., 56, 1988.

[95] Troshichev, O.A., M.G. Gusev, S.V. Nickolashkin and V.P. Samsonov, Features of the polar cap aurorae in the southern polar region, *Planet. Space Sci.*, **36**, No.5, 429-39, 1988.

[96] Tsyganenko, N.A., A magnetospheric field model with a warped tail current sheet. *Planet Space Sci.*, **37**, 5-20, 1989a.

[97] Tsyganenko, N.A., A solution of the Chapman-Ferraro problem for an ellipsoidal magnetopause, *Planet Space Sci.*, **37**, No.9, 1037-46, 1989b.

[98] Tsyganenko, N.A., Quantitative models of the magnetospheric magnetic field: Methods and results, a review, *Space Sci. Rev.*, **54**, No.1/2, 75-186, 1990.

[99] Tsurutani, B.T. and W.D. Gonzalez, The efficiency of 'viscous interaction' between the solar wind and the magnetosphere during intense northward IMF events, *Geophys. Res. Lett.*, **22**, No. A6, 663-6, 1995.

[100] Usadi, A., A. Kegeyama, K. Watanabe, T. Sato, A global simulation of the magnetosphere with a long tail: southward and northward interplanetary magnetic field, *J. Geophys. Res.*, **98**, No. A5, 7503-17, 1993.

[101] Valladares, C.E, H.C. Carlson Jr. and K. Fukui, Interplanetary magnetic field dependency of stable sun-aligned polar arcs, *J. Geophys. Res.*, **99**, No. A4, 6247-72, 1994.

[102] Vo, H.B. and J.S Murphree, A study of day side auroral bright spots seen by the Viking auroral imager, *J. Geophys. Res.*, **100**, No. A3, 3649-55, 1995.

[103] Weber, E.J. and J. Buchau, Polar cap F-layer auroras, *Geophys. Res. Lett.*, **8**, 125-8, 1981.

[104] Weiss, L.A., P.H. Reiff, R.V. Hilmer, J.D. Winningham and G. Lu, Mapping the auroral oval into the magnetotail using Dynamics Explorer plasma data, *J. Geomag. Geoelectr.*, **44**, 1121-44, 1992.

[105] Weiss, L.A., E.J. Weber, P.H. Reiff, J.R. Sharber, J.D. Winningham, F. Primdahl, I.S. Mikkelsen, C. Seifring, and E.M. Wescott, Convection and electrodynamic signatures in the vicinity of a sun-aligned arc: results from polar acceleration regions and convection study (polar arcs). Submitted to *J. Geophys. Res.*, 1994.

[106] Whalen, B.A., J.R. Miller and I.B. McDiarmid, Sounding rocket observations of particle precipitation in the polar cap electron aurora, *J. Geophys. Res.*, **76**, 6847-55, 1971.

[107] Winningham, J.D. and W.J. Heikkila, Polar cap auroral electron fluxes observed with ISIS 1, *J. Geophys. Res.*, **80**, 949-57, 1974.

[108] Wu, B.H., W.E. Mandt, L.C. Lee and J.K. Chao, Magnetospheric response to solar wind dynamic pressure variations: interaction of interplanetary tangential discontinuities with the bow shock, *J. Geophys. Res.*, **98**, No. A12, 21297-311, 1993.

[109] Xu, D. and M.G. Kivelson, Polar cap field-aligned currents for southward interplanetary magnetic fields, *J. Geophys. Res.*, **99**, No. A4, 6067-78, 1994.

[110] Zhang, Y., D.J. McEwen, D.P. Harris, G.R. Hammel, I. Oznovich and A. Maione, Morphological studies of polar arcs at Eureka, *Eos Trans. AGU*, **74**, 457, 1993.

[111] Zhang, Y., D.J. McEwen, K. Yumoto, K. Shiokawa and K. Hayashi, Studies of polar auroras from near the north magnetic pole, *Proceedings of Eighth International Symposium on Solar Terrestrial Physics*, 121, Sendai, Japan, June 5-10, 1994.

[112] Zhang, Y., D.J. McEwen and I. Oznovich, Polar arcs: Their relation to activity in the interplanetary medium, *Eos Trans. AGU*, **75**, 567, 1994.

[113] Zhu, X., How the magnetosphere is driven into substorm, *J. Geophys. Res.*, **100**, No. A2, 1857-56, 1995.

[114] Zwick, R.D., J.R. Asbridge, S.J. Bame, W.C. Feldman and J.T. Gosling, Convective nature of transient solar wind phenomena observed by ISEE 3 and ISEE 1, *Eos Trans. AGU*, **61**, 354, 1980.